

Structure-Function Analysis of a Cyanobacterial Protein Phosphatase 2C Homologue

Dissertation

der Mathematisch-Naturwissenschaftlichen Fakultät
der Eberhard Karls Universität Tübingen
zur Erlangung des Grades eines
Doktors der Naturwissenschaften
(Dr. rer. nat)

vorgelegt von
Jiyong, Su
aus Hebei, China

Tübingen
2011

Tag der mündlichen Qualifikation:

21.11.2011

Dekan:

Prof. Dr. Wolfgang Rosenstiel

1. Berichterstatter:

Prof. Dr. Karl Forchhammer

2. Berichterstatter:

Prof. Dr. Friedrich Götz

Acknowledgmenets

The work of this Ph.D dissertation was performed in the institute of Microbiology/Organismic Interactions, Eberhard Karls University Tuebingen, in the period from July 2007 to October 2011.

My deepest gratitude goes first and foremost to **Prof. Dr. Karl Forchhammer**, my supervisor, for his constant encouragement and guidance.

His excellent scientific guidance, instructive ideas, intensive and critical theoretical discussions are over the period of my Ph.D study. I have enjoyed the experience and learned a lot while working with him.

Secondly, I would like to express my heartfelt gratitude to **Prof. Dr. Klaus Hantke, PD. Dr. Maldener Iris, and Christina Herrmann** for their presence whenever approached with any problems.

I am also greatly indebted to all of the members at the institute of Microbiology/Organismic Interactions who have made the laboratory a wonderful place to work; particularly to Oleksandra, Maximilian, Susanne, Josef, Dai, Peter, Michaela and Frank for their friendly presence at all times.

Last my thanks would go to my beloved family for their loving considerations and great confidence in me. I also owe my sincere gratitude to my friends who gave me their help and time in helping me work out my problems during the difficulties of this thesis

ACKNOWLEDGMENTS.....	4
CHAPTER 1. INTRODUCTION.....	7
1.1 CYANOBACTERIA.....	7
1.2 P _{II} PROTEIN.....	8
1.2.1 <i>E.coli</i> P _{II}	8
1.2.2 <i>Cyanobacteria</i> and plant P _{II}	9
1.3 THE PHOSPHATASE OF P _{II} - A PP2C TYPE PHOSPHATASE.....	11
1.4 PP2C TYPE PROTEIN PHOSPHATASE.....	12
1.4.1 <i>The classification of protein phosphatases</i>	12
1.4.2 <i>Functions of PP2C type protein phosphatase</i>	13
1.4.3 <i>The catalytic mechanism of PP2Cs revealed by the atomic and biochemical studies</i>	15
1.5 AIM OF THIS DISSERTATION.....	24
CHAPTER 2. METHODS AND MATERIALS.....	25
2.1 DNA MATERIALS.....	25
2.1.1 <i>Bacterium</i>	25
2.1.2 <i>Plasmids</i>	26
2.1.3 <i>DNA manipulation enzymes and kits</i>	26
2.1.4 <i>Medium and buffers</i>	27
2.2 DNA METHODS.....	28
2.3 PROTEIN MATERIALS.....	28
2.3.1 <i>Chemicals and materials</i>	28
2.3.2 <i>Buffers for protein manipulations</i>	29
2.4 GENERAL PROTEIN METHODS.....	31
2.4.1 <i>Expression of His-tag tPphA and its variants</i>	31
2.4.2 <i>Purification of his-tPphA and its variants</i>	32
2.4.3 <i>SPS-PAGE protein electrophoresis</i>	32
2.4.4 <i>Preparation of phosphorylated P_{II} and Strep-P_{II}</i>	32
2.4.5 <i>Native PAGE</i>	32
2.4.6 <i>Western-blotting</i>	32
CHAPTER 3. A THIRD METAL IS REQUIRED FOR CATALYTIC ACTIVITY OF THE SIGNAL- TRANSDUCING PPM PHOSPHATASE TPPHA.....	34
CHAPTER 4. DETERMINANTS FOR SUBSTRATE SPECIFICITY OF THE BACTERIAL PP2C PROTEIN PHOSPHATASE TPPHA FROM THERMOSYNECHOCOCCUS ELONGATUS.....	49

CHAPTER 5. INVESTIGATION OF A KEY ARGININE RESIDUE CLOSE TO THE CATALYTIC CENTER OF PPM/PP2C TYPE PROTEIN PHOSPHATASE.....	76
CHAPTER 6. ADDITIONAL DATA.....	90
6.1 THE STUDIES OF P _{II} KINASE.....	90
6.1.2 <i>In vivo</i> P _{II} protein phosphorylation assays.....	90
6.1.2 <i>In vitro</i> P _{II} protein phosphorylation assays.....	91
6.2 TPPHA COULD RECOVER P _{II} -P FROM <i>S. ELONGATUS</i> CRUDE EXTRACT.....	93
6.3 HIS-TPPHA R13C VARIANT CROSS-LINKS WITH STREP-P _{II} S49C VARIANT.....	97
7. SUMMARY.....	99
8. PROSPECTS.....	101
9. REFERENCES.....	102
CONTRIBUTION TO PUBLICATIONS/MANUSCRIPTS.....	106
CURRICULUM VITAE.....	106
ABBREVIATIONS.....	107

Chapter 1. Introduction

1.1 Cyanobacteria

Cyanobacteria are Gram-negative bacteria. They exhibit a broad range of diversity in ecological habitats, including environments that are extremely hot, cold, dry and alkaline (1). Some cyanobacteria can produce cyanotoxins including neurotoxins, hepatotoxins, cytotoxins, and endotoxins. These toxins can be toxic to humans, animals and marine life (2). Chloroplasts of plants have evolved from cyanobacteria and they show many common characters (3). Cyanobacteria have a membranous compartment named thylakoid, which is the site of the light-dependent reactions of photosynthesis. The reaction centers of photosystem II and I are located at the thylakoid membrane. Phycobilisomes which act as light harvesting antennae for the photosystems, are attached at the luminal cytoplasmic side of the thylakoid membranes. Cyanobacteria can use the energy from light to split water molecules (4) into oxygen (O_2), protons (H^+) and electrons (\bullet). The by-product oxygen (O_2) is assumed to have created the ancient oxidizing atmosphere (5). Carbon dioxide (CO_2) can be reduced to carbohydrates by using the primary products (ATP and NADPH) of photosynthesis. Some filamentous cyanobacteria such as *Anabaena* and *Nostoc* (6, 7) are able to reduce and fix nitrogen gas (N_2) into ammonia (NH_3). They show the ability to differentiate into several different cell types: vegetative cells, akinetes and heterocysts, the latter containing nitrogenase. Since nitrogenase is inactivated by oxygen (O_2), the thick-walled heterocyst creates a microanaerobic environment for this enzyme (8). Cyanobacteria of the *Nostoceae* family can form motile filaments termed hormogonia (9). Hormogonia of some *Nostoc* strains are able to colonize host plants to establish a nitrogen fixing symbiosis. Cyanobacteria are valuable model organism to study photosynthesis, carbon-nitrogen assimilation and evolution of plant plastids. Two unicellular cyanobacteria (*Synechocystis* sp. PCC 6803 (*Synechocystis*) and *Synechococcus elongatus* PCC 7942 (*S. elongatus*)) are common experimental strains in the lab. *Synechocystis* (genome size: 3.57 Mb, reference 10) can be easily transformed by exogenous DNA (11, 12) and *S. elongatus* (genome size: 2.7Mb, reference 10) is the first cyanobacterium demonstrated to be reliably transformable by exogenously added DNA (13).

1.2 P_{II} protein

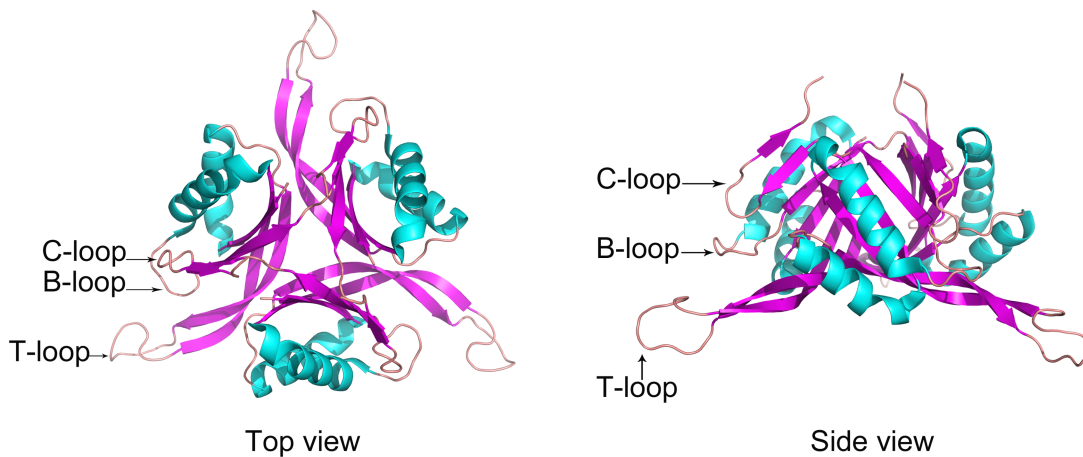


Figure 1.1. Crystal structure of *S. elongatus* P_{II} (PDB: 1QY7). T-loop, B-loop and C-loop are indicated.

P_{II} proteins (12-13 kDa) are small homotrimeric signal transduction proteins that regulate nitrogen metabolism in bacteria, archaea, and plants. The P_{II} family can be sub-divided into three groups including *glnB*, *glnK* and *nifH*. *glnB* and *glnK* homologues are commonly found, but *nifH* is only present in archaea and some strictly anaerobic bacteria (14). Their amino acid sequences are highly conserved. X-ray crystallographic analyses revealed that the structures of P_{II} family proteins in bacteria and plants are nearly identical (15). The trimeric P_{II} architecture resembles a flattened barrel with long and flexible T-loops extending outward, from the flat side (Figure 1.1). These T-loops can adopt multiple conformations and mediate the versatile protein-protein interactions (16). Each subunit further comprises two small loops (B- and C-loop) in the intersubunit clefts, facing each other from opposing subunits.

1.2.1 *E. coli* P_{II}

In 1969, the first P_{II} protein characterized was the *glnB* product from *E. coli*, this protein was identified in a protein fraction as the second peak eluting from a gel filtration column, therefore this protein was named P_{II} (17). *E. coli* has two P_{II} family proteins, P_{II} (product of *glnB*) and GlnK (product of *glnK*), which have distinct functions (18). The key signals of cellular nitrogen and carbon status in *E. coli* appear to be glutamine and 2-oxoglutarate (2-OG). P_{II} can integrate the antagonistic glutamine and 2-OG signals in *E. coli*. The adenylylation status (adenylylation or deadenylylation) of glutamine synthetase (GS) and the transcriptional regulation of nitrogen-regulated genes (Ntr) are directly/indirectly regulated by P_{II}. P_{II} is reversibly uridylylated at tyrosyl residue 51 (Y51) by the signal-transducing uridylyltransferase/uridylyl-removing enzyme (UTase/UR) in response to the glutamine concentration (18). The trimeric *E. coli* P_{II} shows three binding sites for ATP and 2-OG. ATP

and 2-OG interact with P_{II} synergistically (19, 20). The binding of ATP and 2-OG to P_{II} influences the binding between P_{II} with glutamine synthetase adenylyltransferase (ATase) and nitrogen regulator II (NRII) (21, 22). The binding between ADP and P_{II}-protein in *E. coli* has been demonstrated *in vitro* recently (23). The *E. coli glnK* gene is transcriptionally linked to the ammonium transport gene *amtB*. Actually, GlnK controls the activity of AmtB in response to the extracellular ammonium concentration (24, 25). 2-OG bound GlnK can not interact with AmtB. Then, AmtB transports ammonium (NH₄⁺) into the cytoplasm. On the contrary, in the absence of 2-OG, GlnK binds to AmtB and thereby blocks ammonia transport activity by its Arg-47 residue in the T-loop (26). Uridylylation of the nearby Y51 residue prevents the tight contact of the T-loop within the AmtB pore, explaining why only fully de-modified GlnK makes complex with AmtB (14). The four known receptors of P_{II} and GlnK in *E. coli* are NRII, UTase/UR, ATase and AmtB. Structure and function analysis of P_{II} indicated that the T-loop is responsible for interacting with these receptors (18).

1.2.2 Cyanobacteria and plant P_{II}

In the 1980's, ³²P labeling experiments were performed in *Synechococcus elongatus* PPC 6301 to study the effect of different light qualities on protein phosphorylation and thereby the phosphorylated protein P_{II} was discovered in this cyanobacteria (27). In the related strain *S. elongatus* PCC 7942, a *glnB* homologue gene was identified (28). The genome of many cyanobacteria show the absence of *glnK* (15). P_{II} shows highly similarity to *E. coli* GlnB (62-66% identity) (15). Sequencing of the tryptic digested phosphopeptide revealed Ser49 as the phosphorylation site in *S. elongatus* P_{II} homologue (29). The residues (including Ser49) located within or in the vicinity of the T-loop are highly conserved from the alignment of various cyanobacterial GlnB sequences (15). However, P_{II} proteins are not phosphorylated in plant *Arabidopsis thaliana* (*A. thaliana*) and some cyanobacterial strains such as *Nostoc punctiforme* ATCC 29133 and *Prochlorococcus marinus* PCC 9511 (18).

Taking *S. elongatus* as an example, P_{II} senses the nitrogen status only by measuring the cellular concentration of 2-OG. This character is different from the *E. coli* P_{II} system, which mainly integrates the nitrogen signal from the level of the glutamine pool through glutamine-regulated uridylylation. Cyanobacteria have an incomplete tricarboxylic acid (TCA) cycle because of the lack of 2-OG dehydrogenase. The only purpose of 2-OG in cyanobacteria is for glutamate synthesis. The cellular 2-OG level depends on the rate of 2-OG formation and its consumption mainly through the GS-GOGAT cycle (glutamine synthetase-glutamine:2-oxoglutarate amidotransferase). In *E. coli* (having a complete TCA cycle), 2-OG is a catabolic intermediate, and its pool size only partially dependent on nitrogen assimilation (14).

Trimeric *S. elongatus* P_{II} also has three binding sites for ATP and 2-OG and shows similar ATP and 2-OG binding properties as *E. coli* P_{II} although they have some obvious differences (30, 31). ATP and 2-OG can cooperatively assist each other binding to the subunit cleft of P_{II} (15). 2-OG binding to P_{II} requires ATP already bound at P_{II} binding sites. The first 2-OG molecule binds to P_{II} with high affinity (15, 20) and it exerts strong anti-cooperativity on the second and third 2-OG molecule binding to P_{II} (15). Recently, two co-crystals of P_{II} with Mg²⁺-ATP and 2-OG show that the binding site of 2-OG is close to the base of T-loop and the ATP-binding site (16, 32). Binding of Mg²⁺-ATP and 2-OG to P_{II} changes the T-loop conformation from an extended conformation to a compact one that influences the interaction between P_{II} and its partners. The structure analysis showed that the binding of 2-OG to one site affects the two neighbor sites asymmetrically (16).

In cyanobacteria, nitrogen can be stored by synthesizing arginine (33, 34). When cellular nitrogen is abundant, feedback inhibition of arginine synthesis must be relieved. The key enzymes of arginine biosynthesis are inhibited by arginine. The *S. elongatus* N-acetyl-L-glutamate kinase (NAGK) is the rate-limiting enzyme for arginine synthesis. It was proven to be a major P_{II} target by yeast two-hybrid and pull down studies (35, 36). Unphosphorylated P_{II} can make a stable complex with NAGK with a K_d of 3 nM (36). Phosphorylated P_{II} can not bind to NAGK. The P_{II}-NAGK complex is also strongly affected by the ATP/ADP ratio with increasing ADP weakening the interaction (36). The interaction between P_{II} and NAGK relieves the inhibitory effect of arginine on NAGK. The crystal structure analysis showed two polar P_{II} trimers sandwiching one ring-like hexameric NAGK (a trimer of dimers) (37). Plant P_{II} has a conserved chloroplast transit peptide that is cleaved upon entry into the chloroplast. Plant P_{II} can also make a complex with plant NAGK in the chloroplast. The co-crystal structure of *A. thaliana* P_{II} and NAGK show similar architecture as *S. elongatus* (37, 38).

Furthermore, P_{II} affects gene expression in cyanobacteria through binding to the transcriptional coactivator of NtcA, PipX (39, 40). NtcA belongs to the cAMP receptor protein (CRP) transcription factor family (41) and mediates global nitrogen control in cyanobacteria (41, 42). P_{II} is an abundant protein in cyanobacteria and can sequester PipX (39) when the 2-OG level is low. When nitrogen is abundant, the cellular 2-OG level will be low and the sequestration by P_{II} will decrease PipX availability for forming complex with NtcA (43). On the contrary, low nitrogen level results in high concentration of 2-OG, which will lead to the dissociation of the P_{II}-PipX complex (39, 43). Hence more PipX will be available for NtcA activation (43). ADP increases the affinity of P_{II} for PipX: consequently a low cellular energy status blocks NtcA-mediated gene expression by P_{II}-mediated PipX sequestration.

In *Synechocystis*, a transmembrane protein (PamA) was identified as P_{II} partner protein by using yeast two-hybrid screening system and pull down assay (44). The interaction between

PamA and P_{II} was inhibited by ATP and 2-OG, but the interaction was independent of the phosphorylation status of P_{II}.

The P_{II} knockout mutant of *A. thaliana* exhibits an alteration of carbon and nitrogen metabolites like starch and glutamine when grown under certain N-regimes. Therefore, it was suggested that P_{II} is involved in regulating C/N homeostasis in plants (45). P_{II}-affinity chromatography of soluble extracts from *A. thaliana* leaf chloroplasts and mass spectroscopy identified acetyl-CoA carboxylase (ACCase) to specifically bind to P_{II} protein (46). ACCase is a key enzyme initiating the synthesis of fatty acids in plastids. The *in vitro* enzymatic assay showed that *A. thaliana* P_{II} can inhibit ACCase activity but the inhibition could be relieved by adding 2-OG into the reaction buffer. These data provide an additional link between carbon and nitrogen regulation in plants (46).

All P_{II} partner proteins show different structures, but in all cases, the interaction with the targets seems to operate through the T-loop of P_{II}. The conformation of the T-loop is influenced by effector molecules ATP, ADP and 2-OG, which are related to energy, carbon and nitrogen metabolism. Therefore, P_{II} is a key regulatory scaffold protein in bacteria, archaea, and plants.

1.3 The phosphatase of P_{II}- a PP2C type phosphatase

In proteobacteria such as *E. coli*, the P_{II} protein (*glnB*, gene product) can be uridylylated or deuridylylated at a tyrosyl residue (Y51) by uridylyltransferase/uridylyl-removing enzyme (UTase/UR) in response to glutamine concentration. However, the homologous P_{II} protein (*glnB*) in *S. elongatus* was shown to be modified by phosphorylation of a serine residue (S49) in the T-loop (29). By using the crude extract of *S. elongatus* P_{II}-deficient mutant (MP2) to dephosphorylate phospho-P_{II} revealed a Mg²⁺-dependent phosphatase activity (47). This Mg²⁺-dependent phosphatase activity implied P_{II} phosphatase may be a kind of PP2C type phosphatase. The crude extract could also dephosphorylate other phospho-proteins such as phospho-histone, phospho-casein and phospho-kemptid. However, only the dephosphorylation of phospho-P_{II} was synergistically inhibited by ATP and 2-OG (47). The genome of *Synechocystis* reveals eight putative PP2C type phosphatase homologues. The eight PP2C phosphatases of *Synechocystis* were knocked out. One mutant, Δ sll1771, could not dephosphorylate P_{II}-P upon ammonium addition. The corresponding sll1771 phosphatase (termed PphA) was expressed as recombinant protein and purified from *E. coli* and it could dephosphorylate P_{II}-P *in vitro* in the presence of Mg²⁺ or Mn²⁺ (48). Therefore, this PphA was proven to be the specific phosphatase of the P_{II} protein in *Synechocystis*. Low-molecular weight phosphorylated molecules such as ATP are poor substrates of PphA (49). ATP and 2-OG can synergistically inhibit the activity of purified PphA against P_{II}-P. It is assumed that this is a consequence of the fact that ATP and 2-OG can change P_{II} T-loop conformation (49, 16).

1.4 PP2C type protein phosphatase

1.4.1 The classification of protein phosphatases

Reversible protein phosphorylation affects the structure and the function of proteins that are responsible for the regulation of nearly all biological processes in living organisms. Protein kinases and protein phosphatases regulate the state of protein phosphorylation. The former enzymes co-valently attach a phosphate group to an amino acid side chain, and the later enzymes hydrolysis the phosphate group from an amino acid side chain. The protein phosphatases can be subdivided into three main subclasses based upon their substrate specificity and protein structure: protein tyrosine phosphatase (50); protein serine/threonine phosphatase (50); and histidine phosphatase (51).

Protein serine/threonine phosphatase (PSP) comprise three major subfamilies: phosphoprotein phosphatases (PPP), including PP1, PP2A, and PP2B phosphatases; the aspartate-based phosphatases (ABP) represented by FCP/SCP (TFIIF-associating component of RNA polymerase II CTD phosphatase/small CTD phosphatase); and metal-dependent protein phosphatases (PPM), such as PP2C and pyruvate dehydrogenase phosphatase (50, 52). The human PPM member PP2C α (53) has been the defining representative of PPM family, therefore also referred as the PP2C family.

Studies of the crystal structures of the PPPs coupled with kinetic investigations of these enzymes have provided insights into the mechanisms of substrate specificity, catalysis and regulation (53). The catalytic mechanisms of ABP and PP2C were still not fully understood. One thing is clear that PPP, ABP and PP2C utilize three different reaction mechanisms to dephosphorylate substrates.

The crystal structures of PPP subfamily revealed two metal ions, identified as Mn²⁺, Fe²⁺ or Zn²⁺, located in the catalytic site (52). Coordinations of the two divalent cations are provided by invariable residues including three histidines, two aspartates, and one asparagine. These highly conserved residues suggest that PPP family phosphatases utilize one common mechanism of metal-catalyzed reaction to dephosphorylate substrates. The two metal ions share two water molecules and one of them was suggested to initiate a nucleophilic attack on the phosphorous atom (50, 52, 54, 55). Although PPPs have a conserved catalytic center, PPPs have a variety of regulatory domains which target the PPP catalytic center to specific subcellular compartment or modulate substrate specificity.

Members of the ABP family rely on the aspartates of the sequence motif DxDxT/V for phosphatase activity. An unusual feature is that ABP has only one primary substrate-the CTD of RNA polymerase II, which contains tandem repeats of amino acid sequence YSPTSPS (52). The catalytic mechanism of Fcp1/Scp1 might involve two sequential steps (56, 57). First, an

oxygen atom from the carboxylate group of the N-terminal aspartate in the DxTxT motif initiates a nucleophilic attack on the phosphorous atom of a phospho-serine, forming an acylphosphate intermediate. Second, a water nucleophile, likely activated by the second aspartate in the DxTxT motif, attacks the phosphorous atom of the acylphosphate intermediate, resulting in the release of an inorganic phosphate. Mg^{2+} in the catalytic center is thought to facilitate both steps of the reaction by neutralizing the negative charges of the phosphate group (52).

1.4.2 Functions of PP2C type protein phosphatase

PP2C type protein phosphatases are widely present in eukaryotes and prokaryotes and regulate many diverse signal transduction pathways. It seems the main function of PP2Cs is to regulate cellular stress responses in eukaryotes and prokaryotes.

In the human genome, there are 16 distinct PP2C genes (PP2C α , PP2C β , PP2C γ , PP2C δ (Wip1), PP2C ϵ , PP2C ζ , PP2C η , PP2C κ , CaMKP, CaMKP-N, ILKAP, PHLPP, NERRP-2C, TA-PP2C, PDP1 and PDP2) that give rise to at least 22 different isoforms (58). Homologs displaying a high degree of sequence similarity to human PP2Cs have also been identified in mice, rats, and cows. Human PP2Cs participate in many biological processes including regulation of mitogen-activated protein kinase (MAPK) cascades (p38 or Jun N-terminal protein kinase [JNK]), cell cycle progression, ubiquitination and degradation of proteins, and mechanisms for cell death and survival (59).

In plants, there are even more PP2C genes. *A. thaliana* has 82 PP2C genes (60). 76 *A. thaliana* PP2C genes could be classified into ten groups (Group A-J) based on the sequence similarity, except for 6 genes that could not be clustered (60). A significant amount of research is related to Group A PP2Cs. Group A contains some identified genes such as *ABI1*, *ABI2*, *HAB1*, and *HAB2*. These PP2Cs have been shown to act as negative regulators in the abscisic acid (ABA) signaling pathway, which takes part in the response to different environmental stresses such as drought, cold and salinity (59, 61). Recently, atomic studies showed PYR/PYL/RCARs (pyrabactin resistance/pyrabactin resistance-like/regulatory component of ABA receptor), which are the ABA receptors, could interact with the Group A PP2Cs after ABA has bound to the central hydrophobic cavity of PYR/PYL/RCARs (61, 62, 63). In the PYR/PYL/RCARs-bound state, the activities of PP2Cs were inhibited (61). This leads to the activation of the SnRK2 (subfamily 2 of SNF1-related kinases) that phosphorylates downstream effectors, such as the basic leucine-zipper transcription factors called ABFs/AREBs, thus switching on stress response programs (61).

In *Saccharomyces cerevisiae*, 7 PP2C genes (*PTC1* to 7) have been identified (59). The PTCs have been shown to be involved consistently in regulating cell growth and cellular stress

signaling. Ptc1, Ptc2 and Ptc3 were associated with the negative regulation of the HOG (high-osmolarity glycerol) signaling pathway, inducible after osmotic stress, by dephosphorylating and inactivating the Hog1 MAPK (59). Ptc1 was also proven to regulate the signal transduction pathways of the cell wall integrity, the cation homeostasis and the inheritance of cellular organelles (59). Ptc2 regulates negatively the unfolded-protein response in the endoplasmic reticulum and preserves cell viability in the face of agents that compromise the integrity of DNA. Ptc2 and Ptc3 could regulate the cell cycle through desphosphorylating Cdc28 at Thr-169, a residue essential for its activity as a cyclin-dependent kinase. The overexpression of Ptc4 reduces the activity of Hog1 and suppresses the lethality of a *cnb1 stf2* double mutant. The functions of Ptc5, Ptc6 and Ptc7 have not been fully revealed.

A prokaryotic genomic survey revealed a large number of PP2C genes that may exist in putative transmembrane and soluble forms. Putative transmembrane phosphatases are almost exclusively found in actinobacteria and cyanobacteria, while soluble phosphatases appear to be distributed more equally over all bacterial genomes (64, 65). The genomes of *Streptomyces coelicolor* A3(2) and *Streptomyces avermitilis* contain 49 and 48 PP2C genes, respectively (66). The *Bacillus subtilis* genome contains five PP2C genes (67). In contrast, no PP2C gene has been identified in the genomes of *Escherichia coli* or *Salmonella enterica* serovar typhimurium strain LT2.

The SpoIIE PP2C controls the sporulation of *B. subtilis* by dephosphorylating an antitranscription factor SpoIIAA, reversing the actions of the SpoIIAB protein kinase in a process that is governed by the ADP/ATP ration (68). In *B. subtilis*, the energy stress response is controlled by two PP2Cs, RsbP and RsbU, which regulate the phosphorylation status of the RsbV anti-anti-sigma factor (69). The *yloO* gene was identified as a PP2C gene (the overexpressed protein termed PrpC) in *B. subtilis*. A membrane-linked protein kinase (PrkC) gene is located downstream of *yloO* gene. The biochemical assays showed that PrpC could dephosphorylate PrkC *in vitro* (70). In *Bacillus anthracis*, a single phosphatase-kinase gene pair encoding one PP2C type phosphatase (BA-Stp1) and one serine/threonine kinase (BA-Stk1) was identified. BA-Stp1 could dephosphorylate phospho-BA-Stk1 *in vitro*. This phosphatase-kinase pair contributes to the virulence of *B. anthracis*, as mutants lacking BA-Stp1 and BA-Stk1 exhibited decreased lethality in a mouse model of pulmonary anthrax (71). A *Pph1* (PP2C gene) null mutant of *Myxococcus xanthus* showed defects during late vegetative growth, swarming and glycerol spore formation. Under starvation-induced developmental conditions, the mutant showed reduced aggregation and failed to form fruiting bodies with viable spores. The yeast two-hybrid system discovered that there is a strong interaction between Pph1 and the *M. xanthus* protein kinase Pkn5, a negative effector of development (72). The Stp1 PP2C of *Streptococcus agalactiae* has been shown to dephosphorylate an inorganic pyrophosphatase.

The *ΔStp1* mutant exhibited pleiotropic effects on growth, virulence, and cell segregation of *S. agalactiae*. (73). In *Mycobacterium tuberculosis*, the PstP PP2C plays a role in regulating cell division by dephosphorylating the Serine/Threonine kinases PknA and PknB (74, 75). In the cyanobacterium *Anabaena* sp. PCC 7120, PrpJ, a PP2C-type protein phosphatase located on the plasma membrane, is involved in heterocyst maturation (76).

1.4.3 The catalytic mechanism of PP2Cs revealed by the atomic and biochemical studies

Initially, PP2C was isolated in conjunction with PP2A from rat liver (77), it was placed alongside the other PPP family members. However, the sequence alignment with PP1, PP2A and PP2B showed no homology to that of PP2C, suggesting that PP2C was unrelated to the PPP family (77). Recently, several PP2Cs were crystallized. The crystal structures of PP2Cs showed different architecture than PPP implying that the two phosphatase families use different catalytic mechanism to dephosphorylate substrates.

1.4.3.1 Human PP2C α

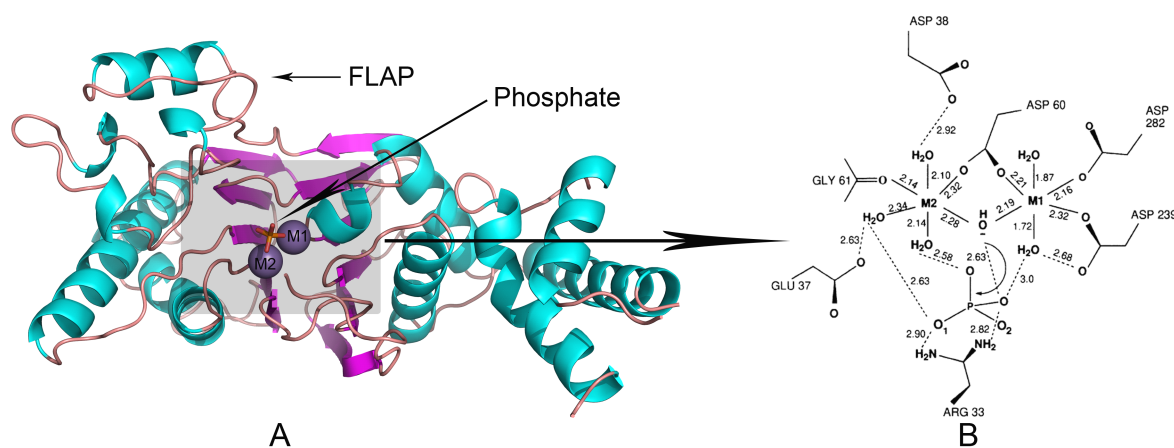


Figure 1.2. A. The crystal structure of human PP2C α (PDB: 1A6Q). The shadowed area is the catalytic center of human PP2C α . Two Mn²⁺ ions (M1 and M2) are labeled by purple. A phosphate ion was crystallized in the catalytic center of human PP2C α . The phosphate is labeled by orange and the oxygen atoms are labeled by red. Close to the catalytic center, there is a flexible loop termed FLAP. B. This figure was drawn based on the structure of the shadowed area in picture A (cited from reference 53). A reaction mechanism catalysed by human PP2C α was proposed. The water coordinated by M1 and M2 could act as a nucleophile to attack the phosphorus atom in an S_N2 mechanism.

The crystal structure of human PP2C α was the first PP2C structure (Figure 1.2. A). Although the crystallization procedures for human PP2C α had some defects that made the structure of human PP2C α abnormal, this structure still facilitated the subsequent PP2C research. In the crystal structure of human PP2C α (53), four aspartate residues and one glutamate residue directly or indirectly (by bridging water molecules) coordinate two manganese (Mn²⁺) ions (M1 and M2) in the catalytic center (Figure 1.2. B). These residues are situated at the top of a central β -sandwich. The binuclear metal center indirectly coordinates a phosphate ion by bridging two water molecules. (Actually, the two oxygen atoms of this phosphate ions could directly interact with M1 and M2. This point of view was proved by the crystal structure of MspP (PP2C) with a phosphate ion. The human PP2C α crystal was grown under a pH 5.0 condition. Under this condition, the phosphate can not properly interact with the metal ions in the catalytic center). Further phosphate-enzyme interactions are provided by the guanidinium group of Arg-33, which forms bifurcated hydrogen bonds with two phosphate oxygen atoms. The presence of M1, M2 and Arg-33 creates a local positive electrostatic potential on human PP2C α for recognizing the phosphate group of the substrate. One water molecule bridged by M1 and M2 was supposed to act as a nucleophile to attack the phosphorus atom in an S_N2 mechanism (Figure 1.2. B).

The two metal ions were proven to be not essential for stabilizing human PP2C α fold. Human PP2C α crystals were incubated for 12 h with 2 mM EDTA and the electron density maps calculated using data collected from these PP2C crystals indicated dissociation of the metal ions and accompanying water molecules and phosphate ion from the catalytic center. Refinement of the metal-free human PP2C α structure revealed that it was identical to the metal-bound enzyme form with a root mean square deviation of 0.4 Å between all atoms. The guanidinium group of Arg-33 shifts by 1 Å in response to phosphate dissociation (53).

Upon the crystal structure of human PP2C α , site-directed mutagenesis of this PP2C phosphatase was performed and the enzyme kinetic parameters of the generated variants were obtained from the assays with *p*NPP as substrate (78). The aspartate residues (Asp-38, Asp-60, Asp-239 and Asp-282) which coordinate M1 and M2 in the catalytic center of human PP2C α were changed to asparagine. The variants (D60N and D239N) showed ≥ 1000 -fold decrease in K_{cat} and ≥ 30 -fold increase in K_m value for Mn²⁺. This result proved that the dinuclear metal center is critically important for the activity of human PP2C α and also support the point of view that the water coordinated by M1-M2 attacks the phosphorus atom in an S_N2 mechanism. D282N showed a 100-fold decrease in K_{cat} , but no significant effect on K_m value for metal and *p*NPP. D38N displayed little alterations on K_{cat} and K_m values for substrate or Mn²⁺. His-62 was supposed to be a general acid during the cleavage of the P-O bond by using Brønsted analyses. Brønsted analyses is useful in examining general-acid catalysis in related phosphatases and the

enzymes (78). (But this conclusion must be taken with caution. In the crystal structure of human PP2C α , His-62 was located close to the catalytic center but the side chain was positioned too far away to act as a general acid and, instead, hydrogen bonds with Asp-199. It is difficult to propose a role for many of the residues that reside near the active site, because at the crystal growing condition of pH 5.0, the environment surrounding the active site may not represent the active form of the enzyme (77).)

The variant R33A showed a 8-fold higher K_m than wild-type phosphatase suggesting that this arginine residue is important for binding p NPP. In the enzymatic assays of human PP2C α towards p NPP, the presteady-state studies of human PP2C α revealed an exponential product burst at pH 8.5, followed by a slower linear rate. The amplitude of the observed burst was proportional to human PP2C α concentration. The burst phase yielded first order rate constants between 20-200 s $^{-1}$, while the linear phase corresponded to the steady-state initial velocity. This initial "burst" means the reaction velocity of human PP2C α is surprisingly high when p NPP was added into the reaction solution. In the presteady-state, human PP2C α only releases the leaving group but not the phosphate ion from the catalytic center. The phosphate ion in the catalytic center of human PP2C α would impede the new round dephosphorylation reaction. After the initial boost, the reaction quickly entered into a steady-state in which the reaction velocity tend to be constant but slower than the reaction velocity in the presteady-state. This character of human PP2C α towards p NPP means that the phosphate release is the rate-limiting step of the dephosphorylation reaction. (77, 78).

1.4.3.2 PstP

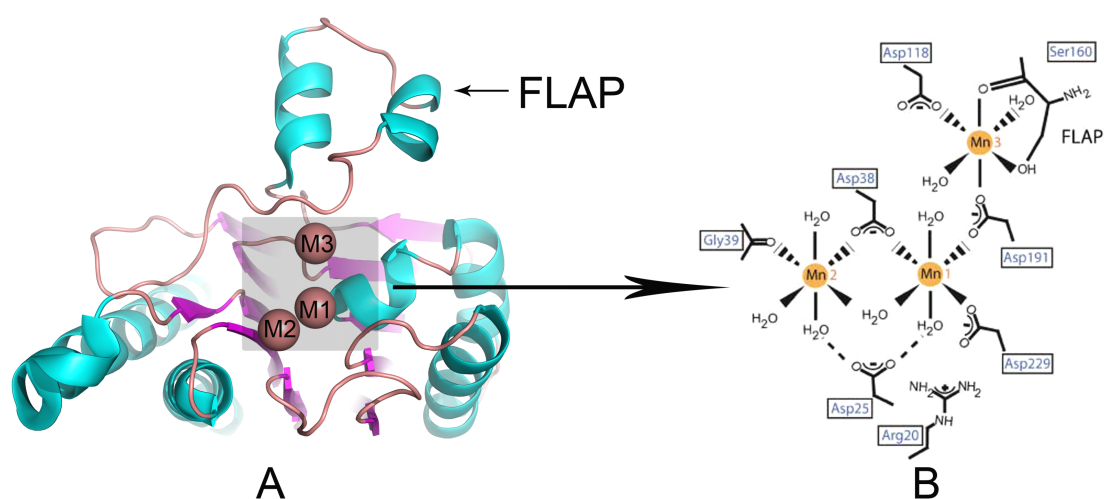


Figure 1.3. A. The crystal structure of PstP (PDB: 1TX0). The shadow area is the catalytic center of PstP. Three Mn²⁺ (M1, M2, and M3) ions are labeled by purple. B. This figure was

drawn based on the structure of the shadow area of figure A (cited from reference 79). There is a third metal ion (M3) in the catalytic center of PstP.

The second crystallized PP2C was PstP from *Mycobacterium tuberculosis* (79). Although PstP shares the fold and dinuclear center of human PP2C α , the PstP catalytic center binds a third Mn²⁺ (M3) which is close to the FLAP subdomain. Two highly conserved aspartates residues (Asp-118 and Asp-191) and one serine residue (Ser-160) directly coordinate the third Mn²⁺ (Figure 1.3. B). Mutations in Asp-118 and Ser-160 increased the K_m value of PstP towards *p*NPP, but the mutations had little effect on K_{cat} towards *p*NPP. Based on these enzymatic assay results, Wehenkel *et al.* (65) concluded that M3 is not essential for PP2C to dephosphorylate substrate. However, the author used a pH 7.5 buffer to assay the activity of wild type PstP and the variants. PP2Cs have more activity towards *p*NPP in basic condition than in the neutral condition. Since PstP and the variants were assayed under pH 7.5 condition that all of them had only residual activity towards *p*NPP, and, no correct conclusion can be drawn.

1.4.3.3 MspP

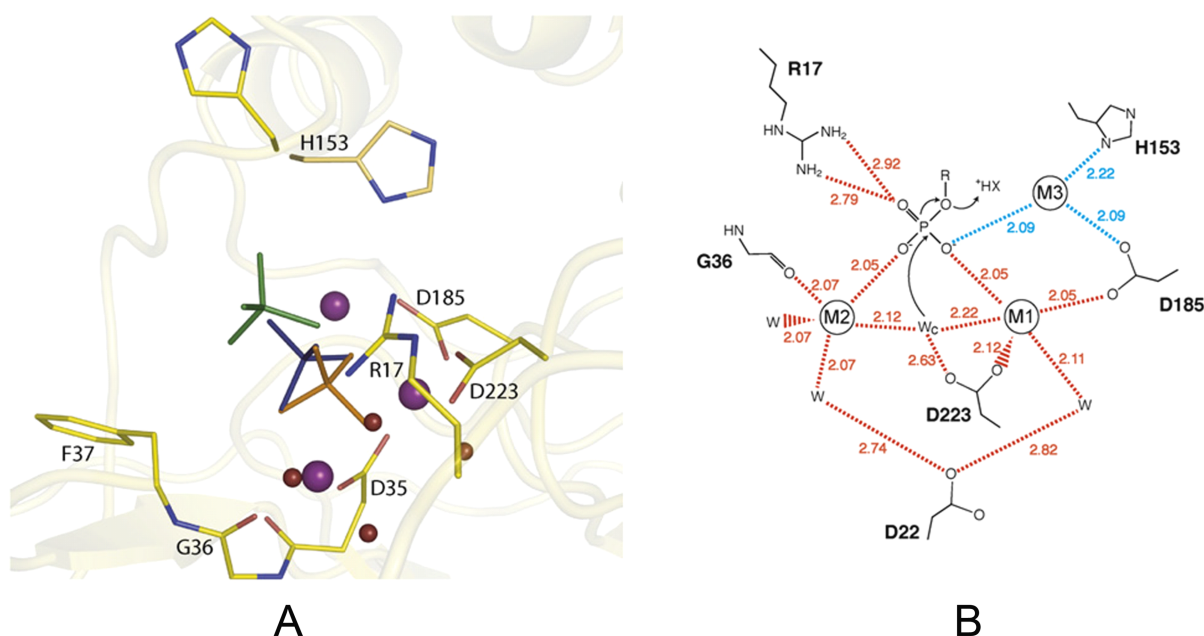


Figure 1.4. A. and B. are from reference 64. A. The catalytic center of MspP with sulphate (green), phosphate (orange) and cacodylate (blue). The metal ions are labeled by purple. This figure was drawn from the overlay of the catalytic centers of three MspP crystal structures (PDB: 2JFS, 2JFR, and 2JFT). B. A new PP2C catalytic mechanism was proposed based on the crystal structures of MspP in complex with three different molecules. The proton donor for leaving group (R) was still not found.

A PP2C type protein phosphatase (termed MspP) from *Mycobacterium smegmatis* was crystallized (64). The architecture of the enzyme closely resemble those observed for PstP and human PP2C α . The crystal structure also showed a trinuclear metal ions center. M3 is octahedrally coordinated and occupies the equivalent position as in PstP, except that the imidazole ring of His-153 replaces the equivalent residue Ser-160 in PstP (Figure 1.4. B). The protein structure has been determined in complex with a cacodylate ion, a sulfate ion, and an inorganic phosphate in different forms.

In the crystal structure of MspP with the phosphate ion, two phosphate oxygens directly bind respectively to M1 and M2 (in human PP2C α structure, M1 and M2 indirectly coordinate the phosphate ion by bridging two water molecules), a third oxygen atom pointing towards the bulk solvent, forms a hydrogen bond with the Arg-17 guanidinium group. The fourth phosphate oxygen bridges the two metal ions and occupies the position of the water nucleophile, suggesting that the structure of phosphate-bound MspP represents the enzyme-product complex (Figure 1.4. A, B). This crystal structure is more reasonable than human PP2C α structure, since the MspP crystal was obtained under a neutral condition.

In the crystal structure of MspP with cacodylate, two oxygens of cacodylate bidentately bind to M1 and M2. This complex was suggested to mimic the binding of enzyme to substrate, since the catalytic water bridging M1 and M2 remains close enough for nucleophilic attack. A water molecule that is hydrogen bonded to Arg-17 occupies the site of the fourth phosphate oxygen, likely because this position is energetically unfavorable for the cacodylate methyl group.

The third crystal form of MspP showed a sulfate ion far away from metal center makes hydrogen bond with Arg-17. The sulfate position was suggested to correspond to that of the incoming phospho-protein substrate or the outgoing inorganic phosphate.

1.4.3.4 *MtPstP* and MspP crystal structure

Recently, new *MtPstP*/PstP (from *Mycobacterium tuberculosis*) and MspP (from *Mycobacterium smegmatis*) crystal structures were reported (65). *MtPstP*/PstP was crystallized in two different forms crystal. The structure of *MtPstP*/PstP in monoclinic crystal form showed a trinuclear metal ion center and the structure of *MtPstP*/PstP in trigonal crystal form only showed a dinuclear metal ion center, M3 was lost from trigonal crystal form. The trigonal crystal form *MtPstP*/PstP was shown to still have activity towards 10 mM *p*NPP in a pH 7.5 reaction buffer with 10 mM MnCl₂. Therefore Wehenkel *et al.* concluded that M3 is not essential for *MtPstP*/PstP to dephosphorylate *p*NPP (65). However, Wehenkel *et al.* did not considered the possibility that Mn²⁺ could be soaked into the catalytic center of *MtPstP*/PstP

and occupy the M3 position. Thus, it could not rule out that M3 is essential for PP2C to dephosphorylate substrate.

M3 is very close to the FLAP subdomain. M3 and the FLAP subdomain could influence the position of each other. The reason why M3 was lost from the trigonal crystal form *Mp*PstP/PstP is probably because the conformation of FLAP was affected by two neighboring *Mp*PstP/PstP molecules in the trigonal crystal form that might influence Mn²⁺ occupying the M3 position.

The structures of MspP at neutral or slightly alkaline pH were determined and shown to contain three or more metal ions in the catalytic center. The MspP crystals were grown at pH 7.5 and then lowered gradually to pH 5.5 by stepwise soaking. MspP crystals soaked in different pH were resolved. The acidic pH was proven to induce significant changes in MspP metal binding properties. The structures of MspP at pH 5.5 only showed M1 and M2 in the catalytic center. M3 was lost from MspP catalytic core upon decreasing the pH to 5.5 even 150 mM MgCl₂ was maintained during soaking. As we know, the crystal structure of human PP2C α with a dinuclear metal center was obtained at pH 5.0. Therefore, there is probably an additional metal ion binding site in the human PP2C α catalytic domain at neutral or alkaline pH (65).

1.4.3.5 SaSTP

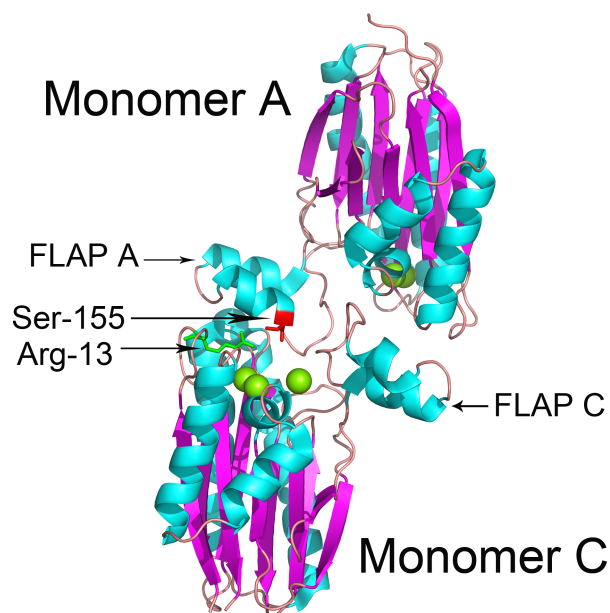


Figure 1.5. Two STP monomers were shown to make packing contacts in the crystal structure of STP (PDB: 2PK0). The FLAP A of monomer A interacts with the catalytic center of monomer C. Ser-155 of monomer A makes hydrogen bond with Arg-13 of monomer C.

The crystal structure of SaSTP (PP2C) from *Streptococcus agalactinae* was resolved (80). The structure consists four monomers (A, B, C and D) The FLAP subdomain of monomer A interacted with catalytic center of monomer C (Figure 1.5.). Rantanen *et al.* suggested that these two monomers with packing interactions might mimic a enzyme-product complex. The Arg-13 of monomer C was shown to make hydrogen bond with a FLAP residue Ser-155 of monomer A. Since the FLAP of monomer A interacted with monomer C, the monomer A FLAP adopted a conformation different from the normal conformation that led to the third metal ion can not occupy M3 position.

In human PP2C α and MspP studies, the water coordinated by M1 and M2 was proven to act as a nucleophile to attack the phosphorus atom in an S_N2 mechanism. But the proton donor for the leaving group was still not found in SaSTP studies. The phosphate ion from the active site of human PP2C α was superpositioned into the catalytic center of SaSTP. The distance between the phosphate and a water molecule coordinated by M3 is only 4 Å. Rantanen *et al.* suggested that this water molecule (termed W_H) could be the proton donor for the leaving group, since the pK_a value should be significantly less than 14 (80).

1.4.3.6 tPphA

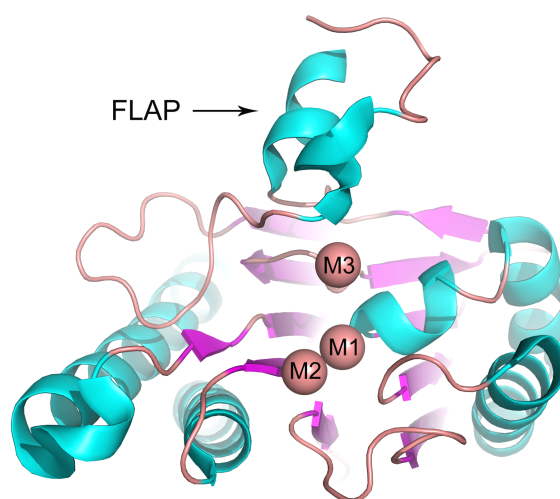


Figure 1.6. The crystal structure of tPphA (PDB:2J86, monomer B). Three divalent cations (M1, M2 and M3) were found in the catalytic center of tPphA.

The crystal structure of tPphA (a PP2C member from *Thermosynechococcus elongatus* (*T. elongatus*)) was resolved (Figure 1.6). tPphA is the homologue protein of PphA and they show high similarity in primary sequence. tPphA is able to dephosphorylate P_{II}-P in the presence of either Mn²⁺ or Mg²⁺, similar to the data reported for PphA. This reaction responds to the addition of the effector molecules ATP, ADP and 2-OG in a manner very similar to that for

PphA (48). P_{II} -P dephosphorylation is partially inhibited by ADP and ATP alone. The inhibition is strongly enhanced by the presence of 2-OG, whereas GTP has no effect on P_{II} -P phosphorylation. Together, these assays revealed a high degree of functional similarity between tPphA and PphA (81).

Native crystals of tPphA were obtained under two different conditions in two different space groups: $C222_1$ with one monomer in the asymmetric unit and $P4_12_12$ with two monomers in the asymmetric unit. All three monomers of tPphA showed highly conserved catalytic center and overall fold as other PP2C type phosphatases. Five conserved aspartates coordinate three divalent metal ions (M1, M2 and M3) in the catalytic center. In tPphA, M3 is coordinated by Asp-119 and Asp-193. The FLAP subdomain of tPphA could adopt different conformations in three different crystal forms.

M3 is always in the catalytic site of tPphA and sometimes in other bacterial PP2Cs (PstP, MspP, and SaSTP) that suggests M3 must play a role in the catalysis process. In the catalytic center of all bacterial PP2Cs whose structure was resolved so far, one water molecule coordinated by M3 close to the catalytic center of PP2C is very suitable for supplying a proton for leaving group, since its pK_a value is significantly lower than 14.

In PP2C phosphatases, the primary sequence of PP2C FLAP subdomains showed high variability. The overlay of all PP2C structures resolved so far shows that the FLAP subdomain can adopt various conformations (Figure 1.7). Some bacterial PP2Cs are devoid of a regulatory domain, but they still can specifically recognize the substrates. It implies this special FLAP subdomain might help PP2Cs recognize substrates.

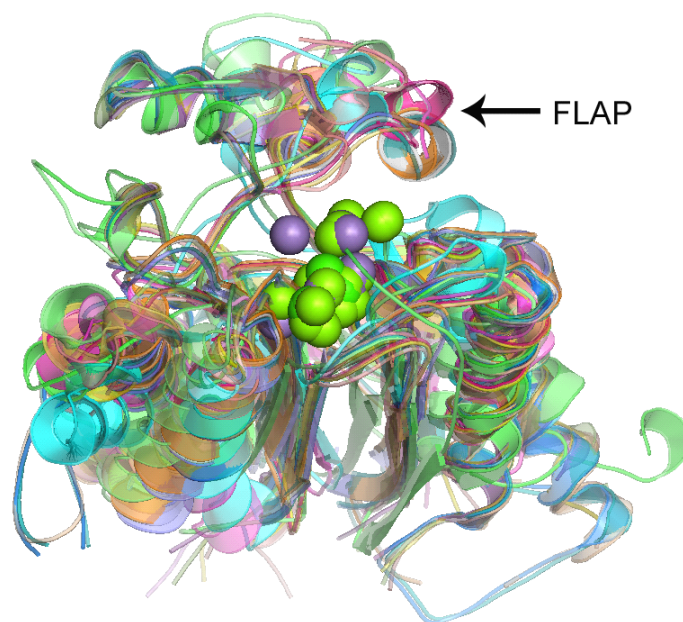


Figure 1.7. Overlay of all PP2Cs structure resolved so far. FLAP subdomains show different conformation. (Green: human PP2C α , PDB:1A6Q; Cyan: PstP, PDB: 1TX0; Magenta: MtPstP, PDB: 2CM1; Yellow: tPphA (C222₁), PDB: 2J82; Salmon: tPphA (P4₁2₁2), PDB: 2J86; White: MspP, PDB: 2JFR; Slate, MspP, PDB: 2JFS; Orange: MspP, PDB: 2JFT; Lime: STP, PDB: 2PK0; Deep teal: MspP, PDB: 2V06; Hotpink: tPphA variant D119A, PDB: 2XZV; Paleyellow: tPphA variant D193A, PDB: 2Y09; Violetpurple: ABI1, PDB: 3JRQ; Marine: HAB1, PDB: 3KB3; Yelloworange: ABI1, PDB: 3KDJ; Smudge: ABI1, PDB: 3NMN; Teal: HAB1, PDB: 3NMT; Darksalmon: ABI2, PDB: 3NMV; wheat: HAB1, PDB: 3QN1)

Close to the catalytic center of PP2C, there is also a conserved arginine residue. The highly conserved arginine residue (in tPphA is Arg-13) and M1-M2 constitute a positive pocket at the active site of tPphA which, may help tPphA recognize the phosphate of substrate. Although the site-directed mutagenesis and enzymatic assay studies of human PP2C α already revealed M1 and M2 are critical important for PP2C activity, if M1 and M2 play roles in binding proteinous substrates were not known. Thus, pull down assay should be applied to study the interaction between PP2C and proteinous substrates. However, since PP2Cs dephosphorylate the substrates very rapidly, it is impossible to directly pull down their proteinous substrates. Therefore, new methods should be designed to test the interaction between PP2Cs and the proteinous substrates. In addition, the variant (R33A) of human PP2C α showed a 8-fold higher K_m than wild-type phosphatase suggesting that this arginine residue is important for binding ρ NPP. But if this arginine residues is important for binding or turn-over other kinds of substrates was unknown.

1.5 Aim of this dissertation

The catalytic mechanism of PP2C was still not fully understood. The questions about why there is a third metal (M3) in the catalytic center and who is the proton donor for the leaving group were not answered. Taking tPphA as an example, the aspartate residues coordinating the three metal ions were mutated by site-directed mutagenesis. The enzyme kinetic parameters of these tPphA variants were obtained as to explain the function of tPphA metal center. The crystal structures of tPphA variants D119A and D193A were resolved in this dissertation to gain a clear idea of the function of metal three (M3).

Structural determinant for specific substrate recognition were not known for PP2C phosphatase. In the catalytic center of *Mp*StP, the metal ions make ionic bonds with the oxygen atoms of a phosphate. However, whether the metal center is important for PP2Cs binding proteinous substrates was not clear. In addition, tPphA is devoid of a regulatory domain and only has a flexible loop (termed FLAP subdomain) close to the catalytic center. This FLAP subdomain may help tPphA recognize P_{II}-P. In order to know if FLAP subdomain and the metal center help tPphA recognize P_{II}-P, a binding assay combined with chemical cross-linking and pull down was designed to test the binding between tPphA variants and P_{II} protein.

A highly conserved arginine residue (in tPphA is Arg-13) can make hydrogen bond with one oxygen atom of the phosphate, which was co-crystallized in the catalytic center of human PP2C α and MspP. The function of this arginine residue was proven to be important for binding substrate. However, the role of this residue during catalytic process was not checked. Thus, various site-directed mutations of this conserved arginine residue and investigation the activity of the variants by different substrates could give more insights into the role of this residue.

Chapter 2. Methods and materials

2.1 DNA Materials

2.1.1 Bacterium

Table 2.1

Strain	Gene type	Reference
<i>E.coli</i> 5k	<i>hsR mcrA serB thr lacy rpsL thi fhuA supE leu</i>	Dietrich Welz et al., 1998
<i>E.coli</i> BL21 (DE3)	<i>F+ ompT hsdS Ade3</i>	Studier., 1986
<i>E.coli</i> XL-1 Blue	<i>recA1 endA1 gyrA96 thi-1 hsdR17 supE44 relA1 lac</i> [F' proAB lacI ^q ZΔ M15 Tn10 (Tet ^r)]	Jerpseth et al., 1997
<i>E.coli</i> XL10-GOLD	<i>recA1 endA1 gyrA96 thi-1 hsdR17 supE44 relA1 lac</i> [F' proAB lacI ^q ZΔM15 Tn10 (Tet ^r)]	Jerpseth et al., 1997
<i>E.coli</i> JM109 High Efficiency Competent Cells	<i>endA1 recA1 gyrA96 thi hsdR17</i> (rk- , mk+) <i>relA1 supE44 Δ(lac-proAB)</i> [F' <i>traD36 proAB laqIqZΔM15</i>].	Promega
<i>E.coli</i> RB 9060	Δ <i>glyA hmp glnB Tc^r</i>	Dr. Alex Ninfa (University of Michigan)
<i>Synechococcus elongatus</i> PPC 7942	Wild type	Kuhlemeier et al., 1983,
<i>Synechococcus elongatus</i> PPC 7942 Δ <i>Pph1</i> mutant	Resistance to kanamycin	This mutant was generated in our group
<i>Synechocystis</i> sp. PCC 6803	Wild type	Sergey et al., 1982
<i>Synechocystis</i> sp. PCC 6803 mutant Δ <i>sll0602</i>	Resistance to kanamycin	Angelika et al., 2001
<i>Synechocystis</i> sp. PCC 6803 mutant Δ <i>sll1033</i>	Resistance to kanamycin	Angelika et al., 2001
<i>Synechocystis</i> sp. PCC 6803 mutant Δ <i>sll1770</i>	Resistance to kanamycin	Angelika et al., 2001
<i>Synechocystis</i> sp. PCC 6803 mutant Δ <i>sll1771</i>	Resistance to kanamycin	Angelika et al., 2001

2.1.2 Plasmids

Table 2.2

Plasmid	Gene type	Reference
pET15b+tPphA and its variants	pET15b <i>amp^R+tPphA</i> from <i>Thermosynechococcus elongatus</i>	Constructed in this thesis
No-histag pET15b+tPphA and two variants (D119A, D193A)	pET15b <i>amp^R+tPphA</i> from <i>Thermosynechococcus elongatus</i>	Constructed in this thesis
pET32a+tPphA	pET32a <i>amp^R+tPphA</i> from <i>Thermosynechococcus elongatus</i>	Christine et al., 2007
pASK-IBA3-P _{II} and its variants	<i>amp^R+P_{II}</i> from <i>Synechococcus elongatus</i> PPC 7942	Heinrich et al., 2004
pET15b+Human PP2C and its variant (D146A)	pET15b <i>amp^R+human PP2C</i>	Constructed in this thesis
pET15b+tPphAcore+human PP2C FLAP	pET15b <i>amp^R+hybrid protein</i>	Constructed in this thesis
pET15b+human PP2C core+tPphA FLAP	pET15b <i>amp^R+hybrid protein</i>	Constructed in this thesis
pGME-T	<i>amp^R</i>	Promega

2.1.3 DNA manipulation enzymes and kits

Table 2.3

Enzyme	Company
<i>Taq</i> DNA polymerase	Fermentas
<i>Nde</i> I	Fermentas
<i>Xho</i> I	Fermentas
<i>Bam</i> HI	Fermentas
T4 DNA ligase	Fermentas
<i>Dpn</i> I	STRATAGENE
<i>Pfu</i> Turbo DNA polymerase	STRATAGENE
E.Z.N.A. Plasmid Miniprep Kit II	PEQLAB Biotechnology GmbH
NUCLEOBOND applications AX 100	MACHEREY-NAGEL
NucleoSpin Extract II	MACHEREY-NAGEL
QuickChange XL Site-Directed Mutagenesis	STRATAGENE

2.1.4 Medium and buffers

LB (Luria-Bertani) medium:	NaCl	1.0%
	Tryptone	1.0%
	Yeast extract	0.5%
LB medium with ampicillin:	LB medium	
	Ampicillin	100 µg/ml
LB plates with ampicillin:	LB medium	
	Agar	1.5%
	Ampicillin	100 µg/ml
SOC Medium:	NaCl	0.05%
	Tryptone	2.0%
	Yeast extract	0.5%
	MgCl ₂ / MgSO ₄	20 mM
	Glucose	20 mM
NZY ⁺ broth:	NaCl	0.5%
	Yeast extract	0.5%
	Casmino acids	1.0%
	MgCl ₂ / MgSO ₄	12.5 mM
	Glucose	20 mM
DNA electrophoresis loading buffer:	Tris/HCl, pH 7.4	100 mM
(5×)	EDTA	50mM
	Ficoll	15%(w/v)
	SDS	0.5%(w/v)
	Bromphenol blue	0.05%(w/v)
	Xylencyanol	0.05%(w/v)
TAE buffer:	Tris	2M
(50×)	Acetic Acid	57.1ml/L
	EDTA	50mM
TE buffer:	Tris	10mM
	EDTA	1.2mM

2.2 DNA Methods

2.2.1 PCR

PCRs were accomplished by the standard protocol everywhere.

2.2.2 DNA agar electrophoresis

PCR products, restricted DNA fragment, and plasmids were analyzed by 0.8%-1.5% agarose gel electrophoresis. The samples were mixed with 5×DNA loading buffer. Gel electrophoresis was performed at 80V-100V. A gel tank with 1× TAE buffer was used to run the gel. DNA was visualized by using a photo imager after ethidium bromide staining. To determine their size, DNA molecules were compared to DNA length standard ladders.

2.2.3 Subclone tPphA gene into pET15b

The PCR fragment containing tPphA gene (tlr2243) amplified from pET32a+tPphA (54) was cloned into Tvector pGME-T (Promega). After restriction enzymes (*NdeI*, *XhoI*) cutting, tPphA gene was cloned into pET15b.

2.2.4 Site-directed mutation of pET15b+tPphA

The experiment procedure followed the instruction manual of QuickChange XL Site-Directed Mutagenesis from *STRATAGENE*.

2.3 Protein Materials

2.3.1 Chemicals and materials

Lumi-light Western blotting Substrate	Pierce chemical company
Pure Nitrocellulose Blotting Membrane	Pall Corporation
L-methionine sulphoximine	Sigma
HIS-Select Cartridge	Sigma
Econo-Pac heparin cartridge	Bio-Rad
Econo-Pac High Q cartridge	BIO-RAD
HiLoad™ 26/60-Superdex™ 200pg	GE Healthcare
Superdex 200 10/300 GL column	Amersham Pharmacia
p-nitrophenyl phosphate	Sigma
Glutardialdehyde	Carl Roth
Ni-NTA magnetic agarose beads	Qiagen
Chelex 100	Sigma
Phosphopeptides	Pineda
PVDF membrane	Pall Corporation
ATP	Sigma

ADP	Sigma
AMP	Sigma
2-OG	Sigma
Protein kinase A (PKA)	BIAFFIN GMBH
Protein kinase C (PKC)	BIAFFIN GMBH
Casein kinase II (CK II)	BIAFFIN GMBH

2.3.2 Buffers for protein manipulations

<i>E.coli</i> BL 21 (DE3)+tPphA lysis buffer:	Tris-HCl, pH 7.8	20 mM
	KCl	75 mM
	NaCl	500 mM
	EDTA, pH 7.8	0.5 mM
	MgCl ₂	5 mM
	PMSF	0.2 mM
Dialyze buffer for tPphA:	Hepes, pH 7.4	40mM
	KCl	150mM
	MgCl ₂	4 mM
	EDTA	1 mM
	DTT	2 mM
	NaCl	1 M
	Add equal volume of Glycerol	
<i>Synechococcus</i> PCC 7942 lysis buffer, pH 7.0, for P _{II} -P purification:	K ₂ HPO ₄	20 mM
	KH ₂ PO ₄	20 mM
	EDTA	4 mM
SDS-PAGE loading buffer: (4×)	Glycerol	2 ml
	Tris-HCl pH 6.8	1.5 ml
	DTT	0.3 g
	SDS	4 ml 10% SDS
	Bromophenol blue	8 mg
	Add water to final volume of 10 ml	
BG11 medium: for culturing cyanobacteria (Rippka, 1998)	NaNO ₃	17.6 mM
	K ₂ HPO ₄ ·7H ₂ O	0.175 mM
	MgSO ₄ ·7H ₂ O	1.3 mM

	CaCl ₂ ·2H ₂ O	0.25 mM
	Citric acid	0.028 mM
	Ferric citrate	0.028 mM
	EDTA	0.0034 mM
	Na ₂ CO ₃	0.19 mM
	Micronutrient solution	1ml/L
Micronutrient solution:	61.0 mg of H ₃ BO ₄ 169 mg of MnSO ₄ ·H ₂ O 287 mg of ZnSO ₄ ·7H ₂ O 2.5 mg of CuSO ₄ ·5 H ₂ O 12.5 mg of (NH ₄) ₆ Mo ₇ O ₂₄ ·4 H ₂ O Add deionized water to 1 liter	
Native-PAGE loading buffer I:	H ₂ O	7 ml
	Tris-HCl, pH6.8 0.5 M	1 ml
	Glycerin	2 ml
	Bromphenol blue	0.008 g
Native-PAGE loading buffer II:	H ₂ O	8 ml
	K ₂ HPO ₄ /KH ₂ PO ₄ buffer 1 M, pH 7.4	0.5 ml
	MgCl ₂ 1M	50 µl
	DTT 1M	50 µl
	EDTA 0.5 M	10 µl
	KCl 1M	0.5 ml
	Benzamidin 1 M	20 µl
Native-PAGE loading buffer II:	80mg BSA in 2ml buffer I Mix 4ml buffer I, 4ml buffer II, and 800ul buffer III to get the 2×native-PAGE loading buffer.	
Native-PAGE electrophoresis buffer:	Tris	15.1 g
	Glycerin	94 g
	Add water to final volume of 1 liter	
Native-PAGE separating Gel 7.5%	H ₂ O 1.45 ml, 30% native acrylamid 1.5 ml	
	Tris-Hcl pH 8.9 (1.5 M) 3 ml	
	APs 30 µl, 5% NP-40 60 µl, TEMED 5 µl	
Native-PAGE stacking Gel	H ₂ O 1.35 ml, 30% native acrylamid 0.5 ml	
	Tris-Hcl pH 6.8 (0.5M) 625µl	

	APs 12.5 μ l, 5% NP-40 25 μ l, TEMED 2.5 μ l	
TBS buffer	Tris-HCl pH 7.4	10 mM
	NaCl	150 mM
Western blotting Anode buffer I:	Tris	1.8 g
	Methanol	100 ml
	Add water to final volume of 500 ml	
Western blotting Anode buffer II:	Tris	1.51 g
	Methanol	100 ml
	Add water to final volume of 500 ml	
Western blotting Kathode buffer:	Tris	1.51 g
	Methanol	100 ml
	Amino- <i>n</i> -caproic acid	2.62 g
	Add water to final volume of 500 ml	
Wash buffer for Qiagen Ni-NTA agarose beads, pH 8.0	Tris/HCl, pH 8.0	10 mM
	NaCl	100 mM
	CaCl ₂	2.5 mM
	Imidazole	20 mM

2.4 General protein methods

2.4.1 Expression of His-tag tPphA and its variants

E. coli BL 21 (DE3) was applied to express his-tPphA and tPphA variants. Plasmids pET15b+tPphA and its variants were transformed into *E. coli* BL 21 (DE3). In the next day, a 5 ml volume of overnight culture of *E. coli* BL 21 (DE3) with plasmid pET15b+tPphA or its variants were prepared. The overnight culture medium was transferred into a glass bottle containing 200 ml LB medium with an ampicillin concentration of 100 μ l/ml. The bottle was shaking at 37°C. When O.D. at 600 nm of the medium arrived 1-1.5, IPTG was added into the medium to the final concentration of 0.5 mM to induce his-tag protein expression. The proteins were induced for 3-5 hours at 25°C. The cells were harvested by centrifuging at 10000 rpm for 10 minutes. The cells were resuspended by lysis buffer and sonicated for 4 times/2 minutes (40% duty). The cell lysis solution was centrifuged at 13000 rpm for 30 minutes. The supernant was centrifuged again at 13000-20000 rpm for 30 minutes. The clarified cell extract was used for protein purification.

2.4.2 Purification of his-tPphA and its variants

Before the cell extract loaded onto HIS-Select Cartridge, 5–10 ml of deionized water and 5–10 ml of wash buffer were used to wash the cartridge. Then, the clarified cell extract was loaded onto the cartridge. The cartridge was washed by 15 ml wash buffer. The protein was eluted from the cartridge by 5 ml elution buffer. The elution fractions contained most of protein were detected by Bradford and dialyzed against the dialyzing buffer at 4°C, overnight.

2.4.3 SPS-PAGE protein electrophoresis

SDS-PAGEs were made by using the standard protocol everywhere. The protein samples were boiled at 95°C for 5 minutes with 4× protein loading buffer to denature the proteins before load the protein on the lane of the SDS-PAGE. The intensity of the electricity of the SDS-PAGE electrophoresis was 15-30 mA. After the electrophoresis, the proteins were stained by coomassie blue. The PAGEs were cleared by the wash buffer. In this thesis, the concentrations of acrylamide in the separate gels were 12% and 15%

2.4.4 Preparation of phosphorylated P_{II} and Strep-P_{II}.

Phosphorylated P_{II} protein (P_{II}-P) was prepared from *Synechococcus elongatus* PCC 7942 as described previously with modification (21).

2.4.5 Native PAGE

Native PAGE was used to separate proteins according to difference in their charge density natively. Native state of protein means proteins in properly folded state, not denatured or unfolded state. There are no denaturants present in the gel and buffer in the gel maintaining the protein in its native state. In Native PAGE the mobility depends on both the protein's charge and its hydrodynamic size. The charge depends on the amino acid composition of the protein as well as post-translational modifications. The hydrodynamic size and mobility of native protein on the gel will vary with the nature of the conformation. Proteins with compact conformations have higher mobility and larger structures like oligomers have lower mobility. P_{II} protein can be phosphorylated. From our formerly results, P_{II} can form a trimer. There are four phosphorylated status including P_{II}⁰, P_{II}¹, P_{II}², and P_{II}³ in the native PAGE. The native PAGE was performed as ours former protocol (30).

2.4.6 Western-blotting

After SDS-PAGE or Native PAGE electrophoresis, the proteins were transferred to nitrocellulose membrane. Anode buffer I, Anode buffer II and Kathode buffer (refer to 2.3.2)

were used to make the papers wet. The “sandwich” of paper, PAGE, and Nitrocellulose membrane was installed. The proteins were transferred from SDS-PAGE or Native PAGE to nitrocellulose membrane at electricity intensity of 50-200mA/13-20V for 60 minutes. After the transferring, the nitrocellulose membranes were incubating in 5% degrease milk (TBS diluted) for 1 hour at room temperature. The nitrocellulose membrane was incubating in 1% degrease milk (TBS diluted) with 1:20000-1:10000 diluted primary antibody of P_{II} protein at 4°C, overnight. The next day, the nitrocellulose membrane was washed by TBS buffer four times. The nitrocellulose membrane was incubating in 1% degrease milk (TBS diluted) with 1:20000-1:10000 secondary antibody at room temperature for 1-2 hours. The nitrocellulose membrane was washed four times/1 minute by TBS. The proteins were illuminated by the Lumi-light Western blotting Substrate. Exposed 2-60 minutes at Kodak Gel Logic 1500 system.

Chapter 3. A third metal is required for catalytic activity of the signal-transducing PPM phosphatase tPphA



A Third Metal Is Required for Catalytic Activity of the Signal-transducing Protein Phosphatase M tPphA^{*[S]}

Received for publication, June 22, 2009, and in revised form, January 25, 2011. Published, JBC Papers in Press, February 10, 2011, DOI 10.1074/jbc.M109.036467

Jiyong Su (苏纪勇)[†], Christine Schlicker[§], and Karl Forchhammer^{*†1}

From the [†]Interfaculty Institute of Microbiology and Infection Medicine, Department of Organismic Interactions, University of Tübingen, Auf der Morgenstelle 28, D-72076 Tübingen and the [§]Department of Biophysics, Ruhr-University Bochum, Universitätsstrasse 150, D-44801 Bochum, Germany

Protein phosphatase M (PPM) regulates key signaling pathways in prokaryotes and eukaryotes. Novel structures of bacterial PPM members revealed three divalent metal ions in their catalytic centers. The function of metal 3 (M3) remained unclear. To reveal its function, we created variants of tPphA from *Thermosynechococcus elongatus* in all metal-coordinating residues, and multiple variants were created for the M3 coordinating Asp-119 residue. The structures of variants D119A and D193A were resolved, showing loss of M3 binding but unaffected binding of M1 and M2 in the catalytic center of D119A, with the nucleophilic water molecule in the correct place. The catalytic activity of this variant was highly impaired. This and further structure-function analyses showed that M3 is required for catalysis by providing a water molecule as a proton donor during catalysis. Mutation of the homologue Asp residue in human PP2C α also caused loss of function, suggesting a general requirement of M3 in PPM-catalyzed reactions.

Serine/threonine phosphatases of the PPM² family are widely present in eukaryotes and prokaryotes and regulate key signaling pathways involved in cell proliferation, stress responses, or metabolic control (1). PPM phosphatases are metalloenzymes requiring Mg²⁺ or Mn²⁺ ions, which are coordinated by a universally conserved core of aspartate residues.

The human PPM member PP2C α has been the defining representative of this family. As shown by structural analysis and site-directed mutagenesis studies, a binuclear metal center (with metals M1 and M2) activates a catalytic water molecule for nucleophilic attack of the phosphate group (2, 3). The importance of the M1-M2 core was also demonstrated for other PPM members, such as BA-Stp1, a bacterial PPM member from *Bacillus anthracis* (4). Recently, the structure of several bacterial members (tPphA from *Thermosynechococcus elongatus* (5), MtPstP from *Mycobacterium tuberculosis* (6), MspP from

Mycobacterium smegmatis (7), STP from *Streptococcus agalactiae* (8), as well as the structure of Hab1 from *Arabidopsis thaliana* in co-crystal with its inhibitor, abscisic acid receptor Pyl2 (9)) has been solved. A third metal ion (M3) in proximity of the M1-M2 core could be revealed in several crystal forms of these proteins; however, the function of the third metal was controversially discussed. It was proposed to directly take part in catalysis in the case of SaSTP (8) or to have a regulatory role in the conformation of the flexible FLAP subdomain, which may be important for substrate recognition (10).

The PPM tPphA from the thermophilic cyanobacterium *T. elongatus* is ideally suited to elucidate the role of M3. Because of its thermophilic origin, it has a robust structure, and the M3 coordination was almost invariant in various crystal forms (Fig. 1) (5), whereas M3 coordination was variable in other PPM members (7, 8). Furthermore, tPphA reacts readily with the artificial substrate pNPP, and moreover, its natural substrate, the phosphorylated P_{II} signal transduction protein (P_{II}-P), is available (11). In this study, mutant tPphA variants affected in M3 coordination were generated and analyzed with respect to enzymatic properties, metal binding, and three-dimensional structures, demonstrating a catalytic role of M3 in the dephosphorylation reaction.

EXPERIMENTAL PROCEDURES

Detailed protocols are available in the [supplemental material](#).

Cloning, Overexpression, and Purification of tPphA and Its Variants—The tPphA gene was cloned into the His tag vector pET15b (Novagen) according to standard procedures. Site-directed mutagenesis of tPphA was carried out with the QuickChange XL site-directed mutagenesis kit (Stratagene).

Artificial genes for human PP2C fragment (residues 1–297) and the corresponding PP2C-variant D146A were synthesized and cloned into His tag pET15b vector by GENEART (Regensburg, Germany). Overexpression and purification of His-tagged proteins were performed as described in the [supplemental material](#).

His tag-free tPphA variants D119A and D193A for crystallization were constructed from the plasmids pET15b + D119A and pET15b + D193A by standard PCR methods. Protein overproduction and purification were carried out as described previously for wild-type tPphA (5).

Crystallization, Data Collection, and Structure Determination—Crystals of the tPphA mutants D119A and D193A were obtained by mixing 0.8 μ l of protein solution (36 mg/ml)

* This work was supported by Deutsche Forschungsgemeinschaft Grant Fo195 and GRK 685 "Infection Biology" and Prof. Dr. Eckhard Hofmann.

† This article was selected as a Paper of the Week.

[S] The on-line version of this article (available at <http://www.jbc.org>) contains supplemental "Experimental Procedures," Figs. 1–3, and Table 1.

The atomic coordinates and structure factors (codes 2xzv and 2y09) have been deposited in the Protein Data Bank, Research Collaboratory for Structural Bioinformatics, Rutgers University, New Brunswick, NJ (<http://www.rcsb.org/>).

¹ To whom correspondence should be addressed. Fax: 49-7071-295843; E-mail: karl.forchhammer@uni-tuebingen.de.

² The abbreviations used are: PPM, protein phosphatase M, pNPP, p-nitrophenyl phosphate; ITC, isothermal titration calorimetry; ICP-OES, inductively coupled plasma-optical emission spectrometry.

TABLE 1
Data collection and refinement statistics

r.m.s.d. means root mean square deviation.

	tPpHA D119A	tPpHA D193A
Space group	C222 ₁	C222 ₁
Unit cell constants	$a = 38.71 \text{ \AA}$ $b = 151.68 \text{ \AA}$ $c = 82.78 \text{ \AA}$ $\alpha, \beta, \gamma = 90^\circ$	$a = 38.65 \text{ \AA}$ $b = 151.44 \text{ \AA}$ $c = 82.60 \text{ \AA}$ $\alpha, \beta, \gamma = 90^\circ$
Resolution	36.33 to 1.7 \AA	36.26 to 1.6 \AA
Unique reflections	27,138	30,657
$\langle I/\sigma \rangle$	19.20 (2.67)	13.64 (3.00)
Completeness ^a	99.1% (97.0%)	94.1% (76.2%)
$R_{\text{merge}}^{a,b}$	3.73% (40.34%)	4.37% (31.77%)
Refinement resolution	36.33 to 1.7 \AA	36.26 to 1.6 \AA
Reflections used for refinement	26,135	26,135
Protein atoms	1795	1784
Ligand atoms	4	4
Solvent atoms	112	99
r.m.s.d. bond lengths	0.007	0.007
r.m.s.d. bond angles	1.13	1.02
Average B factor	21.8 \AA^2	28.0 \AA^2
Final $R_{\text{crist}}/R_{\text{free}}^{c,d}$	19.2/21.9%	21.0/24.2%

^a Numbers in parentheses are for the outermost shell.^b $R_{\text{merge}} = \sum(I - \langle I \rangle) / \sum I$, where I is the intensity of an individual measurement, and $\langle I \rangle$ is the corresponding mean value.^c R factor = $\sum |F_{\text{obs}} - k|F_{\text{calc}}| / \sum |F_{\text{obs}}|$, where $|F_{\text{obs}}|$ is the observed and $|F_{\text{calc}}|$ is the calculated structure factor amplitude.^d R_{free} was calculated from 5% of measured reflections omitted from refinement.

and 0.8 μl of reservoir at 293 K after 1 day. The reservoir consists of 30% PEG3350, 0.2 M CaCl_2 , and 0.1 M Tris, pH 8.0, for the D119A mutant and 0.1 M Hepes, pH 7.4, for the D193A mutant. Before x-ray measurement, the crystals were transferred to a cryosolution containing the reservoir solution and 15% 2,3-butanediol as cryoprotectant. Data sets were collected at ESRF beamline BM14 at 100 K and 0.97625 \AA . Indexing, integration, and scaling of the data were done in HKL2000 (Table 1) (12).

Structure solutions were carried out by molecular replacement with Phaser (13) using the wild-type structure (Protein Data Bank code 2J82) as a search model. The models were refined by manual building with COOT (14) alternated with positional and B factor refinement with Phenix (15). The final structure was analyzed with Procheck (16), and no outliers were detected in the Ramachandran plot. In the structure of the D119A mutant, the following residues are split: Arg-54, Ser-135, Cys-166, Ile-180, and His-227. In the structure of the D193A mutant, only Ser-135 and His-227 are split residues. Structural figures were generated with PyMol. The Protein Data Bank code for the D119A mutant is 2y09 and for the D193A mutant 2xzv.

Preparation of Phosphorylated PII—Phospho- P_{II} protein was extracted from *Synechococcus elongatus* PCC 7942 as described previously (11).

Assay of Phosphatase Activity with pNPP as Artificial Substrate—The activities of the phosphatase variants toward pNPP were assayed in principle as described previously (5). Standard assays in a volume of 250 μl contained 0.25 μg of WT tPpHA or 10 μg of mutant proteins in a buffer consisting of 10 mM Tris-Cl, pH 8.0, 50 mM NaCl, 1 mM DTT, and 2 mM MnCl_2 . Reactions were started by the addition of 2 mM pNPP at 30 $^\circ\text{C}$, and the increase in absorbance at 400 nm was measured in an ELx808 absorbance microplate reader (BioTek) against a blank reaction without enzyme. To determine the K_m value for Mn^{2+} ,

the pNPP concentration was fixed at 1.5 mM, and the Mn^{2+} concentration was varied from 0.1 to 8 mM. For pNPP catalytic constants, the pNPP concentration was varied from 0.1 to 2 mM. From the linear slope of each reaction, the kinetic parameters K_m and V_{max} were calculated by nonlinear hyperbolic fitting using the GraphPad Prism 4 program (GraphPad Software Inc.).

Reactivity of Phosphatase Variants toward Phosphoserine and Phosphopeptides—Peptides G(pS)E, RG(pS)EY, and CRYRG(pS)EYTV, corresponding to the sequence environment in the natural substrate, were synthesized by Pineda (Berlin, Germany). RRA(pT)VA and RRA(pS)VA are commercially available PP2C substrates (Promega). The standard assay conditions are described in the supplemental material. The released P_i was quantified colorimetrically by the malachite green assay (17, 18). The absorbance of the solution at 630 nm was measured in ELx808 absorbance microplate reader (BioTek) against a blank reaction.

Reactivity of Phosphatase Variants toward PII-P—Dephosphorylation assays of $\text{P}_{\text{II}}\text{-P}$ were carried out in 10 mM Tris-Cl, pH 8.0, 50 mM NaCl, 1 mM DTT, and 2 mM MnCl_2 . 30- μl reactions contained 5 μl of *Synechococcus* extract containing 60 ng of highly phosphorylated P_{II} and 100 ng of phosphatase. Reactions were started by the addition of purified phosphatase. After incubation at 30 $^\circ\text{C}$, the reactions were stopped by adding 2.5 μl of 100 mM EDTA on ice. Subsequently, the phosphorylation state of P_{II} was determined by nondenaturing PAGE and immunoblot analysis as described previously (19).

Isothermal Titration Calorimetry (ITC)—All thermodynamic data were collected on a VP-ITC titration calorimeter (MicroCal, GE Healthcare). To remove any divalent cations from the purified proteins, all buffers were treated with Chelex 100 (Sigma), and the proteins were dialyzed four times at 4 $^\circ\text{C}$ in divalent metal-free buffer (25 mM Tris-HCl, pH 8.0, 150 mM NaCl) in the presence of excess Chelex 100 in the dialysis reservoir buffer. ITC experiments were performed at 25 $^\circ\text{C}$. Protein samples (50 μM) were titrated in the calorimeter cell (1.43 ml) by 50 successive injections (4 μl) of 500 μM MnCl_2 solution containing 250 μM DTT. The data were evaluated using the ORIGIN 7.0 software, provided by the manufacturer. Human PP2C ITC procedures were same as for tPpHA.

Elemental Analysis by Inductively Coupled Plasma-Optical Emission Spectrometry (ICP-OES)—ICP-OES (Optima 5300DV, PerkinElmer Life Sciences) was used to quantify the amount of Mn^{2+} in tPpHA variants. The sensitivity of ICP-OES to measure Mn^{2+} in liquid condition is 1 $\mu\text{g}/\text{liter}$. Chelex 100 was used to remove any divalent cations in the protein samples and buffers (same ITC procedure as above). After removing divalent cations, tPpHA variants were incubated with 2 mM MnCl_2 and 1 mM DTT on ice for 30 min. To remove unbound Mn^{2+} , the samples were loaded onto Centri-Spin columns (from Princeton Separations) equilibrated by the final dialysis buffer (25 mM Tris-HCl, pH 8.0, 150 mM NaCl). The columns were centrifuged at $750 \times g$ for 2 min. Only Mn^{2+} tightly bound to tPpHA should pass through the column. The average protein recovery was 70%. Identical concentrations of the protein variants were adjusted using the final dialysis buffer before ICP-OES analysis. As a background control for ICP-OES calibration,

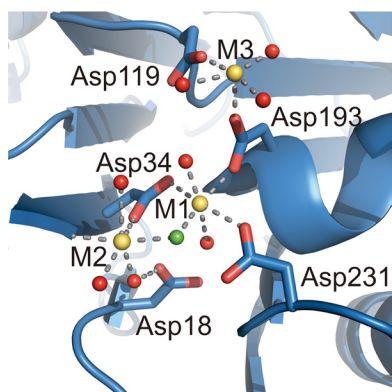


FIGURE 1. **Catalytic center of tPphA.** The water molecule (green ball) in the ion-dipole interaction with M1 and M2 was considered as the nucleophile attacking at the phosphorus atom in an S_n2 mechanism (3).

50 μ l of the final dialysis buffer was supplemented with 2 mM $MnCl_2$ and 1 mM DTT, and the mixture was subjected to the same desalting procedure as the protein samples. The Centri-Spin column eluate, collected in parallel with the protein samples, was used as background control for unspecific carry-over of Mn^{2+} . The concentration of Mn^{2+} was calculated according to a Mn^{2+} standard (0–1000 μ g/liter) prepared in the final dialysis buffer.

RESULTS AND DISCUSSION

Initial Characterization of tPphA Variants—To study the catalytic core of tPphA (Fig. 1), the highly conserved aspartate residues (Asp-18, Asp-34, Asp-119, Asp-193, and Asp-231) coordinating the three metal ions in the trinuclear metal center were site-directed mutated. Asp-18, Asp-34, Asp-193, and Asp-231 were changed to alanine. Asp-119 coordinating M3 was changed to alanine, threonine, glutamate, or asparagine. The recombinant proteins were purified to apparent homogeneity and characterized biochemically. First, the effect of the mutations on catalytic activity was investigated with *p*NPP as substrate. *p*NPP is a commonly used artificial substrate to characterize the catalytic activity of protein phosphatases (20). Previously, we showed that *p*NPP hydrolysis by tPphA requires Mn^{2+} as a divalent metal ion, as is the case for many other PP2C members (6, 7, 21, 22). Under standard assay conditions, all aspartate variants except D119N lost any detectable activity toward *p*NPP. Only after increasing the enzyme concentration 40-fold compared with standard assay conditions could a marginal activity be detected in variants D119A, D119E, D119T, and D231A; variants D18A, D34A, and D193A remained completely inactive (see Table 2). To confirm that the latter mutants were completely inactive, the Mn^{2+} concentration was further increased 5-fold, and the assays were incubated for prolonged periods. However, under no conditions could *p*NPP hydrolysis be detected. Therefore, it is safe to assume that D18A, D34A, and D193A have completely lost the ability to dephosphorylate *p*NPP. Variants D119A, D119E, D119T, and D231A lost about 97.6, 99.9, 99.9, and 99.7% catalytic efficiency compared with the wild type in *p*NPP assay (as derived from the K_m/K_{cat} values in Table 2). The complete loss of activity of variants impaired in M1 or M2 coordination confirms the pivotal role of the M1-M2 core in PPM catalysis (3, 4). The very low activities of Asp-119

TABLE 2

Kinetic parameters of tPphA and its variants towards *p*NPP

*p*NPP assays were carried out as described under “Experimental Procedures.” From the apparent reaction velocities of three independent repetitions, the kinetic parameters were calculated by linear fitting using the program GraphPad Prism 4. The \pm sign is a standard error.

Enzyme variant	K_m	K_{cat}	K_{cat}/K_m
	(<i>p</i> NPP)	(<i>p</i> NPP)	
	<i>mM</i>	<i>s</i> ⁻¹	<i>s</i> ⁻¹ <i>M</i> ⁻¹
tPphA WT	0.47 \pm 0.07	0.85 \pm 0.055	1809 \pm 117
D18A	— ^a	—	—
D34A	—	—	—
D119A	0.27 \pm 0.07	0.012 \pm 0.001	44 \pm 4
D119E	1.67 \pm 0.77	0.032 \pm 0.01	19 \pm 6
D119N	1.22 \pm 0.21	0.15 \pm 0.015	123 \pm 12
D119T	0.8 \pm 0.03	0.027 \pm 0.001	33 \pm 0.001
D193A	—	—	—
D231A	2.90 \pm 0.59	0.018 \pm 0.002	6 \pm 1
hPP2C α WT	0.57 \pm 0.03	2.69 \pm 0.06	5725 \pm 105
hPP2C α D146A	—	—	—

^a — means not determined.

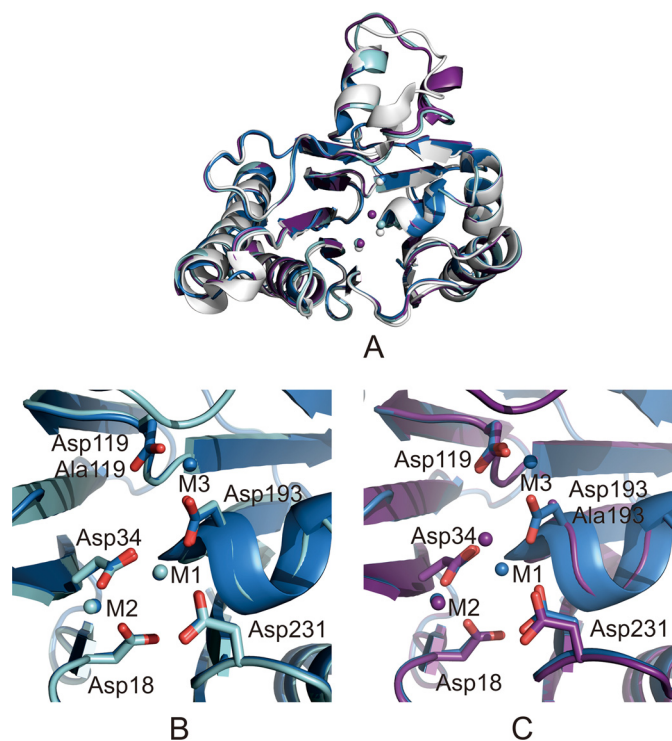


FIGURE 2. **Merge figure of wild-type tPphA and its D119A and D193A variants.** A, wild-type tPphA is shown in gray (Protein Data Bank code 2j86) and in blue (Protein Data Bank code 2j82). Cyan represents the D119A variant and violet the D193A variant. B, merge picture of wild-type tPphA (Protein Data Bank code 2j82) and D119A. C, merge picture of wild-type tPphA (Protein Data Bank code 2j82) and D193A.

variants could either indicate a role of M3 in catalysis or may be explained by an indirect effect on the coordination of the M1-M2 center. To distinguish between these possibilities, the crystal structures of two representative tPphA variants, D119A and D193A, were solved.

Structure of tPphA Variants D119A and D193A—The crystallization conditions for variants D119A and D193A are nearly identical for wild-type tPphA (5). The overall structure of these variants is very similar to wild-type tPphA (Fig. 2A). The centrally buried β -sheets and the two anti-parallel α -helices of the variants fully merged with wild-type tPphA. In contrast to the wild type, only two metal ions (M1 and M2) are resolved in

Thermosynechococcus PPM Function

the catalytic center of D119A and D193A (Fig. 2, B and C). Furthermore, the variants differed from the wild type in the structure of the lower part of the FLAP subdomain near the M3 site. This indicates that the occupation of the M3 site could affect the structure of the FLAP subdomain proximal to the catalytic cavity, as suggested previously (10).

Compared with the wild type, the catalytic core of the D119A variant displayed identical positions of M1 and M2 and all residues, except for the lack of the aspartyl side chain and the lack of M3, revealing that the Asp-119 mutation specifically affected the coordination of M3. By contrast, the Asp-193 mutation causes a shift in the position of M1, probably due to the lack of coordination by the Asp-193 carboxyl group (Fig. 2C). The complete loss of activity of the D193A variant can therefore be explained by the destruction of the binuclear metal core that activates the nucleophilic water. However, in case of the D119A variant, this metal core was entirely preserved, but nevertheless activity was drastically reduced. Activity was lost due to a highly reduced K_{cat} , whereas the K_m value for *p*NPP was almost not affected. Similarly, variants D119T and D119E also displayed greatly reduced K_{cat} values but only slightly different K_m values, indicating that substrate turnover rather than substrate binding was affected.

Mutation of the Asp-119 homologue residue in PstP to asparagine has previously revealed only a minor effect on catalytic activity at high Mn^{2+} concentrations (6), which was taken as evidence against a catalytic role of M3. However, the carbonyl oxygen of asparagine could still coordinate M3, although less efficiently, explaining the high Mn^{2+} requirement of this variant. To reveal if such an explanation could also apply for the tPphA D119N variant, the K_m value of Mn^{2+} was determined (Table 3). Indeed, a 10-fold higher K_m value for Mn^{2+} com-

pared with the wild type was measured, whereas the K_{cat} of the reaction at saturating Mn^{2+} was only moderately (about 2-fold) lowered. This result is in perfect agreement with the above assumption of a decreased efficiency in M3 binding.

Reactivity of tPphA Variants toward Phosphoserine and Phosphopeptides—Next, the reactivity of the various tPphA variants was determined toward phosphoserine and five different phosphopeptides. Two peptides were commonly used artificial protein phosphatase substrates as follows: the hexapeptides containing either a phosphothreonyl residue (RRA(pT)VA subsequently termed pT peptide) or a phosphoseryl residue (RRA(pS)VA, subsequently termed pS peptide). The other three peptides were derived from the sequence surrounding the phosphorylated seryl residue in the natural substrate, the T-loop of the P_{II} protein (G(pS)E, RG(pS)EY, and CRYRG(pS)EYTV) (Table 4). Phosphoserine alone was not used as a substrate by any tPphA variant. Wild-type tPphA turns over the pT peptide (7.73 ± 1.10 nmol/min/ μ g) more rapidly than any of the other phosphoseryl-containing peptides. The preference for pT over the pS peptides is frequently found in PP2C-like phosphatases (19, 23, 24). Activity correlates with the length of the peptides as follows: toward longer peptides the activity was higher than toward smaller substrates; the three-residue peptide (G(pS)E) is apparently too short to be recognized as a substrate (Table 4). As for *p*NPP dephosphorylation, variants D18A, D34A, and D193A had no detectable activity toward any of the peptides, even when the incubation time was prolonged up to 2 h, and D119A, D119T, and D231A variants had some marginal activity (Table 4). The D119E variant showed no residual activity toward any phosphopeptide, highlighting the severe defect of this variant. The D119N variant displayed variable defects; only a low activity (5–10%) was measured against “foreign” peptides; however, more than 50% of wild-type activity was recorded toward the 10-amino acid T-loop peptide, suggesting that the sequence surrounding the phosphoseryl residue can partially compensate the D119N mutation.

Reactivity of tPphA Variants toward Phosphorylated PII Protein as Substrate—The various mutants were also tested with phosphorylated PII protein (P_{II} -P) as substrate. Because the recombinant P_{II} protein cannot be phosphorylated *in vitro* until now, P_{II} -P extracted from the cyanobacterium *S. elongatus* was used as substrate. The phosphorylation status of P_{II} was detected by a well proven procedure, in which unphosphory-

TABLE 3
Kinetic parameters of tPphA and its mutants towards Mn^{2+} (*p*NPP used as substrate)

The assays were carried out as described under “Experimental Procedures.” From the apparent reaction velocities of three independent repetitions, the kinetic parameters were calculated by linear fitting using the program GraphPad Prism 4. The \pm sign is a standard error. Besides WT, D119N, and human PP2C α , the kinetic parameters of other protein towards Mn^{2+} cannot be determined. Activities are in nmol/min/ μ g.

	K_m (Mn^{2+})	K_{cat} (Mn^{2+})
	<i>mM</i>	<i>s⁻¹</i>
WT	0.58 ± 0.088	1.16 ± 0.048
D119N	5.25 ± 0.78	0.47 ± 0.037
Human PP2C α	0.24 ± 0.013	2.51 ± 0.034

TABLE 4
The activity of tPphA and its mutants toward three phosphopeptides

Reactions were performed in the buffer as described under “Experimental Procedures.” Triplicate assays were used. The \pm sign is a standard error.

Variant	RRA(pT)VA	RRA(pS)VA	Phosphoserine	G(pS)E	RG(pS)EY	CRYRG(pS)EYTV
WT	7.73 ± 1.10	3.06 ± 0.21	— ^a	—	0.50 ± 0.02	4.22 ± 0.36
D18A	—	—	—	—	—	—
D34A	—	—	—	—	—	—
D119A	—	0.03 ± 0.01	—	—	—	0.18 ± 0.13
D119E	—	—	—	—	—	—
D119N	0.72 ± 0.02	0.16 ± 0.01	—	—	0.17 ± 0.01	2.36 ± 0.46
D119T	—	—	—	—	—	0.24 ± 0.02
D193A	—	—	—	—	—	—
D231A	0.04 ± 0.02	0.10 ± 0.01	—	—	—	—
hPP2C α	3.732 ± 0.184	1.82 ± 0.12	—	—	0.23 ± 0.03	1.89 ± 0.39
hPP2C α D146A	—	—	—	—	—	—

^a — means the activity is below 0.01 nmol/min/ μ g.

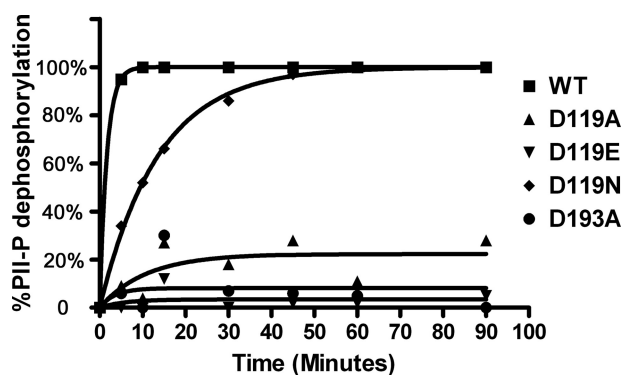


FIGURE 3. Time course assay of phospho- P_{II} dephosphorylation by wild-type tPphA and the mutants. Quantification of the experiment shown in supplemental Fig. 1 using an imaging system (Kodak Gel Logic 1500, Kodak Image Molecular Software). From the phosphorylation status of P_{II} in each lane, the percent of P_{II}-P dephosphorylation was calculated.

lated and the three phosphorylated forms (each subunit of the trimeric P_{II} may be phosphorylated on Ser-49) are separated by nondenaturing PAGE and detected by immunoblot analysis (11). P_{II} -P extract was incubated with the various tPphA variants, and at different time points, aliquots were removed, and the phosphorylation status of P_{II} was analyzed. The resulting electrophoretic pattern, after incubating P_{II} -P with the phosphatase variants, is shown in supplemental Fig. 1. From this pattern, the degree of P_{II} dephosphorylation was determined densitometrically (19) and plotted against the reaction time (Fig. 3). In Mn^{2+} -supplemented buffer, wild-type tPphA dephosphorylated P_{II} -P already after 5 min (Fig. 3). Under these assay conditions, the D119N variant was fairly active, and a marginal background activity could be observed for the D119A variant, but D119E and D193A remained completely inactive. Also variants D18A, D34A, and D231A were completely inactive, as expected (data not shown).

Metal Binding Studies—ITC is a thermodynamic technique that directly measures the heat released during a biomolecular binding event, and this method was successfully used to study the binding of divalent metal ions to various phosphatases (10, 25). The ITC measurements were highly reproducible and yielded almost identical results in three repetitions. Before the tests, all buffers were extensively treated by Chelex 100 to remove any divalent cations. The ITC data for wild-type tPphA, D119E, and D119N variants could be reasonably fitted according to a three-step sequential binding model. The affinity constants and enthalpy changes (ΔH) of the three binding sites calculated according to the sequential binding model are shown in Table 5. The quantity of the heat released from the binding between D119E and Mn^{2+} is similar to WT. The ITC result of D119E suggests that this variant still binds three metals; however, M3 must be shifted by the difference in length between Asp and Glu, compared with the wild-type position. The binding isotherm of D119A shows a similar amount of heat released as the wild type, but the integrated saturation curve adopts a different shape compared with the wild type and cannot be fitted according to a three sequential binding model. The observed heat release must be caused by the binding of M1 and/or M2 to the catalytic core.

TABLE 5

The affinity and thermodynamic parameters of WT and the mutants from ITC assay

K_d is given in micromolars, and ΔH is given in kcal/mol.

Fitting model	WT			D119E			D119N		
Three-step sequential binding model	K_{d1}	K_{d2}	K_{d3}	K_{d1}	K_{d2}	K_{d3}	K_{d1}	K_{d2}	K_{d3}
	18	61	18	85	178	8.2	58	550	48
	ΔH_1	ΔH_2	ΔH_3	ΔH_1	ΔH_2	ΔH_3	ΔH_1	ΔH_2	ΔH_3
	-26	69	-74	-24	283	-282	-27	161	-33
Two-step sequential binding model	hPP2C α			hPP2C α			D146A		
	K_{d1}			K_d			K_{d1}	K_{d2}	
	0.05			0.05			0.02	0.03	
	ΔH_1			ΔH_2			ΔH_1	ΔH_2	
	-15			17			-13	13	

TABLE 6

The stoichiometry of Mn^{2+} and proteins calculated from ICP-OES measurement

Mn^{2+} :WT	1.9:1
Mn^{2+} :D18A	0.7:1
Mn^{2+} :D34A	0.3:1
Mn^{2+} :D119A	0.8:1
Mn^{2+} :D119E	1.5:1
Mn^{2+} :D119N	2.2:1
Mn^{2+} :D119T	1.4:1
Mn^{2+} :D193A	1.2:1
Mn^{2+} :D231A	1.1:1

The Asp-34 mutant shows the strongest impairment in Mn^{2+} binding, with almost no heat release upon $MnCl_2$ addition. The Mn^{2+} -binding isotherms of the mutants D18A (close to M2), D193A (close to M1 and M3), and D231A (close to M1) show that these mutants were still able to bind Mn^{2+} ; however, binding was clearly impaired and released less heat (calorimetric signals decreasing by 70, 50, or 60% for D18A, D193A, or D231A mutants, respectively) compared with wild-type enzyme. The calorimetric signals could not be unambiguously fitted to a unique binding model; therefore, only a qualitative evaluation can be safely performed, because fitting to different models yields different thermodynamic constants (Table 5). The decreased binding isotherms indicate reduced but nevertheless clearly detectable metal binding. The observed residual binding signals in these variants probably represent binding of either M2 (in case of D193A and D231A mutants) or M1 (in case of D18A mutant) to the enzyme.

The amount of firmly bound Mn^{2+} to tPphA variants was determined by ICP-OES, a very sensitive method for quantitative elemental analysis. Before ICP-OES analysis, the protein samples were passed through a Centri-Spin desalting column, equilibrated with a Mn^{2+} -free buffer, to remove unbound or loosely bound Mn^{2+} ions from the protein. Only Mn^{2+} , which was tightly bound, can pass through the column. From the Mn^{2+} concentration measured by ICP-OES and the protein concentration, the stoichiometry of tightly bound Mn^{2+} to tPphA was calculated (Table 6). Wild-type tPphA and variants D119E and D119N had Mn^{2+} :protein stoichiometries close to 2:1, whereas that of the D34A variant was 0.3:1. The latter result agrees with the ITC measurement, which showed that D34A was almost completely impaired in metal binding. This low value indicates that the experimental procedure only reveals tightly protein-bound Mn^{2+} . Asp-34 is placed in the middle of the catalytic metal center, and the oxygen atoms of its carbonyl group coordinates both M1 and M2 (see Fig. 1), explaining the strongly reduced metal binding. Variants D18A, D193A, and D231A have stoichiometries near 1:1, indicating that they can

Thermosynechococcus PPM Function

only tightly bind one metal, either M1 or M2, depending on their mutation. What happens to M3? We suggest an inherent weak binding of M3 to explain the 2:1 stoichiometry found in wild-type tPphA. In agreement with the rather weak and superficial coordination of M3 by the enzyme, it probably binds loosely to the catalytic core and is therefore never observed by this experimental procedure, which involves a gel filtration step. Under conditions of protein crystallization, however, the M3 site is always occupied in wild-type tPphA, due to high surrounding divalent metal ion concentration.

Comparison with Human PP2C α —The results of this study strongly argue in favor of a catalytic role of M3, most likely in activating a water molecule as proton donor (see below). The absolute conservation of the M3-coordinating residue Asp-119 in all other PPM phosphatases, including human PP2C α (hPP2C α), raises the question of a general mechanism in this class of enzymes. We addressed this question by producing recombinant hPP2C α and a variant, in which the homologue residue Asp-146 was changed to Ala, and characterized the phenotype of these variants as described above for tPphA. The enzymatic constants of hPP2C α toward *p*NPP were similar to tPphA; the K_m value for *p*NPP was almost the same, and the K_{cat} was ~ 3 -fold higher. Strikingly, the hPP2C α variant D146A was completely inactive toward *p*NPP (Table 2). When using the various phosphopeptides as substrate, again the wild-type variant of hPP2C α turned out to be similar to wild-type tPphA, whereas the D146A variant had no obvious activity toward any phosphopeptide. Intriguingly, hPP2C α wild type was completely inactive toward P_{II}-P, either in the presence of Mn²⁺ or in the presence of Mg²⁺ (supplemental Fig. 2). This result illustrates a high degree of specificity toward the substrate phosphoprotein, which deserves further investigation. When assaying the binding of Mn²⁺ to hPP2C α by ITC, the calorimetric signals of the wild-type variant were very similar to the D146A variant (Fig. 4), and both could be fitted according to a two-step sequential binding model. This result indicates that only two metals, presumably M1 and M2, bound to hPP2C α in such a manner that they yielded a calorimetric signal. Nevertheless, Asp-146 is essential for catalysis. As shown by the tPphA D119A structure, this mutation did not cause a distortion of the M1-M2 core. Taking into consideration the high degree of structural conservation in the catalytic site of PP2C homologues, including tPphA, it is conceivable that Asp-146 coordinates a loosely bound divalent metal to the M3 site. The assumption of a loosely bound M3 would explain the stoichiometry of Mn²⁺ binding to tPphA; the short passage through a desalting column is obviously sufficient to loosen M3, which therefore seems to be a “volatile” metal in PPM. The degree of volatility could differ between the different enzymes, in agreement with the variable occupation of M3 in various PPM crystals (STP and MtPstP). The M3 site is always occupied in the tPphA crystal, indicating that M3 in tPphA may be less volatile than in other PP2C homologues, possibly because this enzyme is derived from a thermophilic organism and is therefore more rigid.

Conclusions—This study has provided clear evidence that the correct coordination of M3 in tPphA is decisive for catalytic activity. As shown by the structure-function study of the D119A variant, the M1-M2 metal core is not sufficient for catal-

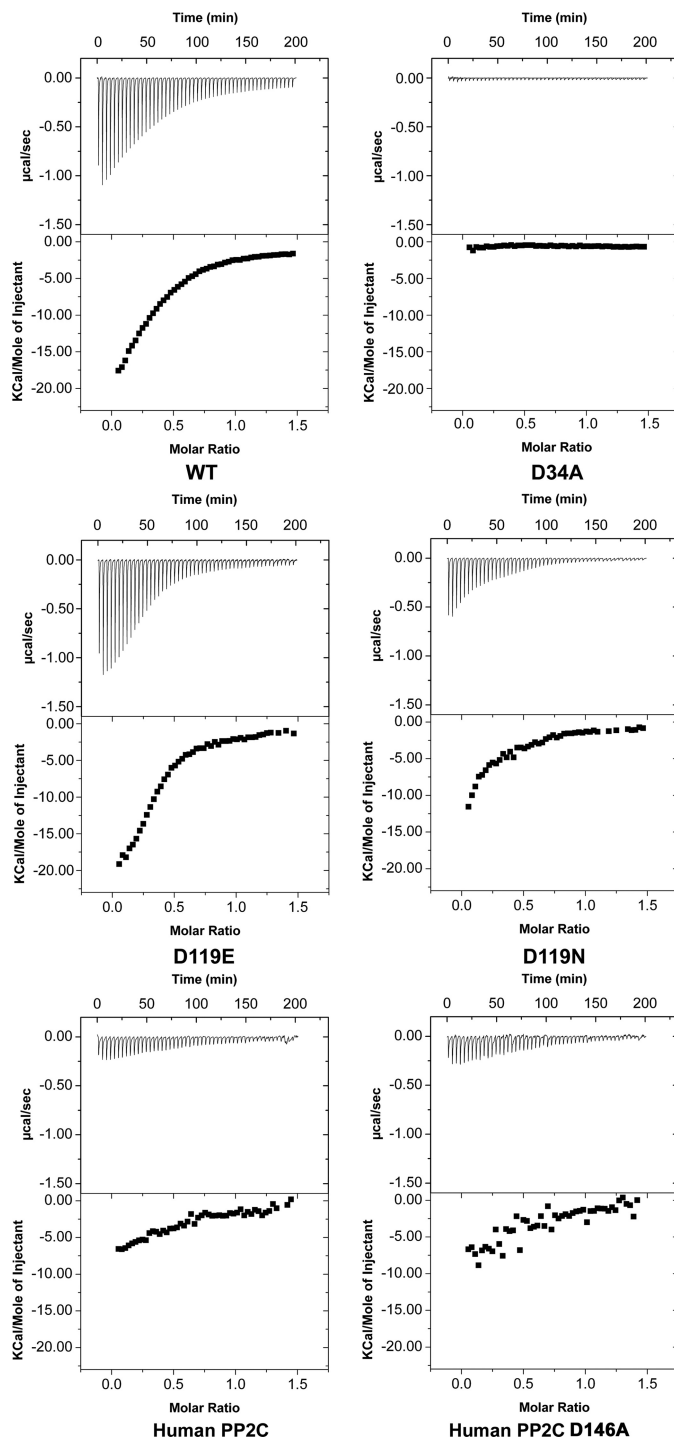


FIGURE 4. Mn²⁺ binding to wild-type and mutant tPphA proteins studied by ITC. For all titrations, each performed at 25 °C, the raw data are shown in the upper panel, and the integrated heat data, corrected for the heat of dilution, are shown in the lower panel. All measurements were done under the same experimental conditions (for details see “Experimental Procedures”). The ITC condition of hPP2C and its D146A variant were identical as for tPphA.

ysis. The absence of M3 causes a highly reduced substrate turnover, implying a catalytic role for M3. The requirement for the M3-coordinating residue Asp-119 was not only confined to tPphA but a similar phenotype was obtained with the defining member of this family, hPP2C α . One contradicting report concerns the *M. tuberculosis* PPM member MtPstP, where the homologue D118A

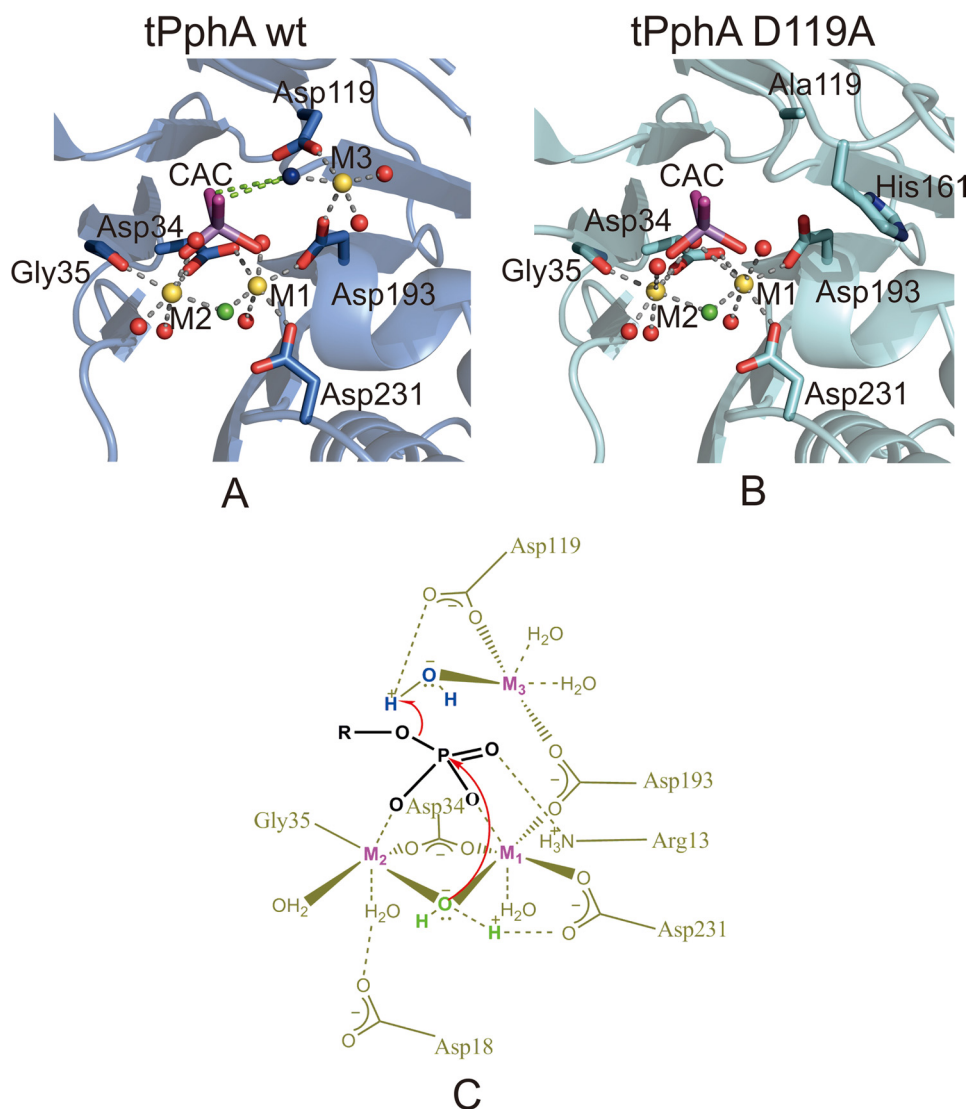


FIGURE 5. *A*, modeling the cacodylate (CAC) from the MspP structure (7) into the tPphA structure. The distances (green line) of M3 coordinated water molecule 2067 to cacodylate are 3.17 and 3.94 Å. *B*, modeling the cacodylate from the MspP structure into the tPphA D119A. *C*, catalytic mechanism of tPphA. The water molecule (green) in ion-dipole interaction with M1 and M2 is considered as the nucleophile, which attacks the phosphorus atom in an S_N2 mechanism. M3 activates as Lewis acid a water molecule (blue) to donate a proton for the phosphate leaving group.

mutation resulted in no significant alteration in *p*NPP hydrolysis activity (10). However, the activity of this enzyme toward *p*NPP (K_{cat}/K_m , $76 \pm 9 \text{ M}^{-1} \text{ s}^{-1}$) was almost as low as the activity of the tPphA variant D119A, suggesting that *p*NPP may not be a suitable substrate for MtPstP. The reported activity could therefore correspond to the slow background reaction that is observed in the tPphA variant D119A, which occurs in the absence of M3.

Structures at the atomic resolution of the PPM member MspP (from *M. smegmatis*) in various complexes with phosphate, sulfate, or the phosphate analogue cacodylate gave insight into potential reaction intermediates (7). According to these structures, the oxygens of the substrate phosphate group can directly interact with M1 and M2 by bidentate coordination, rather than indirectly through water-mediated interactions (2). This configuration places the catalytic water between M1 and M2 in a very favorable position for nucleophilic attack of the phosphorus atom. The MspP-cacodylate complex was suggested to mimic the competent enzyme-substrate complex (7).

Modeling the cacodylate molecule from the MspP structure into the tPphA structure in such a way that the distance between cacodylate and M1 and M2 remained constant shows that the cacodylate oxygen atoms would replace water molecules coordinated by M1 and M2 in tPphA (Fig. 5, *A* and *B*). If a phospho-substrate binds to this position, water molecule 2067 coordinated by M3 (colored in blue in Fig. 5, *A* and *B*) is now in a very favorable distance (3.17 Å) to function as a proton donor for the phosphate leaving group. This general acid for catalysis has previously been assumed to be a histidine residue in hPP2C α . However, this residue is not conserved in bacterial PPM members, and it has been suggested that a water molecule or a functional group from the protein substrate could function as a general acid (7). This work strongly argues in favor of the water molecule 2067 coordinated by M3 to act as proton donor; M3 can act as Lewis acid to facilitate the proton transfer from water 2067 to the phosphate leaving group, as depicted in Fig. 5*C*. The phenotype of the hPP2C α variant D146A suggests that

the proposed mode of reaction may be general for PPM phosphatases, because the M3 coordinating aspartate residue is universally conserved, and mutation to alanine causes a loss of function phenotype, similar to that in tPphA.

The proposed mechanism explains all observed phenotypes of the Asp-119 variants; the variants with Ala or Thr in place of Asp display a very slow substrate turnover. When the M3 is vacant and consequently no Mn²⁺-dependent activation of water molecule 2067 occurs, a water molecule from the solvent could occasionally act as a proton donor, explaining the background reaction with a highly reduced K_{cat} of the D119A variant. When Asp is replaced by Glu, metal analysis suggests that M3 could still bind, however, shifted by the length of a -CH₂ unit (1.54 Å), thus placing the metal in improper reaction distance and resulting in loss of function. However, when Asp is replaced by Asn, M3 could still bind at the same position as in the wild type, albeit with reduced affinity (implied by the elevated K_m for Mn²⁺). When at high Mn²⁺ concentrations the site becomes occupied, the reaction proceeds almost as efficiently as in the wild type. According to the structure of the two tPphA variants D119A and D193A and as shown for the structure of the bacterial PPM member SaSTP (8), binding of M3 affects the conformation of part of the FLAP subdomain, which is close to the catalytic site. Conversely, conformational changes of this part of the FLAP domain could modulate the binding of M3. If the conformation of the FLAP domain is influenced by substrate binding, the connection between FLAP conformation and M3 binding could provide a functional link between substrate binding and catalytic activity and could contribute to the mechanistic basis of substrate specificity of PPM-catalyzed dephosphorylation reactions.

Acknowledgments—We thank Christina Herrmann and Jie Su for excellent technical assistance, Olexandra Fokina for help with ITC experiments, and Peter Kühn for performing the ICP-OES measurements. We appreciate Vicente Rubio for critically reading the manuscript. We also thank the beamline staff of BM14 at the ESRF (Grenoble, France) for support during data collection.

REFERENCES

- Ariño, J., Casamayor, A., and González, A. (2011) *Eukaryot. Cell* **10**, 21–33
- Das, A. K., Helms, R., Cohen, P. T., and Barford, D. (1996) *EMBO J.* **15**, 6798–6809
- Jackson, M. D., Fjeld, C. C., and Denu, J. M. (2003) *Biochemistry* **42**, 8513–8521
- Shakir, S. M., Bryant, K. M., Larabee, J. L., Hamm, E. E., Lovchik, J., Lyons, C. R., and Ballard, J. D. (2010) *J. Bacteriol.* **192**, 400–409
- Schlicker, C., Fokina, O., Kloft, N., Grüne, T., Becker, S., Sheldrick, G. M., and Forchhammer, K. (2008) *J. Mol. Biol.* **376**, 570–581
- Pullen, K. E., Ng, H. L., Sung, P. Y., Good, M. C., Smith, S. M., and Alber, T. (2004) *Structure* **12**, 1947–1954
- Bellinzoni, M., Wehenkel, A., Shepard, W., and Alzari, P. M. (2007) *Structure* **15**, 863–872
- Rantanen, M. K., Lehtiö, L., Rajagopal, L., Rubens, C. E., and Goldman, A. (2007) *FEBS J.* **274**, 3128–3137
- Melcher, K., Ng, L. M., Zhou, X. E., Soon, F. F., Xu, Y., Suino-Powell, K. M., Park, S. Y., Weiner, J. J., Fujii, H., Chinnusamy, V., Kovach, A., Li, J., Wang, Y., Li, J., Peterson, F. C., Jensen, D. R., Yong, E. L., Volkman, B. F., Cutler, S. R., Zhu, J. K., and Xu, H. E. (2009) *Nature* **462**, 602–608
- Wehenkel, A., Bellinzoni, M., Schaeffer, F., Villarino, A., and Alzari, P. M. (2007) *J. Mol. Biol.* **374**, 890–898
- Irmeler, A., Sanner, S., Dierks, H., and Forchhammer, K. (1997) *Mol. Microbiol.* **26**, 81–90
- Otwinowski, Z., and Minor, W. (1997) *Methods Enzymol.* **276**, 307–326
- McCoy, A. J., Grosse-Kunstleve, R. W., Storoni, L. C., and Read, R. J. (2005) *Acta Crystallogr. D Biol. Crystallogr.* **61**, 458–464
- Emsley, P., and Cowtan, K. (2004) *Acta Crystallogr. D Biol. Crystallogr.* **60**, 2126–2132
- Adams, P. D., Grosse-Kunstleve, R. W., Hung, L. W., Ioerger, T. R., McCoy, A. J., Moriarty, N. W., Read, R. J., Sacchettini, J. C., Sauter, N. K., and Terwilliger, T. C. (2002) *Acta Crystallogr. D Biol. Crystallogr.* **58**, 1948–1954
- Laskowski, R. A., Moss, D. S., and Thornton, J. M. (1993) *J. Mol. Biol.* **231**, 1049–1067
- Van Veldhoven, P. P., and Mannaerts, G. P. (1987) *Anal. Biochem.* **161**, 45–48
- Ekman, P., and Jäger, O. (1993) *Anal. Biochem.* **214**, 138–141
- Ruppert, U., Irmeler, A., Kloft, N., and Forchhammer, K. (2002) *Mol. Microbiol.* **44**, 855–864
- MacKintosh, C., and Moorhead, G. (1999) in *Protein Phosphorylation: A Practical Approach* (Hardie, D. G., ed) pp. 153–180, Oxford University Press, Oxford
- Sugiura, T., and Noguchi, Y. (2009) *Biometals* **22**, 469–477
- Marley, A. E., Sullivan, J. E., Carling, D., Abbott, W. M., Smith, G. J., Taylor, I. W., Carey, F., and Beri, R. K. (1996) *Biochem. J.* **320**, 801–806
- Lai, S. M., and Le Moual, H. (2005) *Microbiology* **151**, 1159–1167
- Treuner-Lange, A., Ward, M. J., and Zusman, D. R. (2001) *Mol. Microbiol.* **40**, 126–140
- Conner, S. H., Kular, G., Pegg, M., Shepherd, S., Schüttelkopf, A. W., Cohen, P., and Van Aalten, D. M. (2006) *Biochem. J.* **399**, 427–434

Supplemental Experimental Procedures

Cloning, Overexpression and Purification of tPphA and its mutants

tPphA was amplified from plasmid pET32a+tPphA [5] by using the T7 primers (supplementary Table 1), which amplify genes between the T7 promoter and T7 terminator in the pET (Novagen) series plasmids and contain *NdeI* and *XhoI* restriction sites. The tPphA containing PCR product was cloned into plasmid pGME-T (Promega). Following restriction with *NdeI* and *XhoI*, the tPphA fragment was cloned into pET15b-vector (Novagen), generating an N-terminal fusion to the 6×His-tag sequence from the vector. The procedure of site-directed mutagenesis of tPphA was carried out with the QuickChange XL site directed mutagenesis kit (*Stratagene*). The primers for amplifying and mutation are shown in Table. 7. All constructs were checked by DNA sequencing. For overproduction of the recombinant enzymes, the constructs were transformed into *E. coli* BL21 (DE3) cells and grown in LB medium supplemented with Ampicillin (100µg/ml). When the optical density (O.D₆₀₀) of the culture reached to an optical density of 1 - 1.5, IPTG was added to a final concentration of 0.5 mM to induce protein overproduction. After 4-5 hours induction at 25 °C, the cells were harvested by centrifugation and lysed by sonification on ice in a buffer consisting of 20 mM Tris/HCl pH 7.8, 75 mM KCl, 500 mM NaCl, 5 mM MgCl₂, 0.5 mM EDTA, 0.2 mM PMSF. The lysate was centrifuged for 30 minutes at 13,000 rpm. The supernatant was centrifuged again for 30 minutes at 13,000 rpm. The clarified cell extract was used for protein purification. HIS-Select Cartridges (Sigma) were used to purify His-tag proteins. After purification, the proteins were dialyzed in buffer (20 mM Hepes, pH 7.4, 75 mM KCl, 500 mM NaCl, 2 mM MgCl₂, 0.5 mM EDTA, 1 mM DTT, 50% Glycerol) and analyzed by SDS-PAGE. The concentrations of the purified proteins were determined by the Bradford method (Carl Roth) and from UV spectra calculating with an absorption coefficient at 280 nm of 27960 M⁻¹cm⁻¹ (calculated from www.expasy.ch/tools/protparam.html).

Artificial genes for human PP2C fragment (1-297) and the corresponding PP2C-variant D146A were synthesized and cloned into His-tag pET15b vector by GENEART (Regensburg). Overexpression and purification of His-tagged proteins was performed as his-tPphA purification.

His-tag free tPphA variants D119A and D193A for crystallisation were constructed from the plasmids pET15b+D119A and pET15b+D193A by standard PCR methods. Protein overproduction and cell lysis procedures were carried out as his-tPphA. The protein purification was performed same as WT tPphA [5]. Econo-Pac High Q cartridge (BIO-RAD) was used to purify the protein at the first step. The clarified cell extract was 1:50 diluted by H₂O before loaded onto the Econo-Pac High Q cartridge. Afterwards, the Econo-Pac High Q cartridge was washed by 50 ml 10 mM Hepes pH 7.4. Then the protein was eluted from the cartridge by NaCl in a linear gradient concentration from 0-1 M. The fractions containing the mutant proteins were found by SDS-PAGE. 80% saturation (NH₄)₂SO₄ were used to precipitate the fractions containing tPphA. After incubated at 4 °C for 16 hours,

the precipitated protein was collected by centrifuge and redissolved in the buffer (20 mM Hepes, pH 7.4, 75 mM KCl, 150 mM NaCl, 5 mM MgCl₂, 0.5 mM EDTA, 3 mM DTT). The redissolved protein was loaded onto a gel filtration column (HiLoad™ 26/60-Superdex™ 200pg from GE Healthcare) for the second step purification. The column was equilibrated with the buffer (20 mM Hepes, pH 7.4, 75 mM KCl, 150 mM NaCl, 5 mM MgCl₂, 0.5 mM EDTA, 3 mM DTT). After purification, the fractions containing tPphA were pooled and precipitated again by 80% saturation (NH₄)₂SO₄. After incubated at 4 °C for 16 hours, the precipitated protein was collected by 15 minutes centrifuge at 16,000 rpm and redissolved in the buffer (20 mM Hepes, pH 7.4, 75 mM KCl, 150 mM NaCl, 5 mM MgCl₂, 0.5 mM EDTA, 3 mM DTT). The purity of protein was above 95%. The protein was concentrated to 36 mg/ml by a protein concentrator.

Crystallization, data collection and structure determination.

Crystals of the tPphA mutants D119A and D193A were obtained by mixing 0.8 µl protein solution (36 mg/ml) and 0.8 µl reservoir at 293 K after 1d. The reservoir consists of 30% PEG3350, 0.2M CaCl₂ and 0.1M Tris pH 8.0 for the D119A mutant and 0.1M Hepes pH 7.4 for the D193A mutant. Before x-ray measurement the crystals were transferred to a cryo solution containing the reservoir solution and 15 % 2, 3-butandiol as cryo protectant. Data sets were collected at ESRF beamline BM14 at 100K and 0.97625 Å. Indexing, integration, and scaling of the data were done in HKL2000 [12]. (Table 1).

Structure solutions were carried out by molecular replacement with Phaser [13] using the wildtype structure (pde code 2J82) as search model. The models were refined by manual building with COOT [14] alternated with positional and B factor refinement with Phenix [15]. The final structure was analyzed with Procheck [16] and no outliers were detected in the ramachandran plot. In the structure of D119A mutant the following residues are split: Arg54, Ser135, Cys166, Ile180 and His 227, in the structure of the D193A mutant only Ser135 and His227 are splitted residues.

Structural figures were generated with PyMol (<http://pymol.sourceforge.net>).

The pdb code for the D119A mutant is 2y09 and for the D193A mutant 2xzv.

Preparation of phosphorylated P_{II}

Phospho-P_{II} protein was prepared from *Synechococcus elongatus* PCC 7942 mutant Pph1. To achieve a maximal degree of *in vivo* P_{II} phosphorylation, the cells were grown in BG 11 medium [11] containing 17.6 mM NaNO₃ supplemented with 10 mM NaHCO₃ and ferric ammonium citrate was replaced by ferric citrate. When the O.D of the cells arrive at 1.0, the cells were treated with 0.5 mM L-methionine sulphoximine (MSX) for 4 hours and were then harvested by centrifugation. Preparation of P_{II}-P enriched extract was carried out according to [11].

Assay of phosphatase activity with pNPP as artificial substrate

The activities of the phosphatase variants towards pNPP were assayed in principle as described previously [5]. Standard assays in a volume of 250 µl contained 0.25 µg WT tPphA or 10µg mutant proteins in a buffer consisting of 10 mM Tris-Cl, pH 8.0, 50 mM NaCl, 1 mM DTT and 2 mM MnCl₂.

Reactions were started by the addition of 2 mM *p*NPP at 30°C and the increase in absorbance at 400 nm was measured in an ELx808 absorbance microplate reader (BioTek) against a blank reaction without enzyme. To determine the K_m for Mn^{2+} , the *p*NPP concentration was fixed at 1.5 mM and the Mn^{2+} concentration was varied from 0.1 mM to 8 mM. For *p*NPP catalytic constants, the *p*NPP concentration was varied from 0.1 mM to 2 mM. From the linear slope of each reaction, the kinetic parameters K_m and V_{max} were calculated by non-linear hyperbolic fitting using the GraphPad Prism 4 program (GraphPad Software Inc.).

Reactivity of tPphA and its mutants towards phospho-serine and phosphopeptides

Phospho-serine and five different phosphopeptides were used to assay the activities of tPphA and its mutants. The sequence of the five peptides are G(pS)E, RG(pS)EY, CRYRG(pS)EYTV, RRA(pT)VA, and RRA(pS)VA. G(pS)E, RG(pS)EY, CRYRG(pS)EYTV correspond to the T-loop sequence of the P_{II} protein. In a standard assay, 0.25 μ g of purified tPphA or 10 μ g mutant proteins were reacted with 2 mM phospho-serine or 100 μ M phosphopeptides in a reaction volume of 100 μ l containing 50 mM Tris-Cl pH 8.0, 50 mM NaCl, 2 mM $MnCl_2$ and 1 mM DTT. Reactions were incubated at 30°C for 2-10 minutes, then stopped by the addition of 50 μ l 4.7 M HCl. The released P_i was quantified colorimetrically by the malachite-green assay [17, 18]. The absorbance of the solution at 630 nm was measured in ELx808 absorbance microplate reader (BioTek) against a blank reaction which was stopped at the start point by 50 μ l 4.7 M HCl. The activity of WT tPphA and its mutants toward peptides was calculated with a phosphate standard.

The activities of tPphA and its mutants towards P_{II} -P

Dephosphorylation assays of P_{II} -P were carried out in 10 mM Tris-Cl, pH 8.0, 50 mM NaCl, 1 mM DTT and 2 mM $MnCl_2$. 30 μ l reactions contained 5 μ l *Synechococcus* extract containing 60 ng highly phosphorylated P_{II} and 100 ng phosphatase. Reactions were started by the addition of purified phosphatase. After incubation at 30°C the reactions were stopped by adding 2.5 μ l 100 mM EDTA on ice. Subsequently, the phosphorylation state of P_{II} was determined by non-denaturing PAGE and immunoblot analysis as described previously [19].

Isothermal Titration Calorimetry

All thermodynamic data were collected on a VP-ITC titration calorimeter (MicroCal, GE Healthcare). To remove any divalent cations from the purified proteins, all buffers were treated with Chelex-100 (Sigma-Aldrich) and the proteins were dialyzed four times at 4°C in divalent metal-free buffer (25mM Tris-HCl, pH 8.0, 150 mM NaCl) in the presence of excess Chelex-100 in the dialysis reservoir buffer. ITC experiments were performed at 25°C. Protein samples (50 μ M) were titrated in the calorimeter cell (1.43 ml) by 50 successive injections (4 μ l) of 500 μ M $MnCl_2$ solution containing 250 μ M DTT. The data were evaluated using the ORIGIN 7.0 software, provided by the manufacturer. Human PP2C ITC procedures were same as for tPphA.

Elemental analysis by Inductively Coupled Plasma-Optical Emission Spectrometry (ICP-OES)

ICP-OES (Perkin Elmer Optima 5300DV) was used to quantify the amount of Mn^{2+} in tPphA variants. The sensitivity of ICP-OES to measure Mn^{2+} in liquid condition is $1\mu g/l$. Chelex-100 was used to remove any divalent cations in the protein samples and buffers (same ITC procedure above). After removing divalent cations, tPphA variants were incubated with 2 mM $MnCl_2$ and 1 mM DTT on ice for 30 minutes. To remove unbound Mn^{2+} , the samples were loaded onto CENTRI.SPIN Columns (from PRINCETON separations) equilibrated by the final dialysis buffer (25mM Tris-HCl, pH 8.0, 150 mM NaCl). The columns were centrifuged at $750 \times g$ for 2 minutes. Only Mn^{2+} tightly bound to tPphA should pass through the column. The average protein recovery was 70%. Identical concentrations of the protein variants were adjusted using the final dialysis buffer before ICP-OES analysis. As a background control for ICP-OES calibration, 50 μl of the final dialysis buffer was supplemented with 2 mM $MnCl_2$ and 1 mM DTT and the mix was subjected to the same desalting procedure as the protein samples. The CENTRI.SPIN column eluate, collected in parallel with the protein samples, as used as background control for unspecific carry-over of Mn^{2+} . The concentration of Mn^{2+} was calculated according to a Mn^{2+} standard (0-1000 $1\mu g/l$) prepared in the final dialysis buffer.

Supplementary Fig. 1

Time course assay of phospho- P_{II} dephosphorylation by wild type tPphA and the mutants. Following the indicated incubation times in presence of phosphatase, the phosphorylated forms of P_{II} were separated by non-denaturing PAGE and visualized by immunoblotting. The non-phosphorylated form P_{II0} and the phosphorylated forms containing one, two or three phosphorylated subunits (P_{II}^1 ; P_{II}^2 and P_{II}^3) are indicated.

Supplementary Fig. 2

P_{II} -P dephosphorylation by human PP2C and its mutant D146A.

Supplementary Fig. 3

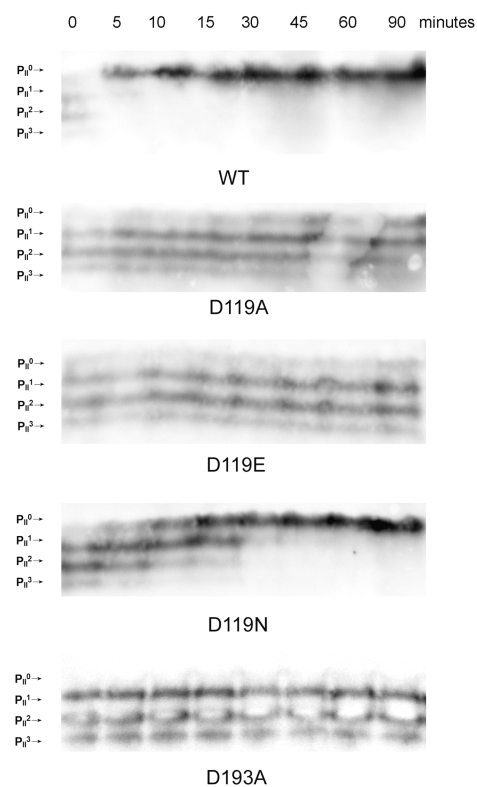
Mn^{2+} binding to mutant tPphA proteins studied by Isothermal Titration Calorimetry (ITC). For all titrations, the raw data of the six experiments each performed at $25^\circ C$ are shown in the upper panel, and the integrated heat data, corrected for the heat of dilution, are shown in the lower panel. All measurements were done under the same experimental conditions (for details see Experimental Procedures).

Supplementary table 1: Primers used for PCR amplification of tPphA and for site-directed mutagenesis

T7	5'; 5'-TAATACGACTCACTATAGGG-3'
	3'; 5'-GCTAGTTATTGCTCAGCGG-3'
D18A	5'; 5'-CGCAAAGCAATCAGGCCGCTTTTTATATTGATG-3'
	3'; 5'-CATCAATATAAAAAGCGGCCTGATTGCTTTTGCG-3'
D34A	5'; 5'-CTTTTTTATTGTTGCAGCCGGCATGGGGGGACACG-3'
	3'; 5'-CGTGTCCCCCATGCCGGCTGCAACAATAAAAAAG-3'
D119A	5'; 5'-GCCCATGTGGGCGCTTCCCGCATCTACC-3'
	3'; 5'-GGTAGATGCGGGAAGCGCCACATGGGC-3'
D119E	5'; 5'-GCCCATGTGGGCGAATCCCGCATCTACC-3'
	3'; 5'-GGTAGATGCGGGATTCGCCACATGGGC-3'
D119N	5'; 5'-GCCCATGTGGGCAATTCCCGCATCTACC-3'
	3'; 5'-GGTAGATGCGGGAATTGCCACATGGGC-3'
D119T	5'; 5'-GCCCATGTGGGCACTTCCCGCATCTACC-3'
	3'; 5'-GGTAGATGCGGGAAGTGCCACATGGGC-3'
D193A	5'; 5'-GCTGCTGTGCAGTGCCGGCCTGACCGAAG-3'
	3'; 5'-CTTCGGTCAGGCCGGCACTGCACAGCAGC-3'
D231A	5'; 5'-CCATGGCGGGCGTGCTAATGTCACCGTCG-3'
	3'; 5'-CGACGGTGACATTAGCACGCCCGCCATGG-3'
Histagremove	5'; 5'-Pho-ATGGACGTTGCTGGCTTA-3'
	3'; 5'-Pho-GGTATATCTCCTTCTTAAAG-3'

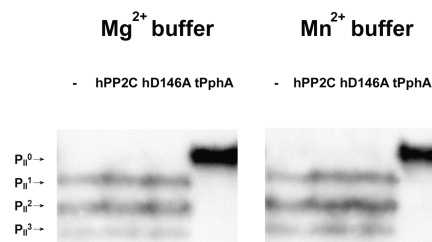
Supplementary Fig. 1

Supplementary Figure 1 Karl Forchhammer



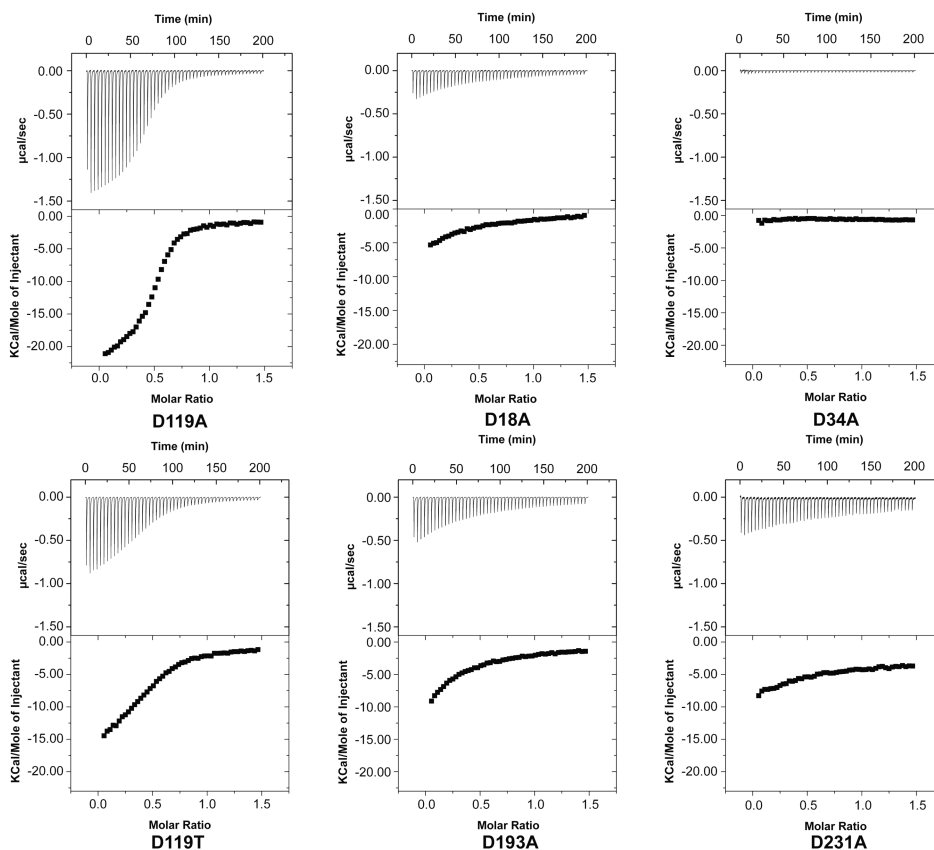
Supplementary Fig. 2

Supplementary Figure 2 Karl Forchhammer



Supplementary Fig. 3

Supplementary Figure 3 Karl Forchhammer



Chapter 4. Determinants for substrate specificity of the bacterial PP2C protein phosphatase tPphA from *Thermosynechococcus elongatus*

Jiyong Su and Karl Forchhammer*

From the Interfaculty Institute for Microbiology and Infection Medicine, Department of Organismic Interactions, University of Tübingen, Auf der Morgenstelle 28, D-72076 Tübingen, Germany

Running title: Determinants for protein phosphatase substrate specificity

* Corresponding Author: Karl Forchhammer, Auf der Morgenstelle 28, D-72076 Tübingen, Germany;

Fax: 49 7071 295843. E-mail: karl.forchhammer@uni-tuebingen.de

The abbreviations used are: PPM, Mg²⁺- or Mn²⁺-dependent protein phosphatase, PP2C, PP2C-like serine/threonine phosphatase; *p*NPP, *p*-nitrophenyl phosphate; P_{II}-P, phosphorylated P_{II} protein; GDA, glutaraldehyde; PD, pull-down; 2-OG, 2-oxoglutarate; ITC, isothermal titration calorimetry; ICP-OES, inductively coupled plasma-optical emission spectrometry

Subdivision: Signal transduction

This Chapter was submitted to FEBS. J.

Summary

Members of the PPM/PP2C protein phosphatases are abundant and widely distributed in prokaryotes and eukaryotes, where they regulate diverse signal transduction pathways. Despite of low sequence conservation, the structure of their catalytic core is highly conserved except of a flexible region termed FLAP subdomain. Bacterial PPM/PP2C members without C- or N-terminal regulatory domains still recognize their substrates. Based on the crystal structure of tPphA (a PPM/PP2C-member from the cyanobacterium *Thermosynechococcus elongatus*), variants of tPphA were generated by site-directed mutagenesis to identify substrate specificity determinants. Furthermore, a PPM/PP2C chimera containing the tPphA catalytic core and the FLAP subdomain of human PP2C α was also generated. tPphA variants and the chimera were tested towards different artificial substrates and native phosphorylated P_{II}. A histidine residue (His-39) of tPphA was thereby identified to play a key role in recognizing protein substrate. A binding assay combining chemical cross-linking and pull-down was designed to analyze the binding of tPphA variants, human PP2C α and chimera to phosphoprotein P_{II}. According to this analysis, metal 1- metal 2 cluster in the catalytic centre, but not metal 3 is required for the binding of phosphorylated substrate. The flexible FLAP subdomain, which protrudes on the top of the catalytic centre, not only affects catalytic activity, but also substrate specificity and binding. The chimera protein, despite being active towards *p*-nitrophenyl phosphate, could not dephosphorylate and bind to phosphorylated P_{II} protein, indicating that the entire FLAP subdomain is required for substrate recognition.

Introduction

Reversible protein phosphorylation affects the structure and the function of proteins that are responsible for the regulation of nearly all biological processes in living organisms. Protein kinases and protein phosphatases control the state of protein phosphorylation. Protein phosphatases can be divided into three main subclasses based upon their substrate specificity and protein structure: protein tyrosine phosphatase (1); protein serine/threonine phosphatase (2); and histidine phosphatase (3). Protein serine/threonine phosphatase could be further classified into three major subfamilies: phosphoprotein phosphatases, the aspartate-based phosphatases, and metal-dependent protein phosphatases (PPM/PP2C) (2). The human PPM member PP2C α (4) has been the defining representative of PPM family, therefore also referred as the PP2C family.

Serine/threonine phosphatases of the PP2C family are widely present in eukaryotes and prokaryotes where they regulate diverse signaling pathways involved in central cellular processes, such as cell proliferation, metabolic activity or stress responses (5). The PP2C phosphatases require Mg²⁺ or Mn²⁺ ions as ligands, which are coordinated by a universally conserved core of aspartate residues. The structural analysis of bacterial and plant PP2C members revealed that these enzymes contain three metal ions in their catalytic center and the structure of the catalytic core is almost invariant (6-11). In the catalytic centre, metal 1 (M1) and metal 2 (M2) coordinate a catalytically active nucleophilic water molecule and according to novel structures, they directly interact with two oxygen atoms of the substrate phosphate group during catalysis, respectively (8). Recently, we could show by site-directed mutagenesis of the highly conserved aspartate residues in the catalytic core of tPphA (a PP2C type phosphatase from *Thermosynechococcus elongatus*), that the loosely bound metal 3 (M3), which was occasionally observed in several bacterial and plant PP2C homologues, is required for catalysis, presumably by activating a water molecule as proton donor (12). Close to the catalytic center of PP2C, there is a flexible loop termed FLAP subdomain. The greatest structural variability in the structures of PP2C homologues is observed in this FLAP subdomain.

P_{II} proteins are homotrimeric proteins of 12-13 kDa subunits, and they may be post-translationally modified. P_{II} proteins can sense in an integrative manner of the state of nitrogen, carbon and energy metabolism (14, 19 - 23). Three ATP-binding sites are located in the intersubunit clefts, and in the presence of ATP, up to three 2-oxoglutarate (2-OG) molecules can bind per P_{II} trimer. Binding of the effector molecules modulates the conformation of the T-loop (14, 24). In unicellular cyanobacteria such as *Synechococcus elongatus* PCC 7942 or *Synechocystis* sp. PCC 6803 (*Synechocystis*), P_{II} has been shown to be phosphorylated on a seryl-residue (Ser-49) located at the apex of a large, solvent exposed loop, termed T-loop (13, 14). The genome of *Synechocystis* reveals eight putative PP2C type phosphatase homologues (15, 16). The alignment of the amino acid sequence of the eight PP2Cs showed the greatest variability exists in the FLAP subdomain. The eight PP2C phosphatases of

Synechocystis were knocked out separately. Only one mutant ($\Delta sll1771$) could not dephosphorylate phosphorlate P_{II} (P_{II} -P) under various conditions (17). The recombinant *sll1771* phosphatase (termed PphA) was purified from *E. coli* and it could dephosphorylate P_{II} -P *in vitro* in the presence of Mg^{2+} or Mn^{2+} (17). Phosphorylated P_{II} (P_{II} -P) becomes resistant towards PphA-mediated dephosphorylation, when it is fully occupied by ATP and 2-OG (20, 25), a ligand status which results in a retracted T-loop conformation. Although direct experimental evidence for binding between P_{II} and PphA is lacking, this observation implies that PphA recognizes the T-loop conformation, such that it could be unable to bind to P_{II} with the retracted T-loop. tPphA is the homologue of PphA from *Thermosynechococcus elongatus*: it shows high similarity in the FLAP subdomain sequence to PphA and could specifically dephosphorylate P_{II} -P in an effector molecule-dependent manner (6). Recently, we reported that human PP2C α (amino acid 1-297, without the C- regulatory domain) could not dephosphorylate P_{II} -P under conditions under which tPphA could fully dephosphorylate P_{II} -P (12). The structure of the catalytic core of tPphA and human PP2C α is highly similar, but their FLAP subdomains show huge differences in structure and primary sequence, suggesting that the FLAP subdomain plays a key role in recognizing P_{II} -P.

A clue to understand the specific interaction between PP2C phosphatases and their phosphoprotein substrates comes from the crystallographic analysis of the *Streptococcus agalactiae* PP2C phosphatase *Sa*STP (9). A *Sa*STP crystal with four monomers (A, B, C, and D) in the asymmetric unit revealed monomer C in a conformation, which interacted with the FLAP subdomain of the adjacent monomer A. The interactions in this contact include two salt bridges, Arg12(C)–Glu151(A) and His41(C)–Glu152(A), and three direct hydrogen bonds Ser14(C)–Glu152(A), Arg13(C)– Ser155(A), and Ile162(C)–Pro157(A). Whether this interaction mimicked an enzyme –product complex or was a serendipitous crystallographic artifact was an open question (9). However, *Sa*STP His-41 is highly conserved among bacterial PP2C phosphatases. The corresponding residue in tPphA is His-39, which is located at the tip of a small loop connecting $\beta 4$ - $\alpha 1$. His-39 seems to be flexible, since this residue is invisible in one space group (C222₁) of the wild-type tPphA crystal (6) and in the crystal of the D193A variant (12). Whether this residue is indeed involved in substrate recognition or product interaction needs to be resolved.

Recently, a co-crystal structure of PYR1 (pyrabactin resistance1, abscisic acid receptor protein) with HAB1 (hypersensitive to ABA1, PP2C) was resolved (18). PYR1 and HAB1 are important regulatory proteins in abscisic acid signal transduction pathway in *Arabidopsis thaliana*. The co-crystal structure showed the PYR1 $\beta 3/\beta 4$ loop containing Ser-85 takes part in a hydrogen bond network with the backbone amine of Gly-246 and the carboxylic group of Glu-203 of HAB1. This interaction was suggested to mimic the interaction of a serine containing peptide with the catalytic center of a PP2C phosphatase. In addition, the phosphate ion from the catalytic center of human PP2C α crystal structure was superimposed into the catalytic core of HAB1. This phosphate ion is only 2.9 Å away from the

carboxylic group of PYR1 Ser-85, which suggests that a phospho-serine substrate might enter PP2C catalytic site in a similar manner as PYR1 β 3/ β 4 loop goes into the catalytic center of HAB1 (18). tPphA Gln-17 is the homologue residue of HAB1 Glu-203. In the catalytic center of tPphA, Gln-17 indirectly coordinates M2 by bridging a water molecule (12). Whether tPphA Gln-17 is responsible for recognizing substrates or stabilizing M2 was still not known.

In order to find key residues/domains for tPphA substrate recognition, residues surrounding the catalytic center were site-directed mutagenized (Fig. 1) and a new PP2C chimera protein (tPphA catalytic center + human PP2C α FLAP) was generated. Substrate-specific activities of the variants were assayed and a novel phosphatase binding-assay, based on chemical cross-linking under enzymatically arrested conditions, was developed to determine the direct interaction between the enzymes and the P_{II} protein substrate.

Results

In this study, several new tPphA variants (R13K, S15A, Q17E, Q17K, M36A, H39A, R160A, T138A and T138E) were created. The previously created variants (D18A, D34A, D119A, D193A, D231A (12), H161A and R169A (6) were also included in this research. Fig. 1 shows the location of the mutated residues in the 3D-structure of tPphA. Furthermore, the FLAP subdomains of tPphA and of human PP2C α were mutually exchanged to generate two chimeric proteins (see Fig. 2). In chimera A, the human PP2C α FLAP subdomain was fused to the tPphA catalytic core. In chimera B, the tPphA FLAP subdomain was fused to the human PP2C α catalytic core. Whereas construction of chimera A resulted in soluble and active protein (see below), chimera B was insoluble and could not be re-solubilized (details on the manipulation of chimera B are given in the section "*Cloning, Overexpression and Purification of human PP2C α and the Chimeras*"). Further experiments were therefore only performed with chimera A.

Enzymatic assays of tPphA variants, human PP2C α and chimera A towards artificial substrates and P_{II}-P. The artificial substrates *p*-nitrophenyl phosphate (*p*NPP), various phospho-peptides and P_{II}-P were used to characterize the effects of amino acid substitutions on tPphA activity (See Table S1 and Table S2 and Fig. S1 A-D). A comprehensive comparison of the relative enzyme activities towards the five different substrates, normalized to the activity of the wild-type tPphA is shown in Fig. 3 A for those variants, which were apparently affected in substrate selectivity. The tPphA crystal structure (PDB file 2J82 (6)) reveals that Gln-17 (Q17) indirectly coordinates M2 by a bridging water molecule. In many other PP2C homologues, the corresponding position is occupied by glutamyl residue [see Supplementary file S1 in ref. (10)]. Interestingly, the Gln-17 to Glu mutation (Q17E) resulted in increased catalytic efficiency of the variant towards artificial substrates, in particular the artificial phosphoseryl-peptide. By contrast, Q17K only showed residual activity towards *p*NPP and *p*T-peptides and no activity towards phosphoseryl-containing substrates. Replacement of highly conserved residue His-39 to Ala (H39A) did not affect the reactivity towards *p*NPP, but, intriguingly, this variant

displayed reduced activity towards artificial phosphopeptides and was almost completely impaired in dephosphorylating P_{II} -P. This clearly indicates that this peripheral part of the enzyme does not directly take part in catalysis but has an important role for assisting substrate recognition. Mutation of Thr-138 to Glu (T138E) resulted in a surprisingly high disturbance of activity. This was unexpected, since in numerous bacterial PP2C members the corresponding position is in fact occupied by Asp or Glu residues (see Supplementary file S1 in ref. (10)). The methyl group of Thr-138 projects into the basis of the FLAP subdomain, pointing towards M3. Introduction of a negative charge at this place may distort the conformation of the entire FLAP subdomain.

The activity of human PP2C α and chimera A (tPphA catalytic core + human PP2C α FLAP) were also assayed towards these five different substrates. Human PP2C α dephosphorylated artificial substrates faster than wild type tPphA but was unable to dephosphorylate P_{II} -P. Chimera A could dephosphorylate p NPP to some extent (17 % residual activity) but could not dephosphorylate phosphopeptides and P_{II} -P (Fig. 3 B, Table S1, Table S2, and Fig. S1, E). The K_m value of chimera A for Mn^{2+} in the p NPP dephosphorylation assay was 0.63 mM, which is very similar to the K_m value (0.57 mM) of wild type tPphA (Table S1). Furthermore, metal binding by chimera A was tested by ITC analysis to reveal whether this protein is still capable to form a metal cluster. The result showed Mn^{2+} binding to chimera A with a similar affinity than between Mn^{2+} and wild type tPphA (Fig S2 and Table S3). The p NPP assay and the ITC results of chimera A indicate that chimera A has a functional tPphA catalytic core. However, the human FLAP subdomain prevents chimera A from recognizing phosphopeptides and P_{II} -P.

An assay to study the interaction between P_{II} and tPphA.

In the structure of tPphA, which was obtained by crystallization in a 100 mM $CaCl_2$ containing buffer, Mg^{2+} was found in the M1 position and Ca^{2+} in M2 and M3 sites (6). Therefore, the effect of Ca^{2+} on wild-type tPphA activity towards the various substrates was assayed. Ca^{2+} was unable to support any activity of tPphA and partially inhibited the Mg^{2+} -supported activity of phosphopeptide and P_{II} -P dephosphorylation (see Fig. S3). To further examine how the various mutations of tPphA residues directly affect the binding of P_{II} -P to the phosphatase, we sought to directly analyze the interaction of the proteins. Initial attempts to pull-down P_{II} -P with His-tagged tPphA on Ni-NTA beads under various buffer conditions (among others, using inhibitors of tPphA activity such as Ca^{2+} or EDTA, see below) were unsuccessful, indicating that the interaction is either very weak and/or transient. Therefore, we tried to stabilize the interaction intermediates by adding glutaraldehyde, followed by affinity purification of tPphA with Ni-NTA beads and examination of recovered P_{II} and tPphA by immunoblot analysis. Finally, conditions could be found, under which P_{II} could be specifically recovered in the tPphA elution fractions after glutaraldehyde treatment. Controls (P_{II} with and without cross-link in the absence of tPphA) revealed that the recovery of P_{II} specifically depended on tPphA interaction (See Fig. S4 A). Apparently, the interaction between P_{II} and tPphA is too weak to withstand affinity purification, but by crosslinking with a *bis*-aldehyde homobifunctional crosslinker glutaraldehyde, the interaction can

be stabilized and analyzed. The cross-linking reaction of glutaraldehyde and protein proceeds through the formation of Schiff bases between aldehyde and lysine residues (ϵ -amino group) (26).

A Ca^{2+} -containing buffer was necessary to efficiently recover $\text{P}_{\text{II}}\text{-P}$ by this procedure, whereas no pull-down occurred in the presence of Mg^{2+} (see the lane termed " Mg^{2+} " in Fig. 4A) or in the absence of divalent cations (see the lane termed "-" in Fig. 4A). Examination of the phosphorylation status of P_{II} incubated under these assay conditions revealed, that $\text{P}_{\text{II}}\text{-P}$ was dephosphorylated in the Mg^{2+} containing buffer, whereas almost no dephosphorylation occurred in the Ca^{2+} containing buffer or in the presence of EDTA (Fig. 4 B). Therefore, the low recovery of $\text{P}_{\text{II}}\text{-P}$ in the presence of Mg^{2+} was probably due to dephosphorylation of $\text{P}_{\text{II}}\text{-P}$ and a weaker interaction of non-phosphorylated P_{II} with tPphA. On the other hand, the lack of pull-down in the absence of any divalent metal may indicate a metal-requirement for phosphoprotein binding (see below). To directly compare the recovery of phosphorylated and non-phosphorylated P_{II} by this procedure, the same amount (0.2 μg) of either $\text{P}_{\text{II}}\text{-P}$ or Strep-tagged P_{II} (Strep- P_{II}) was used in a pull-down experiment in the presence of Ca^{2+} . As shown in Fig. 4C, indeed much more $\text{P}_{\text{II}}\text{-P}$ was recovered than non-phosphorylated Strep- P_{II} . Nevertheless, some residual recovery of Strep- P_{II} was visible. To find out whether the recovery of Strep- P_{II} by tPphA pull-down was also dependent on divalent metals, the same assay as shown in Fig. 4A was carried out with 10-fold higher amounts of Strep- P_{II} . Under these conditions, tPphA could specifically trap Strep- P_{II} in either Ca^{2+} , Mg^{2+} and no divalent cation buffer conditions (see the lanes termed " Ca^{2+} ", " Mg^{2+} ", and "-" in Fig. 4D). The signal intensity of recovered P_{II} was quantified densitometrically and the signal intensity in Ca^{2+} buffer was set to 100% (Fig. 4E). As a comparison, the same quantification was performed with the pull-down of $\text{P}_{\text{II}}\text{-P}$ shown in Fig. 4A, which was strictly Ca^{2+} -dependent. Although the highest recovery of Strep- P_{II} was observed in Ca^{2+} containing buffer, there was substantial recovery in the absence of divalent metals and also in the presence of Mg^{2+} . This indicates that tPphA can weakly interact with non-phosphorylated P_{II} and this interaction is not strictly dependent on divalent metals, whereas the interaction of $\text{P}_{\text{II}}\text{-P}$ with tPphA requires a metal-occupied enzyme.

The fact that almost no cross-link products between P_{II} and tPphA are found after heating the samples in SDS sample buffer can be attributed to the instability of the Schiff base formed through glutaraldehyde cross-linking (26, 27). However, most P_{II} is found cross-linked with itself either in dimeric or trimeric form. This can be explained by the tight packing of the P_{II} subunits in the trimer, which leads to much denser cross-linking between P_{II} subunits than between P_{II} and tPphA, and therefore the intramolecular cross-links remain preserved during sample preparation.

In order to independently investigate the cross-linking between Strep- P_{II} and tPphA, cross-linking solutions were analyzed by gel filtration and the molecular weight of the proteins was determined by dynamic light scattering (Fig. 5A and Fig. 5B). In the absence of glutaraldehyde cross-linking, Strep- P_{II} and tPphA were separated in two peaks, with the first peak containing Strep- P_{II} and the second tPphA (Fig. 5A) as was revealed by immunoblot analysis (data not shown). The mobility of tPphA is slower as

expected from its molecular mass. The reason for the aberrant slow mobility is unknown. Dynamic light scattering estimated a molecular weight of 36 kDa for Strep-P_{II} and 28 kDa for tPphA, which agrees with the expected values (Strep-P_{II}: 38 kDa, calculated from (28); tPphA: 28.9 kDa, calculated from (28)). When the proteins were first cross-linked with glutaraldehyde and then separated by gel-filtration, an additional peak of higher molecular weight appeared in addition to the peaks of Strep-P_{II} and tPphA, indicative of cross-link products with an average molecular weight of 64 kDa (Fig. 5B).

To further confirm that this pull-down assay detects the specific interaction between P_{II}-P and tPphA, the effect of metabolites ATP/ADP and 2-OG was tested in this assay using wild-type tPphA in the presence of different concentrations of metabolites. The recovery of P_{II}-P from these pull-down assays is shown in Fig. 6. A clear correlation between P_{II}-tPphA interaction and dephosphorylation activity, which was reported previously (29) can be noticed. AMP had no effect on P_{II}-P-tPphA interaction, in agreement with its lack of effects on P_{II} interactions (25). ATP and ADP were shown to bind to P_{II} and to partially inhibit P_{II}-P dephosphorylation, whereas 2-OG in the absence of ATP is unable to bind to P_{II} and has no impact on P_{II}-P dephosphorylation activity. In agreement, partial inhibition of binding was observed in the presence of ATP and ADP, whereas 2-OG alone was not inhibitory. In the presence of Mg²⁺-ATP and 2-OG, where P_{II}-P dephosphorylation is strongly impaired (25, 29), tPphA did not cross-link to P_{II}-P. When these metabolites are bound to P_{II}-P, the T-loop is forced in a retracted conformation (30). This coincidence strongly implies that the T-loop in the retracted conformation is not accessible to tPphA, in other words, the phosphatase recognizes the conformation of the P_{II} T-loop. Together, these data confirm the specificity of the present interaction analysis and provide the first direct evidence for effector-molecule regulated (t)PphA-P_{II}-P interaction.

Interaction of tPphA variants, human PP2Ca and chimera A with P_{II}. The interaction of tPphA variants with P_{II}-P was investigated using the glutaraldehyde cross-link and pull-down assay described above. Fig. 7A shows the immunoblot analysis of P_{II} recovered from the pull-down assays with tPphA variants. The control for tPphA recovery is shown in Fig. S5 A. In the following cases, there was a clear correlation between reactivity towards and binding of P_{II}-P: variants Q17K and T138E, which displayed very low P_{II}-P dephosphorylation activity (compare Fig. 3) could not bind to P_{II}-P, whereas same position variants Q17E and T138A, which were only slightly impaired in reactivity towards P_{II}-P, showed apparently equal or more binding of P_{II}-P than wild-type tPphA. The Q17E and T138A variants showed furthermore the same response towards the P_{II} effector molecules than the wild-type enzyme (Figure S6). Furthermore, tPphA variants D18A, D34A and D193A, coordinating the M1-M2 cluster and being enzymatically completely inactive (12), could not bind any P_{II}-P (Fig. 7A). Previous metal binding analysis showed, that the D18A and D34A variants were highly impaired in metal binding (12) and therefore, they are presumably unable to correctly assemble the M1-M2 cluster. Furthermore, the crystal structure of the D193A showed that the position of M1 was shifted by 1.8 Å in this variant (12). By contrast, the variants of the loosely M1 coordinating Asp 231 residue (D231A) and of the M3-

coordinating Asp 119 residue (D119A), which are also unable to dephosphorylate P_{II-P} , could still bind this substrate. In contrast to the D18A and D34A variants, they have retained a higher residual capacity to bind metals (12) and may therefore be able to coordinate the M1-M2 cluster. Indeed, the crystal structure of D119A variant showed that the M1-M2 cluster was unaffected but M3 was missing (12). Together, these data imply that trapping of P_{II-P} by tPphA is dependent on an intact M1-M2 cluster, but M3 is less important for the binding of phosphorylated protein. To reveal whether the metals are also required for binding unphosphorylated substrate, a binding assay was performed with Strep-tagged P_{II} and the tPphA variants D18A and D34A. As shown in Fig. 7B, these variants could bind the unphosphorylated protein, indicating that the metal core is indeed only required for the efficient binding of phosphorylated substrate, in agreement with the metal-dependence of P_{II-P} binding described above.

The human PP2C α and chimera A, which have a active metal centre, as deduced from ITC analysis and the activity towards p NPP, nearly could not recover P_{II-P} (Fig. 7C), which agrees with the lack of P_{II-P} dephosphorylation. This result indicates that the FLAP subdomain is indeed pivotal to recognize and bind the protein substrate P_{II-P} .

Discussion

As deduced from this study, three regions appear to be of particular relevance for selecting the phosphoprotein substrate, here the P_{II-P} protein, and specifying its dephosphorylation: the M1-M2 core, the FLAP subdomain and the opposing region containing the His-39 residue. The catalytic centre of the H39A variant is apparently not impaired, as revealed by the unaffected reactivity towards p NPP. However, already the activity towards phosphopeptides is substantially impaired, and the reactivity towards P_{II-P} almost vanished (Fig. 3). By contrast, H39A could still bind to P_{II-P} (Fig. 7A). This indicates that His-39 could be involved in the fine-tuned placement of the substrate into the catalytic pocket, resulting in a productive substrate-enzyme complex, rather than in a general binding of substrate.

The M1-M2 catalytic core is another important part of tPphA for binding of P_{II-P} . Structures of the PP2C member MspP (from *M. smegmatis*) in various complexes with phosphate, sulfate or the phosphate analogue cacodylate showed that two oxygen atoms of the substrate phosphate group can directly interact with M1 and M2 by bidentate coordination (8). The MspP-cacodylate complex was suggested to mimic the competent enzyme-substrate complex (8). Modelling the cacodylate molecule from the MspP structure into the tPphA structure in such a way that the distance between cacodylate and M1 and M2 remains constant, showed that the cacodylate oxygen atoms would replace the oxygen atoms from water molecules coordinated by M1 and M2 in tPphA (12), which indicates that M1-M2 of tPphA could indeed directly bind the substrate phosphate. In agreement, the tPphA variants D18A and D34A, affected in M1-M2 coordination are unable to bind P_{II-P} (Fig. 7A) but are still able to bind non-phosphorylated P_{II} (Fig. 7B). In the previous ITC and ICP-OES metal binding studies (12), the D34A variant, which coordinates M1 and M2, did not show any Mn^{2+} binding. The D18A variant binds about 0.7 Mn^{2+} per molecule. This indicates that the positively charged M1-M2 core of tPphA is critical for

trapping the phosphate group and this trapping is a crucial step for tPphA dephosphorylation. In the co-crystal structure of PYR1 with HAB1 (from *Arabidopsis thaliana*), HAB1 Glu-203 could directly form a hydrogen bond with PYR1 Ser-85. This interaction was suggested to mimic the interaction of a serine containing peptide with the catalytic center of a PP2C phosphatase (18). In this study, tPphA variant Q17E was shown to bind higher amounts of P_{II} -P than wild-type tPphA. Similar as the interaction of PYR1 and HAB1, it is likely that Glu-17 at this position could make a hydrogen bond with an anonymous residue of P_{II} -P, and this hydrogen bond may be more stable than the hydrogen bond formed by the carboxylate oxygen of Gln-17 of wild type tPphA. Therefore, Q17E could recover more P_{II} -P than wild type tPphA. By contrast, the Q17K variant binds almost no P_{II} -P. The positive charge of lysine in this position is apparently so unfavorable that this variant cannot interact with P_{II} -P (Fig. 7A). These properties of the Q17 variants verify that Gln-17 of tPphA plays an active role in interacting with P_{II} -P. In the tPphA structure (PDB: 2j82), residues Q17 and D18 located on the β 2 strand, constitute a negatively charged pocket and stabilize M2 by two bridging water molecules. In the crystal structure of other PP2Cs (3, 7 - 11), Glu or Gln at the position of tPphA Gln-17 can also indirectly interact with M2 (6).

The last part of tPphA, important for phosphoprotein recognition, appears to be the FLAP subdomain. Mutations in tPphA FLAP subdomain created variants (R160A, T138E, H161A and R169A) that have clearly altered substrate specificities. In particular, the T138E mutation, at the basis of the FLAP, is intriguing. In many other PP2C homologs, this position is occupied by an Asp or Glu residue (see Supplementary file S1 in ref. (10)). In tPphA, this replacement heavily affects enzyme activity and strongly reduces binding to P_{II} -P. The effect on enzyme activity could be caused by a global structural effect on the FLAP subdomain conformation extending to the nearby M3, which is important for catalytic activity (6, 12). Chimera A with the tPphA catalytic core and the human PP2C α FLAP could not bind to and dephosphorylate P_{II} -P but could dephosphorylate p NPP. Since all FLAP subdomain variants (except for T138A) and chimera A show less binding and impaired activity towards P_{II} -P, this part of the enzyme, which is highly variable in the different PP2C members, could play an important role in phosphoprotein selection. In agreement, the FLAP sequence of the bacterial PPM members is the segment of highest sequence variability and could represent a general specificity determinant for protein substrate selection.

We have previously argued that the response of P_{II} -P dephosphorylation towards ATP/ADP and 2-OG is mediated by the binding of these effectors to P_{II} , rather than by affecting the catalytic activity of the phosphatase directly (25). Recent crystallographic analysis showed that the binding of these effectors indeed affects the conformation of the phosphoserine-bearing T-loop (30). The new binding assay showed that in its interaction with P_{II} , tPphA behaves like a typical P_{II} receptor protein such as N-Acetyl-L-Glutamate kinase (NAGK) (32), whose interaction with P_{II} is regulated by the binding of these effector molecules (20, 25). Since the phosphorylated T-loop of P_{II} must fit into the catalytic cavity of

tPphA and expose the phosphorylated Ser-49 residue, it is conceivable that the optimal interaction requires a high degree of flexibility of the T-loop, like in the absence of effector molecules, whereas the contracted T-loop conformation, which is caused by ligation of Mg^{2+} -ATP/2-OG to P_{II} is incompatible with tPphA binding. However, in contrast to a receptor protein like NAGK or AmtB (33), the complex between tPphA and P_{II} -P is transient and could only be detected after chemical cross-linking by glutaraldehyde. The phosphatase must turn-over its substrate, which requires release after catalysis. In agreement, the non-phosphorylated P_{II} protein is a much weaker interaction partner than P_{II} -P. The enhanced binding of phosphorylated P_{II} is probably supported by the interaction between the phosphoserine-residue and M1-M2 metal centre. After catalysis, the substrate can then rapidly dissociate from the phosphatase. The phosphatase must be able to recognize its substrate protein, and therefore, fine-tuned interactions between phosphatase and substrate are necessary. Here, we have shown that the whole face of the phosphatase is involved in this recognition process, from the region around His-39 to the FLAP subdomain. Only when a productive substrate-enzyme complex is formed, then the enzyme is able to dephosphorylate its substrate. This mechanism prevents dephosphorylation of non-cognate phosphoproteins. For many bacterial PP2Cs, this recognition process seems to be sufficient, since they lack further substrate binding domains and solely depend on the specificity provided by the interaction between substrate and enzyme on the face of the phosphatase. The sequence variability of the FLAP subdomain could therefore be a clue to distinguish between the different protein substrate specificities of bacterial PP2Cs.

Experimental procedures

Cloning, Overexpression and Purification of tPphA variants. The *tPphA* gene (tlr2243) encoding tPphA was amplified from plasmid pET32a+tPphA (6) by using the T7 primers (See Table S4), which amplify genes between the T7 promoter and T7 terminator in the pET (Novagen, Darmstadt, Germany) series plasmids. The resulting PCR product, which contains an *NdeI* site at the *tPphA* start codon and a 3' terminal *XhoI* restriction site was first cloned using the pGEM-T easy vector system (Promega, Madison, USA). Following restriction of the resulting plasmid with *NdeI* and *XhoI*, the *tPphA* fragment was isolated and cloned between the *NdeI* and *XhoI* sites of His-tag expression vector pET15b-vector (Novagen, Darmstadt, Germany), generating an N-terminal fusion to the 6×His-tag sequence from the vector. The procedure of site-directed mutagenesis of tPphA was carried out with the QuickChange XL site directed mutagenesis kit (Stratagene, La Jolla, Canada). The primers for site-directed mutagenesis are shown in Table S4. All constructs were checked by DNA sequencing. For overproduction of the recombinant enzymes, the constructs were transformed into *E. coli* BL21 (DE3) cells (New England Biolabs GmbH, Frankfurt am Main, Germany) and grown in LB medium supplemented with Ampicillin (100µg/ml). When the optical density (OD_{600}) of the culture reached a value of 1 - 1.5, IPTG was added to a final concentration of 0.5 mM to induce protein overproduction. After 4-5 hours induction at 25°C, the cells were harvested by centrifugation and lysed by sonification (Branson SONIFIER 250, Danbury,

USA) on ice in a buffer consisting of 20 mM Tris-Cl, pH 7.8, 75 mM KCl, 500 mM NaCl, 5 mM MgCl₂, 0.5 mM EDTA, 0.2 mM PMSF. The lysate was centrifuged for 30 minutes at 13,000 rpm. The supernatant was centrifuged again for 30 minutes at 13,000 rpm. The clarified cell extract was used for protein purification. HIS-Select Cartridges (Sigma, Saint Louis, USA) were used to purify His-tag proteins. After purification, the proteins were dialyzed in a buffer (20 mM Hepes, pH 7.4, 75 mM KCl, 500 mM NaCl, 2 mM MgCl₂, 0.5 mM EDTA, 1 mM DTT, 50% Glycerol) and analyzed by SDS-PAGE. The concentrations of the purified proteins were determined by the Bradford method (Rotiquant, Carl Roth, Karlsruhe, Germany) and from UV spectra calculating with an absorption coefficient at 280 nm of 27960 M⁻¹cm⁻¹ (calculated from (28)).

Cloning, Overexpression and Purification of human PP2C α and the Chimeras.

His-human PP2C α was purified as described previously with no modification (12). Artificial genes for chimera A (tPphA catalytic center (1-137, 174-240) + human PP2C α FLAP (165-219)) and chimera B (human PP2C α catalytic center (1-164, 220-297) + tPphA FLAP (138-173)) were synthesized and cloned into His-tag pET15b vector by GENEART (Regensburg). Overexpression and purification of his-tagged chimeras were performed as the section of "*Cloning, Overexpression and Purification of tPphA variants*". His-tagged chimera A was purified and stored in a buffer (20 mM Hepes, pH 7.4, 75 mM KCl, 500 mM NaCl, 2 mM MgCl₂, 0.5 mM EDTA, 1 mM DTT, 50% Glycerol). Unfortunately, most of chimera B became insoluble inclusion bodies in *E. coli* BL21 (DE3) after induced by IPTG. Only residual soluble chimera B could be purified by HIS-Select Cartridges (Sigma, Saint Louis, USA). After protein purification, the soluble form chimera B could be dialysed against a buffer (20 mM Hepes, pH 7.4, 75 mM KCl, 500 mM NaCl, 2 mM MgCl₂, 0.5 mM EDTA, 1 mM DTT, 50% Glycerol), and it remained soluble. After dialysis, the concentration (0.2 μ g/ μ l) of chimera B was determined by the Bradford method. But it precipitated at once when it was added into any other buffer. Therefore, no further experiment could be performed with chimera B and the characters of chimera B were unknown.

Preparation of phosphorylated P_{II} and Strep-P_{II}. Phosphorylated P_{II} protein (P_{II}-P) was prepared from *Synechococcus elongatus* PCC 7942 as described previously with modification (29). To achieve a maximal degree of *in vivo* P_{II} phosphorylation, the cells were grown in 4.5 l BG-11 medium containing 17.6 mM NaNO₃ supplemented with 10 mM NaHCO₃ and ferric ammonium citrate was replaced by ferric citrate. When the OD₇₅₀ of the cells reached 1.0, the cells were treated with 0.5 mM L-methionine sulphoximine for 4 hours and were then harvested by centrifugation. All subsequent steps were carried out at 0 - 8°C. The cells were broken by sonification (Branson SONIFIER 250, Danbury, USA) in a buffer consisting of 50 mM Tris-Cl, pH 7.4, 4 mM EDTA; 0.1 mM PMSF. Cell debris was removed by 10 minutes centrifugation at 10000 \times g and the crude extract was cleared by high speed centrifugation at 100000 \times g for 60 minutes. This crude extract enriched with phosphorylated P_{II} was used for the section "*The activities of tPphA variants, human PP2C α and chimera A towards P_{II}-P*". The crude extract was applied to a Econo-Pac heparin cartridge (Bio-Rad, Hercules, Canada) equilibrated 10 mM Hepes, pH

7.4. Proteins were eluted with a 100 ml linear gradient of 0 - 400 mM NaCl in 10 mM Hepes, pH 7.4 at a flow rate of 1 ml/min. Fractions (4 ml) were collected in tubes containing 50 μ l of 0.4 M EDTA to prevent dephosphorylation of P_{II}-P. The P_{II}-P containing fractions were detected by immunoblot (dot-blot) analysis using P_{II}-specific antibodies. Ammonium sulphate was added to a saturation of 80% to precipitate proteins. The precipitated proteins were collected and resuspended in 10 mM Tris-Cl, pH 7.4, 150 mM NaCl, 5 mM EDTA. The solution was applied to a Superdex 200 10/300 GL column (Amersham Pharmacia, Freiburg, Germany) equilibrated in a buffer (10 mM Tris-Cl, pH 7.4, 150 mM NaCl, 5 mM EDTA) and developed in the same buffer at a flow rate of 0.5 ml/min. The P_{II}-P containing fractions were concentrated by ultrafiltration (Microcon YM-10, 10kDa cut-off, Millipore, Bedford, USA). This purified Phospho-P_{II} was used for the sections "*P_{II}- tPphA binding assay*" and "*Human PP2C α and chimera bind to P_{II}-P*". Purification of recombinant P_{II} proteins with a C-terminal-fused Strep-tag II peptide were performed according to Heinrich *et al* (34).

Assay of phosphatase activity with pNPP as artificial substrate. The activities of tPphA variants, human PP2C α and chimera A towards pNPP were assayed as described previously with modifications (6, 12). Standard assays in a volume of 250 μ l contained 0.25 μ g - 10 μ g tPphA variants, 0.25 μ g human PP2C α and 0.25 μ g - 10 μ g chimera A in a buffer consisting of 10 mM Tris-Cl, pH 8.0, 50 mM NaCl, 1 mM DTT and 2 mM MnCl₂. Reactions were started by the addition of 2 mM pNPP at 30°C and the increase in absorbance at 400 nm was measured in an ELx808 absorbance microplate reader (BioTek, Winooski, USA) against a blank reaction without enzyme. To determine the K_m for Mn²⁺, the pNPP concentration was fixed at 1.5 mM and the Mn²⁺ concentration was varied from 0.1 mM to 8 mM. For pNPP catalytic constants, the pNPP concentration was varied from 0.1 mM to 2 mM. From the linear slope of each reaction, the kinetic parameters K_m and V_{max} were calculated by non-linear hyperbolic fitting using the GraphPad Prism 4 program (GraphPad Software Inc.).

Reactivity of tPphA variants, human PP2C α and chimera A towards phosphopeptides. Three different phosphopeptides were used to assay the activities of tPphA variants and chimera A. The sequence of the three peptides are CRYRG(pS)EYTV, RRA(pT)VA, and RRA(pS)VA. CRYRG(pS)EYTV corresponds to the T-loop sequence of the P_{II} protein. In a standard assay, 0.25 μ g - 10 μ g tPphA variants, 0.25 μ g human PP2C α and 0.25 μ g - 10 μ g chimera A were reacted with 100 μ M phosphopeptides in a reaction volume of 100 μ l containing 50 mM Tris/HCl, pH 8.0, 50 mM NaCl, 2 mM MnCl₂ and 1 mM DTT. Reactions were incubated at 30°C for 2 - 10 minutes, then stopped by the addition of 50 μ l 4.7 M HCl. The released Pi was quantified colorimetrically by the malachite-green assay (35, 36). The absorbance of the solution at 630 nm was measured in ELx808 absorbance microplate reader (BioTek, Winooski, USA) against a blank reaction, which was stopped at the start point by 50 μ l 4.7 M HCl. The activity of all enzymes toward peptides was calculated with a phosphate standard.

The activities of tPphA variants, human PP2C α and chimera A towards P_{II}-P. Dephosphorylation assays of P_{II}-P were carried out in 10 mM Tris-Cl, pH 8.0, 50 mM NaCl, 1 mM DTT and 2 mM MgCl₂.

30 μ l reactions contained 5 μ l *Synechococcus* extract containing 60 ng highly phosphorylated P_{II} and 100 ng enzymes. Reactions were started by the addition of purified phosphatase. After incubation at 30°C the reactions were stopped by adding 2.5 μ l 100 mM EDTA on ice. Subsequently, the phosphorylation state of P_{II} was determined by non-denaturing PAGE and immunoblot analysis as described previously (25).

P_{II}-tPphA binding assay. Each step of the following binding assay was carried out on ice or 4°C. tPphA (10 μ g wild-type or tPphA variant proteins) was incubated with P_{II} -P (0.2 or 0.5 μ g) or Strep- P_{II} (0.2 μ g or 5 μ g) in 50 μ l of buffer I containing 1 mM Tris-Cl, pH 7.4, 2.5 mM CaCl₂, 110 mM NaCl, 0.05 mM EDTA and 0.08% (w/w) glutardialdehyde (Carl Roth, Karlsruhe, Germany). After 60 minutes, 2.5 μ l of 1 M imidazole (pH 8.0) was added to the reaction. After further incubating on ice for 15 minutes, the reaction was diluted with 420 μ l buffer II of 2.5 mM CaCl₂, 100 mM NaCl and 0.05% v/v tween-20. To extract His-tagged tPphA, 30 μ l Ni-NTA magnetic agarose beads (Qiagen, Hilden, Germany) were added. The mixture was gently mixed by rotation for one hour. Thereafter, the Ni-NTA beads were removed with a magnet and washed three times with 0.5 ml washing buffer (10 mM Tris-Cl, pH 8.0, 2.5 mM CaCl₂, 100 mM NaCl, 20 mM imidazole.). Finally, the bound proteins were eluted by denaturing the sample with 50 μ l SDS-sample buffer (75 mM Tris-Cl, pH 6.8, 1.5% DTT, 1% SDS, 10% glycerol, 0.04% bromphenol blue) at 95°C for 5 minutes. Subsequently, the eluted proteins were visualized by SDS-PAGE and immunoblot analysis as described previously (20). In order to reveal the effect of divalent cations on the binding between P_{II} and tPphA, 2.5 mM CaCl₂ was either removed or changed to 2.5 mM MgCl₂ in buffer I, buffer II and washing buffer. To test the effect of small molecule effectors such as ATP, ADP, AMP, or 2-oxoglutarate (Sigma-Aldrich, neutralized at pH 7.4 by NaOH), these metabolites were added to the cross-link reaction to final concentrations of 0.1, 1 or 3 mM. Other procedures were same as in the standard binding assay.

Human PP2C α and chimera A bind to P_{II}-P

The procedures were same as the section "*P_{II}-tPphA binding assay*".

Size exclusion chromatography and molecular weight determination by dynamic light scattering of Strep-P_{II} and tPphA cross-link products. 450 μ g tPphA was incubated with 200 μ g Strep- P_{II} in 200 μ l cross link Buffer I same as *P_{II}-tPphA binding assay*. After 60 minutes, the cross-link solution was centrifuged at 14000 rpm for 1 minute to remove any aggregate from the solution. Afterwards, 200 μ l solution was loaded onto a Superdex 200 10/300 GL column (Amersham Pharmacia, Freiburg, Germany). Size exclusion chromatography was conducted at a flow rate of 0.5 mL/min at 8°C with a run time of 40 min. The cross link products were eluted by the buffer (10 mM Tris-Cl, pH 7.4, 150 mM NaCl) filtered through a 0.02 μ m filter. Elution fractions of 0.5 ml were collected. Western-blotting was performed to check the contents of each fraction. The molecular weights of Strep- P_{II} and tPphA cross-link products were triplicately determined by dynamic light scattering using the MiniDawn TREOS detector (Wyatt, Dernbach, Germany). As a validation standard 2mg/ml bovine serum albumin (Sigma

A1900, Saint Louis, USA) was used to determine the light scattering parameters for the size exclusion chromatography setup.

Acknowledgements We thank Christina Herrmann and Oleksandra Fokina for practical help. This work was supported by DFG grant Fo195 and by GRK 685 “infection biology”.

Reference

1. Tonks NK (2006) Protein tyrosine phosphatases: from genes, to function, to disease. *Nat. Rev. Mol. Cell Biol.*, **7**, 833-846.
2. Shi Y (2009) Serine/threonine phosphatases: mechanism through structure. *Cell*, **139**, 468-484.
3. Rigden DJ (2008) The histidine phosphatase superfamily: structure and function. *Biochem. J.*, **409**, 333-348.
4. Das AK, Helps NR, Cohen PTW, & Barford D (1996) Crystal structure of the protein serine/threonine phosphatase 2C at 2.0 angstrom resolution. *Embo Journal*, **15**, 6798-6809.
5. Arino J, Casamayor A, & Gonzalez A (2011) Type 2C Protein Phosphatases in Fungi. *Eukaryotic Cell*, **10**, 21-33.
6. Schlicker C, Fokina O, Kioft N, Grune T, Becker S, Sheldrick GM, & Forchhammer K (2008) Structural analysis of the PP2C phosphatase tPphA from *Thermosynechococcus elongatus*: A flexible flap subdomain controls access to the catalytic site. *Journal of Molecular Biology*, **376**, 570-581.
7. Pullen KE, Ng HL, Sung PY, Good MC, Smith SM, & Alber T (2004) An alternate conformation and a third metal in PstP/Ppp, the M-tuberculosis PP2C-family Ser/Thr protein phosphatase. *Structure*, **12**, 1947-1954.
8. Bellinzoni M, Welhenkel A, Shepard W, & Alzari PM (2007) Insights into the catalytic mechanism of PPM Ser/Thr phosphatases from the atomic resolution structures of a mycobacterial enzyme. *Structure*, **15**, 863-872.
9. Rantanen MK, Lehtio L, Rajagopal L, Rubens CE, & Goldman A (2007) Structure of *Streptococcus agalactiae* serine/threonine phosphatase - The subdomain conformation is coupled to the binding of a third metal ion. *Febs Journal*, **274**, 3128-3137.
10. Wehenkel A, Bellinzoni M, Schaeffer F, Villarino A, & Alzari PM (2007) Structural and binding studies of the three-metal center in two mycobacterial PPM Ser/Thr protein phosphatases. *Journal of Molecular Biology*, **374**, 890-898.
11. Melcher K, Ng LM, Zhou XE, Soon FF, Xu Y, Suino-Powell KM, Park SY, Weiner JJ, Fujii H, Chinnusamy V, Kovach A, Li J, Wang YH, Li JY, Peterson FC, Jensen DR, Yong EL, Volkman BF, Cutler SR, Zhu JK, & Xu HE (2009) A gate-latch-lock mechanism for hormone signalling by abscisic acid receptors. *Nature*, **462**, 602-610.

12. Su JY, Schlicker C, & Forchhammer K (2011) A Third Metal Is Required for Catalytic Activity of the Signal-transducing Protein Phosphatase M tPphA. *Journal of Biological Chemistry*, **286**, 13481-13488.
13. Forchhammer K & Demarsac NT (1994) The P-II Protein in the Cyanobacterium *Synechococcus* Sp Strain Pcc-7942 Is Modified by Serine Phosphorylation and Signals the Cellular N-Status. *Journal of Bacteriology*, **176**, 84-91.
14. Forchhammer K (2008) P-II signal transducers: novel functional and structural insights. *Trends in Microbiology*, **16**, 65-72.
15. Kaneko T, Sato S, Kotani H, Tanaka A, Asamizu E, Nakamura Y, Miyajima N, Hirosawa M, Sugiura M, Sasamoto S, Kimura T, Hosouchi T, Matsuno A, Muraki A, Nakazaki N, Naruo K, Okumura S, Shimpo S, Takeuchi C, Wada T, Watanabe A, Yamada M, Yasuda M, & Tabata S. (1996) Sequence analysis of the genome of the unicellular cyanobacterium *Synechocystis* sp. strain PCC6803. II. Sequence determination of the entire genome and assignment of potential protein-coding regions. *Dna Research*, **3**, 109-136.
16. Zhang CC, Gonzalez L, & Phalip V (1998) Survey, analysis and genetic organization of genes encoding eukaryotic-like signaling proteins on a cyanobacterial genome. *Nucleic Acids Research*, **26**, 3619-3625.
17. Irmiler A & Forchhammer K (2001) A PP2C-type phosphatase dephosphorylates the PII signaling protein in the cyanobacterium *Synechocystis* PCC 6803. *Proc. Natl. Acad. Sci. U. S. A*, **98**, 12978-12983.
18. Dupeux F, Antoni R, Betz K, Santiago J, Gonzalez-Guzman M, Rodriguez L, Rubio S, Park SY, Cutler SR, Rodriguez PL, & Marquez JA (2011) Modulation of Abscisic Acid Signaling in Vivo by an Engineered Receptor-Insensitive Protein Phosphatase Type 2C Allele. *Plant Physiology*, **156**, 106-116.
19. Arcondeguy T, Jack R, & Merrick M (2001) P-II signal transduction proteins, pivotal players in microbial nitrogen control. *Microbiology and Molecular Biology Reviews*, **65**, 80-105.
20. Forchhammer K & Hedler A (1997) Phosphoprotein PII from cyanobacteria--analysis of functional conservation with the PII signal-transduction protein from *Escherichia coli*. *Eur. J. Biochem.*, **244**, 869-875.
21. Forchhammer K (2004) Global carbon/nitrogen control by PII signal transduction in cyanobacteria: from signals to targets. *FEMS Microbiol. Rev.*, **28**, 319-333.
22. Ninfa AJ & Jiang P (2005) PII signal transduction proteins: sensors of alpha-ketoglutarate that regulate nitrogen metabolism. *Current Opinion in Microbiology*, **8**, 168-173.
23. Jiang P & Ninfa AJ (2007) *Escherichia coli* PII signal transduction protein controlling nitrogen assimilation. Acts as a sensor of adenylate energy charge in Vitro. *Biochemistry*, **46**, 12979-12996.

24. Yildiz O, Kalthoff C, Raunser S, & Kuhlbrandt W (2007) Structure of GlnK1 with bound effectors indicates regulatory mechanism for ammonia uptake. *Embo Journal*, **26**, 589-599.
25. Ruppert U, Irmeler A, Kloft N, & Forchhammer K (2002) The novel protein phosphatase PphA from *Synechocystis* PCC 6803 controls dephosphorylation of the signalling protein PII. *Mol. Microbiol.*, **44**, 855-864.
26. Migneault I, Dartiguenave C, Bertrand MJ, & Waldron KC (2004) Glutaraldehyde: behavior in aqueous solution, reaction with proteins, and application to enzyme crosslinking. *Biotechniques*, **37**, 790-802.
27. Hermanson, G. (2008) Glutaraldehyde, in *Bioconjugate Techniques*, 2nd Ed., pp 265-268, Academic Press, New York.
28. www.expasy.ch/tools/protparam.html
29. Irmeler A, Sanner S, Dierks H, & Forchhammer K (1997) Dephosphorylation of the phosphoprotein P(II) in *Synechococcus* PCC 7942: identification of an ATP and 2-oxoglutarate-regulated phosphatase activity. *Mol. Microbiol.*, **26**, 81-90.
30. Fokina O, Chellamuthu VR, Forchhammer K, & Zeth K (2010) Mechanism of 2-oxoglutarate signaling by the *Synechococcus elongatus* PII signal transduction protein. *Proc. Natl. Acad. Sci. U. S. A.*, **107**, 19760-19765.
31. Llacer JL, Espinosa J, Castells MA, Contreras A, Forchhammer K, & Rubio V (2010) Structural basis for the regulation of NtcA-dependent transcription by proteins PipX and PII. *Proc. Natl. Acad. Sci. U. S. A.*, **107**, 15397-15402.
32. Beez S, Fokina O, Herrmann C, & Forchhammer K (2009) N-acetyl-L-glutamate kinase (NAGK) from oxygenic phototrophs: P(II) signal transduction across domains of life reveals novel insights in NAGK control. *J. Mol. Biol.*, **389**, 748-758.
33. Heinrich A, Woyda K, Brauburger K, Meiss G, Detsch C, Stulke J, & Forchhammer K (2006) Interaction of the membrane-bound GlnK-AmtB complex with the master regulator of nitrogen metabolism TnrA in *Bacillus subtilis*. *J. Biol. Chem.*, **281**, 34909-34917.
34. Heinrich A, Maheswaran M, Ruppert U, & Forchhammer K (2004) The *Synechococcus elongatus* P signal transduction protein controls arginine synthesis by complex formation with N-acetyl-L-glutamate kinase. *Mol. Microbiol.*, **52**, 1303-1314.
35. Vanveldhoven PP & Mannaerts GP (1987) Inorganic and Organic Phosphate Measurements in the Nanomolar Range. *Analytical Biochemistry*, **161**, 45-48.
36. Ekman P & Jager O (1993) Quantification of Subnanomolar Amounts of Phosphate Bound to Seryl and Threonyl Residues in Phosphoproteins Using Alkaline-Hydrolysis and Malachite Green. *Analytical Biochemistry*, **214**, 138-141.

FIGURE LEGENDS

Fig. 1. The crystal structure of tPphA (PDB: 2J86, generated by PyMOL 0.99). The amino acids that were analyzed by site-directed mutagenesis are indicated. Metal 1, Metal 2 and Metal 3 (M1, M2 and M3) constitute the catalytic center of tPphA.

Fig. 2. The strategy of exchanging the FLAP subdomain in tPphA and human PP2C α to generate two chimeras. In Chimeras A and B, the FLAP subdomains of tPphA and the catalytic core of human PP2C α FLAP were swapped. The tPphA FLAP subdomain is labeled in blue, the human PP2C α FLAP subdomain is labeled in green. Only the catalytic domain (1-297) of human PP2C α was used, whereas the C-terminal segment (298-382, grey α helices in the figure) was truncated.

Fig. 3. Enzymatic assays of wild-type tPphA and the variants A. B. Relative activities of tPphA variants, human PP2C α and chimera A towards different substrates. The activities of wild-type tPphA towards five substrates were set as 100% and the activities of other enzymes towards these five substrates were adjusted accordingly. p NPP indicates the value for K_{cat}/K_m from the p NPP assay (Table S1). pT-peptide indicates the relative activity with RRA(pT)VA as substrate, pS-peptide indicates the activity with RRA(pS)VA peptide as substrate and T-loop peptide indicates the activity towards the CRYRG(pS)EYTV peptide (Table S2). P_{II}-P indicates the initial activity of P_{II}-P dephosphorylation (retrieved from the initial slope as shown in the curves of Fig. S1 C, S1 D and S1 E).

Fig. 4 A. P_{II}-P recovered by co-purification with tPphA after glutaraldehyde crosslinking in buffer containing Ca²⁺, Mg²⁺ or no divalent cation (-). 0.5 μ g P_{II}-P was used in the binding assay. **B.** Dephosphorylation of P_{II}-P during incubation with tPphA. 0.5 μ g P_{II}-P was incubated with 10 μ g tPphA on ice in different buffers for 2 hours, corresponding to the incubation time during the P_{II}-P-tPphA binding assay. The reaction volume was 50 μ l containing 110 mM NaCl together with either 2.5 mM Ca²⁺, 2.5 mM Mg²⁺, 5 mM EDTA, or without additions, as indicated above. After 2 h incubation, the phosphorylation status of P_{II} was determined by non-denaturing PAGE and immunoblot analysis as described previously (20). **C.** Comparison of P_{II}-P (0.2 μ g) and Strep-P_{II} (0.2 μ g) binding to tPphA (10 μ g) in Ca²⁺-containing buffer. **D.** Strep-P_{II} recovered by co-purification with tPphA after glutaraldehyde crosslinking in buffer containing Ca²⁺, Mg²⁺ or no divalent cation (-). 5 μ g Strep-P_{II} was used in the binding assay. **E.** The signal intensity of recovered P_{II} ((P_{II})1, (P_{II})2, (P_{II})3 and cross link products) was quantified by densitometry and the signal intensity of recovered P_{II}-P or Strep-P_{II} in Ca²⁺ buffer was set as 100%.

Fig. 5. Gel filtration analysis of Strep-P_{II} – tPphA cross-link reactions. **A.** Chromatographic separation of a non-cross-linked mixture of 450 μ g of tPphA and 200 μ g Strep-P_{II} on a Superdex 200 10/300 GL column. The molecular weight of Strep-P_{II} and tPphA was determined by the dynamic light scattering as 36 kDa and 28 kDa, respectively. **B.** The same separation as in A, but after the tPphA-Strep-P_{II} cross linking reaction as described in Experimental procedures. The average molecular weight of cross link products was determined by dynamic light scattering as 64kDa.

Fig. 6. Effects of ATP, ADP, AMP and 2-oxoglutarate (2OG) on the binding of P_{II}-P to tPphA. All assays were performed in standard Ca²⁺ buffer. Binding assays of wild-type tPphA with P_{II}-P were performed in the absence of effector molecules (0) or in the presence of either 0.1, 1 or 3 mM ATP, 2-oxoglutarate (2OG), ADP or AMP, or in the presence of a mixture of ATP and 2-oxoglutarate, each present at 0.1, 1 or 3 mM as indicated above. The anti-P_{II} immunoblot revealing the amount of recovered P_{II} protein is shown.

Fig. 7. A. Assay of P_{II}-P binding to wild-type tPphA (WT) and the variants. The recovery of P_{II} is shown by anti P_{II} immunoblotting. **B.** D18A and D34A bind similar amount of non-phosphorylated Strep-P_{II} as wild-type tPphA in Ca²⁺ buffer. **C.** Assay of P_{II}-P binding to tPphA, Chimera A and human PP2C α , recovery of P_{II} as visualized by anti P_{II} immunoblotting. These assays were performed three times with similar results. All assays were performed as described in *Experimental Procedures*.

Fig. 1.

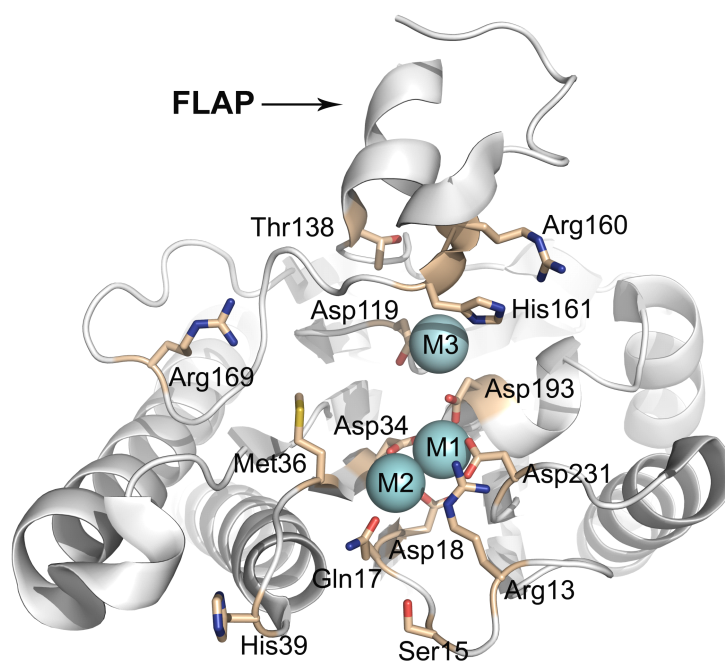


Fig. 2.

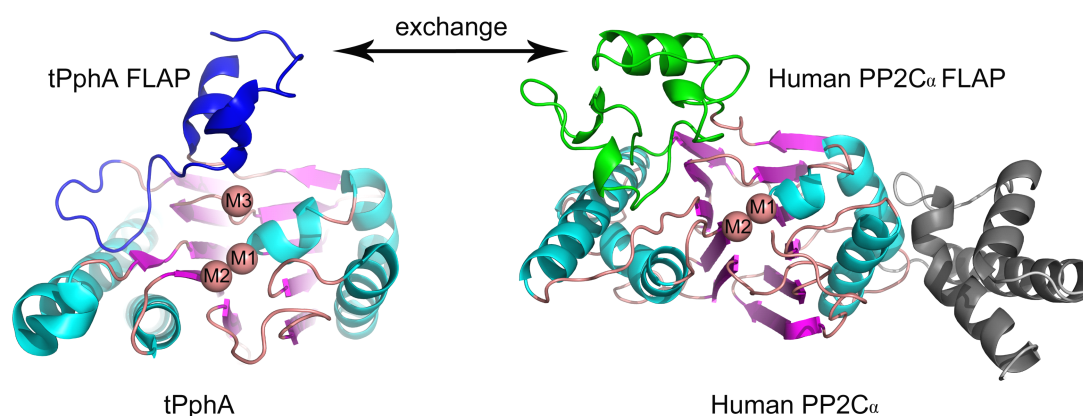


Fig. 3.

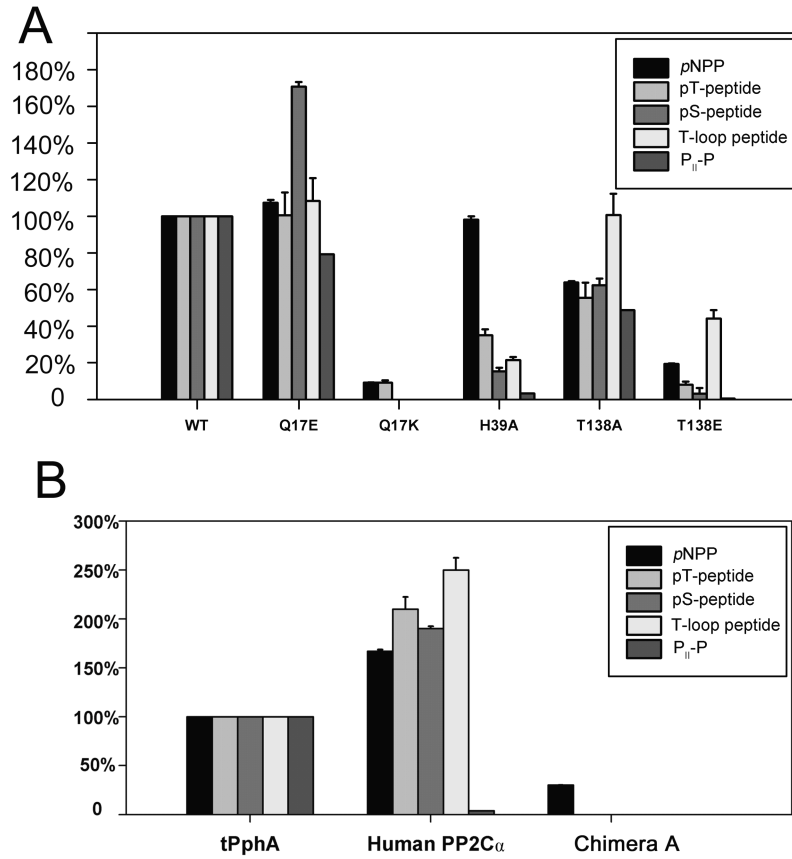


Fig. 4.

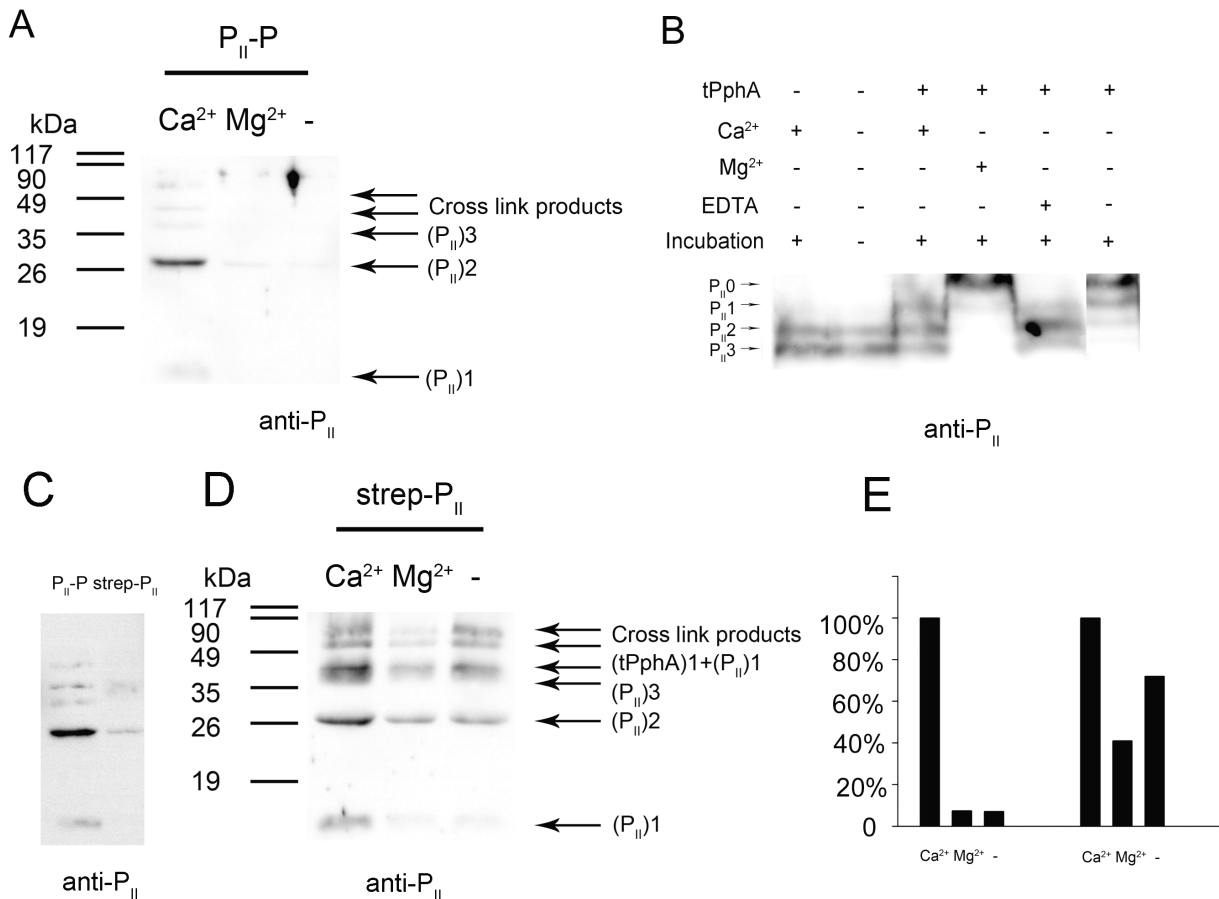


Fig. 5.

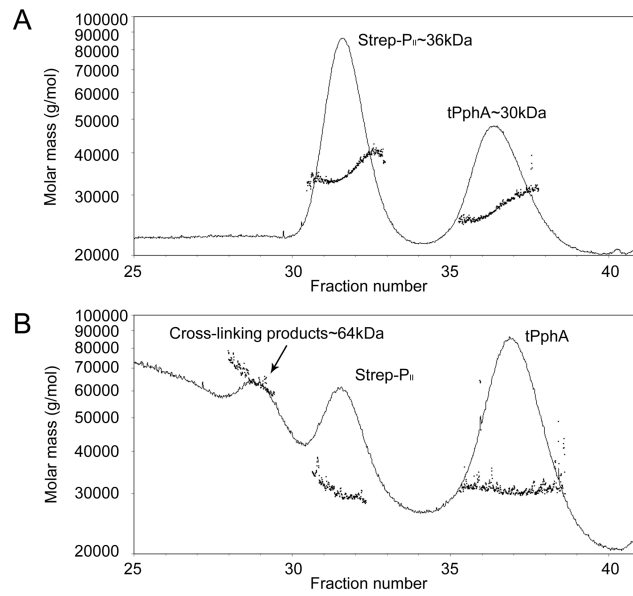


Fig. 6.

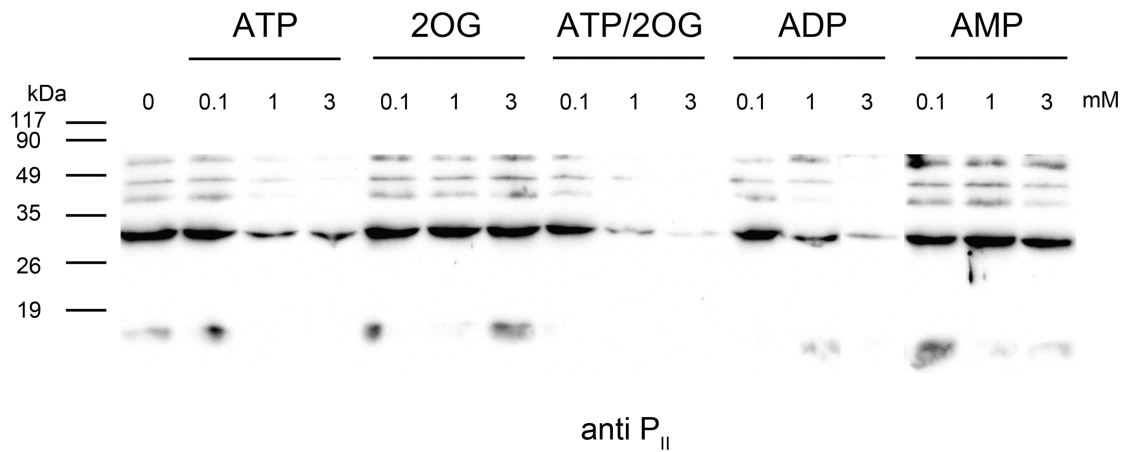
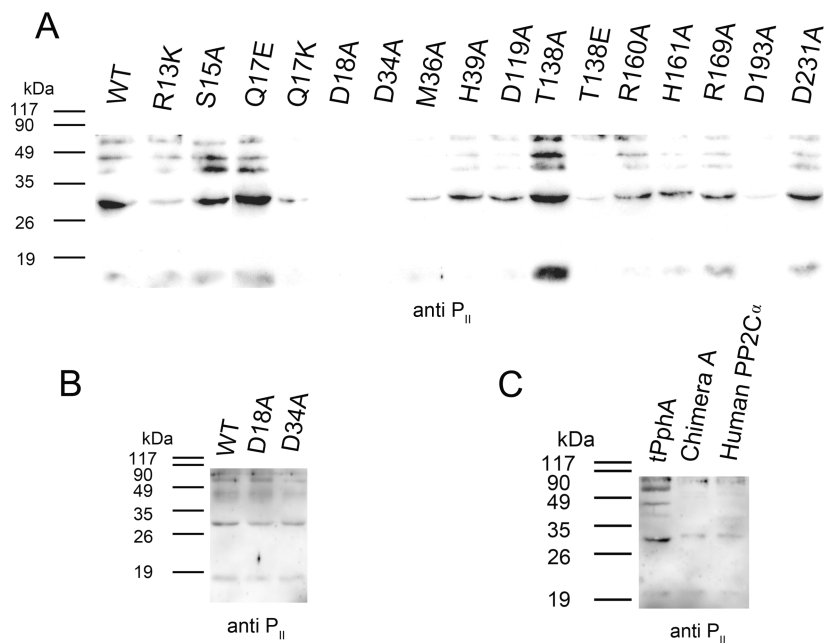


Fig. 7.



Supplementary files

Table S1. Kinetic parameters of tPphA and its variants towards ρ NPP.

ρ NPP assays were carried out as described in Experimental procedures. From the apparent reaction velocities of three independent repetitions, the kinetic parameters were calculated by linear fitting using the program GraphPad Prism 4. \pm sign is a standard error. The results were obtained from single preparations of tPphA variants, human PP2C α and chimera A purifications and the data come from single experiments.

	K_m [mM]	K_{cat} [s^{-1}]	K_{cat}/K_m	K_m [mM]
	(ρ NPP)	ρ NPP	[$s^{-1} M^{-1}$]	Mn ²⁺
WT	0.47 \pm 0.070	0.85 \pm 0.055	1809 \pm 117	0.57 \pm 0.088
R13K	0.88 \pm 0.075	0.60 \pm 0.026	682 \pm 30	0.96 \pm 0.052
S15A	0.42 \pm 0.038	0.83 \pm 0.020	1976 \pm 48	0.57 \pm 0.042
Q17E	0.66 \pm 0.055	1.28 \pm 0.050	1939 \pm 76	0.74 \pm 0.062
Q17K	1.02 \pm 0.090	0.17 \pm 0.008	167 \pm 8	2.03 \pm 0.187
M36A	0.81 \pm 0.059	0.26 \pm 0.009	321 \pm 11	0.78 \pm 0.049
H39A	0.62 \pm 0.044	1.10 \pm 0.036	1774 \pm 58	0.68 \pm 0.071
T138A	0.45 \pm 0.052	0.52 \pm 0.025	1156 \pm 56	0.90 \pm 0.072
T138E	0.74 \pm 0.065	0.26 \pm 0.011	351 \pm 15	4.10 \pm 0.33
R160A	0.83 \pm 0.071	0.26 \pm 0.011	313 \pm 13	1.34 \pm 0.120
H161A	0.57 \pm 0.041	0.57 \pm 0.018	1000 \pm 32	0.82 \pm 0.053
R169A	0.61 \pm 0.062	0.49 \pm 0.023	803 \pm 38	1.29 \pm 0.118
Human PP2C α	0.45 \pm 0.192	1.37 \pm 0.259	3044 \pm 576	0.48 \pm 0.15
Chimera A	0.51 \pm 0.170	0.16 \pm 0.024	314 \pm 47	0.63 \pm 0.093

Table S2. The activity of tPphA and its variants towards three phosphopeptides

Reactions were performed in the buffer as described in Experimental procedures. Triplicate assays were used. \pm sign is a standard error. The results were obtained from single preparations of tPphA variants, human PP2C α and chimera A purifications and the data come from single experiments.

nmol/min/ug	pT-peptide	pS-peptide	T-loop peptide
WT	7.73 \pm 1.10	3.06 \pm 0.21	4.22 \pm 0.36
R13K	4.61 \pm 0.03	0.61 \pm 0.13	1.02 \pm 0.10
S15A	8.96 \pm 0.06	3.11 \pm 0.09	4.34 \pm 0.21
Q17E	7.50 \pm 0.06	5.22 \pm 0.29	4.50 \pm 0.25
Q17K	0.68 \pm 0.01	-	-
M36A	3.77 \pm 0.01	0.52 \pm 0.01	0.61 \pm 0.02
H39A	2.65 \pm 0.17	0.47 \pm 0.07	0.89 \pm 0.02
T138A	4.13 \pm 0.15	1.90 \pm 0.09	4.20 \pm 0.37
T138E	0.59 \pm 0.05	0.098 \pm 0.08	1.83 \pm 0.03
R160A	3.51 \pm 0.06	1.72 \pm 0.21	2.33 \pm 0.12
H161A	0.87 \pm 0.01	0.21 \pm 0.04	1.61 \pm 0.05
R169A	4.26 \pm 0.09	0.70 \pm 0.04	2.17 \pm 0.13
Human PP2C α	16.2 \pm 0.96	5.81 \pm 0.08	10.55 \pm 0.53
Chimera A	-	-	-

-* means the activity is below 0.01 nmol/min/ug

Table S3: The affinity and thermodynamic parameters of tPphA, chimera A and human PP2C α from ITC assay

K_d is given in micromolars, and ΔH is given in kcal/mol

Fitting model	tPphA (from reference 12)			Chimera A		
	Kd ₁	Kd ₂	Kd ₃	Kd ₁	Kd ₂	Kd ₃
Three-step sequential binding model	18	61	18	24	237	35
	ΔH_1	ΔH_2	ΔH_3	ΔH_1	ΔH_2	ΔH_3
	-26	69	-74	-249	453	-365
	hPP2C α (from reference 12)					
Two-step sequential binding model	Kd ₁			Kd		
	0.05			0.05		
	ΔH_1			ΔH_2		
	-15			17		

Table S4: Primers used for PCR amplification of tPphA and for site-directed mutagenesis

T7	5'; 5'-TAATACGACTCACTATAGGG-3' 3'; 5'-GCTAGTTATTGCTCAGCGG-3'
R13K	5'; 5'-CTGACTGTGGTCTGATTAAGAAAAGCAATCAGGATGC-3' 3'; 5'-GCATCCTGATTGCTTTTCTTAATCAGACCACAGTCAG-3'
S15A	5'; 5'-GTGGTCTGATTGCGCAAAGCTAATCAGGATGCTTTTTA-3' 3'; 5'-TAAAAAGCATCCTGATTAGCTTTGCGAATCAGACCAC-3'
Q17E	5'; 5'-CTGATTCGCAAAGCAATGAAGATGCTTTTTATATTGATG-3' 3'; 5'-CATCAATATAAAAAGCATCTTCATTGCTTTTGCGAATCAG-3'
Q17K	5'; 5'-CTGATTCGCAAAGCAATAAAGATGCTTTTTATATTGATG-3' 3'; 5'-CATCAATATAAAAAGCATCTTTATTGCTTTTGCGAATCAG-3'
M36A	5'; 5'-TATTGTTGCAGATGGCGCTGGGGGACACGCCGGCG-3' 3'; 5'-CGCCGGCGTGTCCCCCAGCGCCATCTGCAACAATA-3'
H39A	5'; 5'-GGCATGGGGGGAGCTGCCGGCGGCGAGG-3' 3'; 5'-CCTCGCCGCGGCAGCTCCCCCATGCC-3'
T138A	5'; 5'-GATTACCAGCGACCACGCTTGGATTGCTCAAGCCG-3' 3'; 5'-CGGCTTGAGCAATCCAAGCGTGGTCGCTGGTAATC-3'
T138E	5'; 5'-GATTACCAGCGACCACGAATGGATTGCTCAAGCCG-3' 3'; 5'-CGGCTTGAGCAATCCATTCGTGGTCGCTGGTAATC-3'
R160A	5'; 5'-CGGCAGCATCCGTGGGCTCATGTGCTCTCCAG-3' 3'; 5'-CTGGGAGAGCACATGAGCCCACGGATGCTGCCG-3'

Figure S1 A.B. Time course assay of phospho- P_{II} dephosphorylation by tPphA varieties. Following the indicated incubation times in the presence of phosphatase, the phosphorylated forms of P_{II} were separated by Native-PAGE and visualized by immunoblotting. The non-phosphorylated form P_{II0} and the phosphorylated forms containing one, two or three phosphorylated subunits (P_{II1} ; P_{II2} and P_{II3}) are indicated. **C.** Graphical representation of 45 minutes P_{II} -P dephosphorylation assays analyzed by non-denaturing gels as shown in Fig. S1A, for tPphA variants (WT (wild-type tPphA), R13K, S15A, Q17E, T138A, H161A, R169A). **D.** Graphical representation of 90 minutes P_{II} -P dephosphorylation assays analyzed by non-denaturing gels as shown in Fig. S1 B, for tPphA variants (Q17K, M36A, H39A, T138E, R160A, H161A, D193A). **E.** Time course assay of phospho- P_{II} dephosphorylation by tPphA, human PP2C α and chimera A

Figure S2. Mn^{2+} binding to tPphA, chimera A and human PP2C α studied by ITC. All ITC measurements were performed as described previously with no modification (12). The raw data are shown in this figure. The integrated heat data, corrected for the heat of dilution are shown in the Table S3.

Figure S3 A. Inhibitory effect of Ca^{2+} on the relative activities of tPphA towards ρNPP , pT-peptide, T-loop peptide and $\text{P}_{\text{II}}\text{-P}$. 100% activity of tPphA was achieved with MnCl_2 ; towards ρNPP the 100% value was 2.57 nmol/min/ μg , 100% activity of tPphA towards pT-peptide was 0.87 nmol/min/ μg , 100% activity of tPphA towards T-loop peptide was 0.78 nmol/min/ μg . Inhibitory effect of Ca^{2+} on the dephosphorylation of $\text{P}_{\text{II}}\text{-P}$ by wild-type tPphA. $\text{P}_{\text{II}}\text{-P}$ dephosphorylation assay was carried out under standard conditions for 15 min. The degree of P_{II} dephosphorylation was determined densitometrically from Fig. S3 B. "1 2 3 4 5" in the figure means five assays were performed in the reaction buffers containing 2mM Mn^{2+} , 2mM $\text{Mn}^{2+}/2\text{mM Ca}^{2+}$, 2mM Mg^{2+} , 2mM $\text{Mg}^{2+}/2\text{mM Ca}^{2+}$, and 2mM Ca^{2+} , respectively. **B.** Inhibitory effect of Ca^{2+} on the dephosphorylation of $\text{P}_{\text{II}}\text{-P}$ by wild-type tPphA. Dephosphorylation assay was carried out under standard conditions for 15 min, as described in *Experimental Procedures*, without divalent ions (lane 1), or in the presence of 2 mM divalent cations, separately or in mixtures, as indicated. Ca^{2+} has a stronger inhibitory effect in combination with Mg^{2+} than with Mn^{2+} .

Figure S4 A. B. Glutaraldehyde (GDA) cross-linking followed by Ni-NTA affinity purification (pull-down, PD) using His-tPphA (10 μg) with $\text{P}_{\text{II}}\text{-P}$ (0.5 μg). 15 % SDS gels were loaded with aliquots of the reaction assays before pull down (lanes 1-3) and with the elution fractions after pull-down (lanes 4-7), together with protein mobility controls. From lane 1 to 7 (left to right): the control experiments without pull-down separation (lanes 1-3) and the pull-down assays in lanes 4-7. All the experiments were performed in a buffer containing 2.5 mM Ca^{2+} . Presence or absence of glutardialdehyde (GDA) or P_{II} or tPphA is as indicated on top. Other assay conditions were as described in *Experimental Procedures*. The gels were immunoblot analyzed with **(A)** anti- P_{II} antibodies or **(B)** anti-tPphA antibodies. The mobility of monomeric, dimeric or trimeric P_{II} is indicated as $(\text{P}_{\text{II}})1$, $(\text{P}_{\text{II}})2$ or $\text{P}(\text{II})3$, respectively, the mobility of monomeric tPphA or dimeric tPphA is indicates as $(\text{tPphA})1$ or $(\text{tPphA})2$.

Figure S5 A.B. Recovery of tPphA from pull-down assays shown in Fig. 6 and 7A.

Figure S6 A. Binding assays of $\text{P}_{\text{II}}\text{-P}$ with tPphA variants Q17E and T138A in the absence of effectors (0) or in the presence of 3 mM ATP, 2-oxoglutarate, ATP together with 2-oxoglutarate, ADP or AMP. **B.** Recovery of tPphA from pull-down assays shown in Figure S6A. These assays were performed three times with similar results.

Figure S1

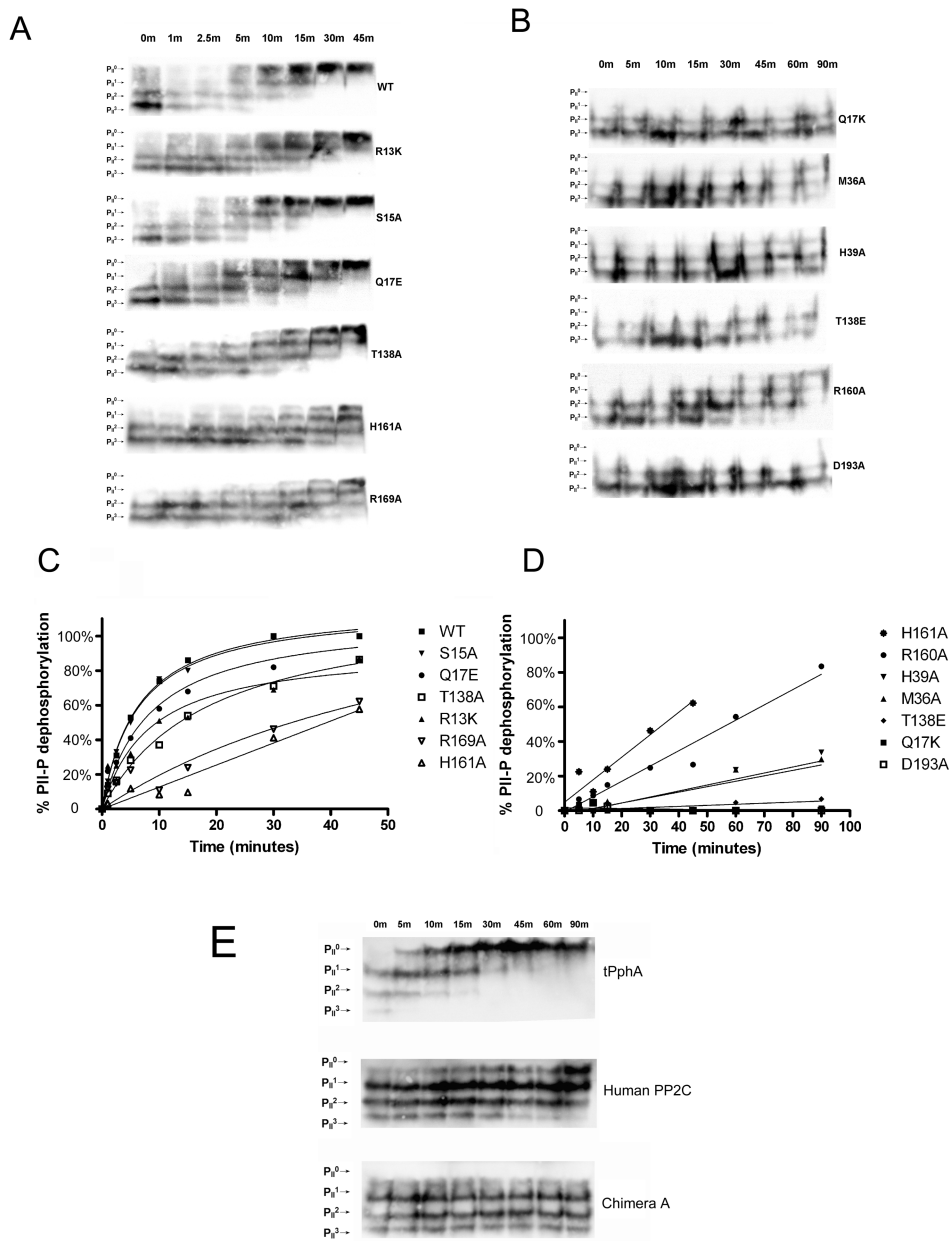


Figure S2

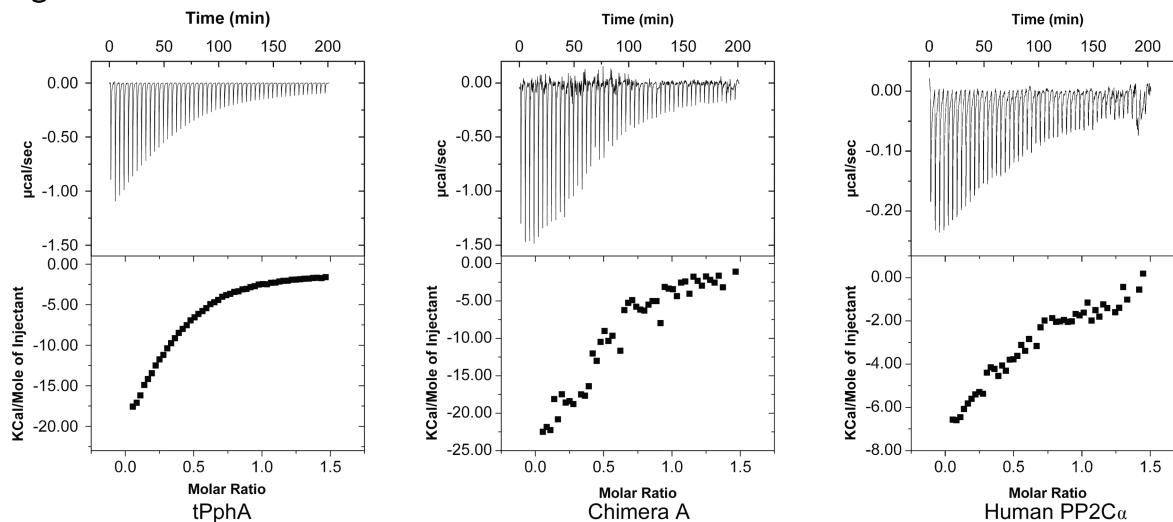


Figure S3

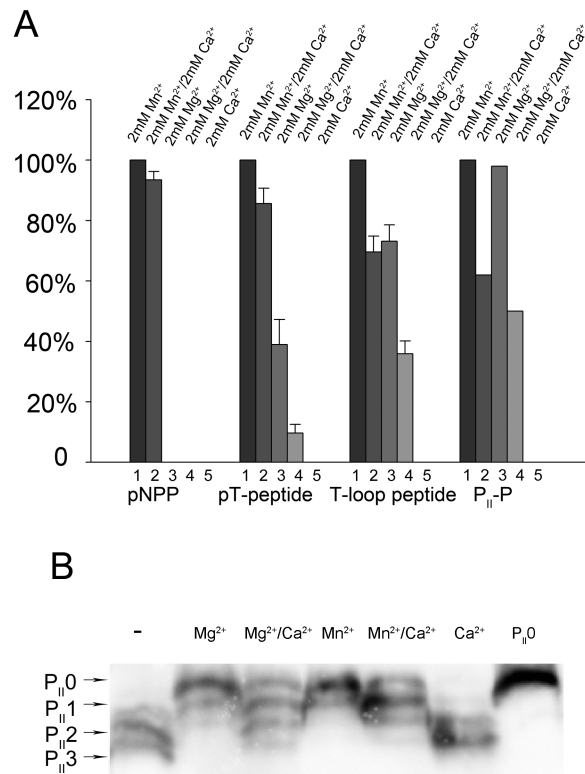


Figure S4

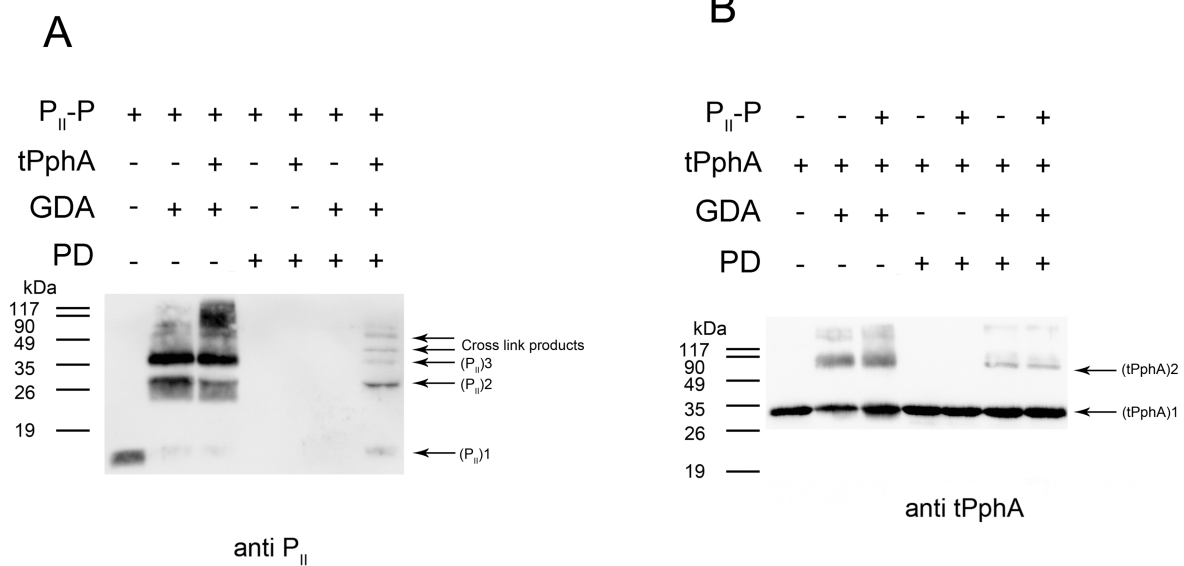


Figure S5

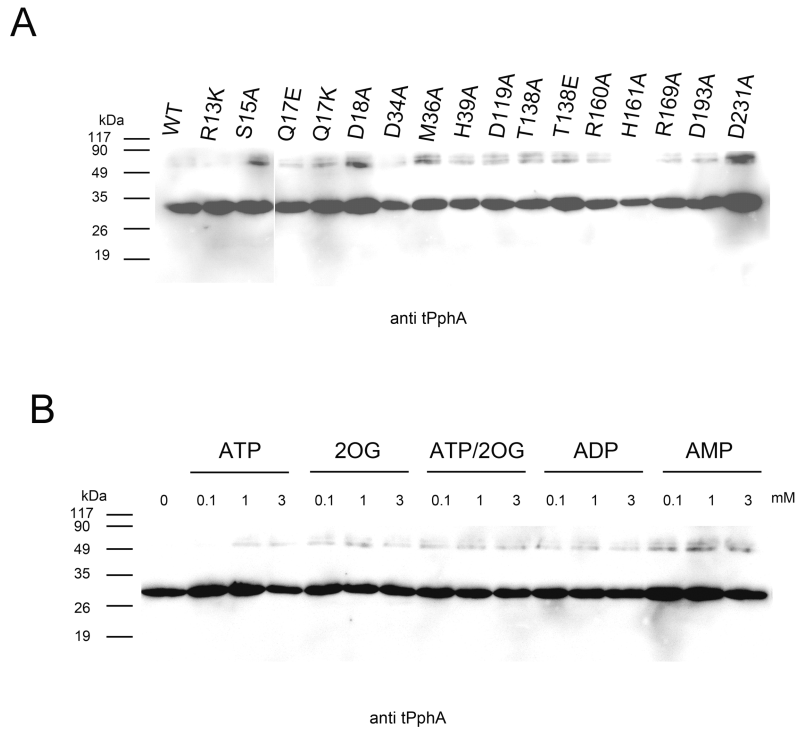
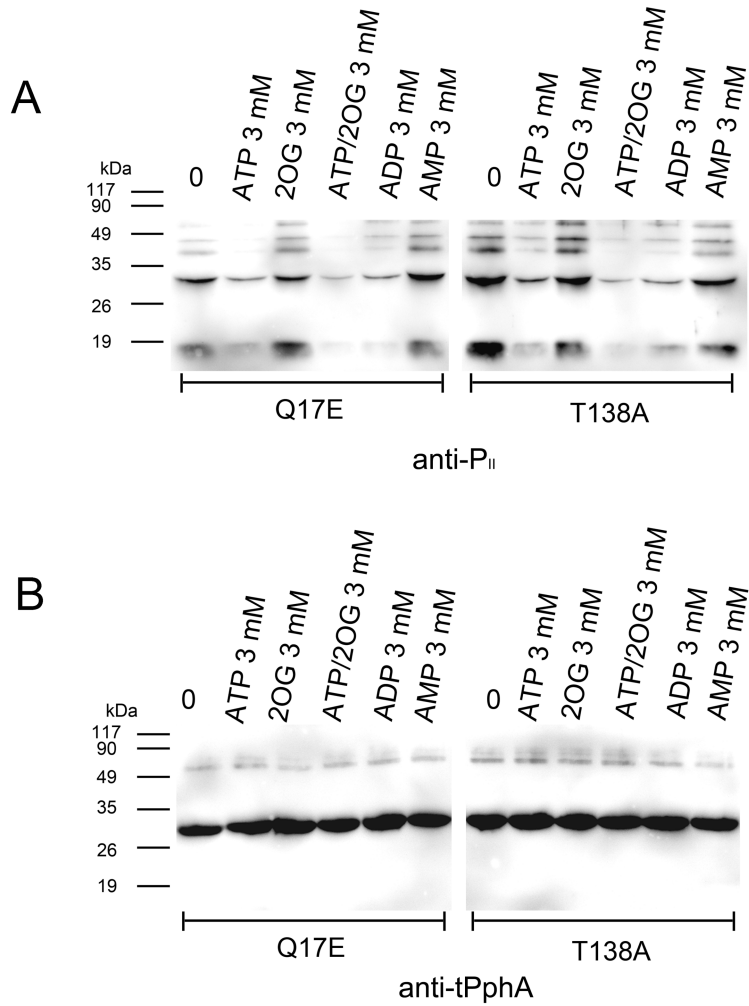


Figure S6



Chapter 5. Investigation of a key arginine residue close to the catalytic center of PPM/PP2C type protein phosphatase

Abstract

A highly conserved arginine residue is close to the catalytic center of PPM/PP2C type protein phosphatase. The crystal structures of PPM/PP2Cs revealed that the guanidium side chain of this arginine residue can adopt different conformations and bind different ligands, suggesting this residue could play different roles during PPM/PP2C catalysis. Arginine 13 of tPphA, a PPM/PP2C type phosphatase from *Thermosynechococcus elongatus*, was mutated to 16 different amino acids in this report. The generated variants were tested towards *p*-nitrophenyl phosphate and phosphopeptides. Arginine 13 of tPphA was proven to assist tPphA to bind *p*-nitrophenyl phosphate, since twelve variants showed 3-7 times higher K_m values than wild type tPphA towards *p*-nitrophenyl phosphate and four variants (R13D, R13F, R13L, and R13W) had no activity towards *p*-nitrophenyl phosphate. The fact that all variants could dephosphorylate phosphopeptides means that this arginine residue is not critically important for binding phosphopeptides. Except R13K, all variants showed low activity towards different substrates, suggesting that this highly conserved residue might play a role in stabilizing the transition state of the phosphate of substrates.

Introduction

Protein serine/threonine phosphatase comprises three main subfamilies: phosphoprotein phosphatases, the aspartate-based phosphatases, and metal-dependent protein phosphatases (PPM) (1). The human PPM member PP2C α (2) has been the defining representative of PPM family, therefore also referred as the PP2C family. PP2C phosphatases are widely present in eukaryotes and prokaryotes where they regulate diverse signaling pathways involved in central cellular processes, such as cell proliferation, stress responses or metabolic activity (3).

Recently, the crystal structures of bacterial and plant PP2Cs show that five highly conserved aspartate residues constitute a negative charged pocket that coordinates three Mg²⁺/Mn²⁺ (M1, M2, and M3) ions to form the catalytic center (4-9). All these three metal ions were proven to be essential for the activity of PP2Cs, since the variants of the five conserved aspartate residues showed no or residual activity towards different substrates (2, 10, 11). The biochemical and atomic studies of human PP2C α revealed that one water molecule bridged by M1 and M2 was

supposed to nucleophilically attack the phosphorous atom of substrates in an S_N2 mechanism (2, 12). Recently, we could show by site-directed mutagenesis of the M3 coordinating aspartate residues in the catalytic core of tPphA (a PP2C member from *Thermosynechococcus elongatus*), that M3 is required for catalysis, presumably by activating a water molecule as proton donor for the leaving group (10).

Close to the catalytic center of PP2C, there are several highly conserved residues. The function of these highly conserved residues were not fully understood. The crystal structures of PP2C showed that the guanidium side chain of a arginine residue could adopt different conformation suggesting this residue could play different roles during catalysis. The crystal structures of human PP2C α (2) and MspP (a PP2C member from *Mycobacterium smegmatis*) (6) in complex with a phosphate ion revealed one oxygen atom of phosphate ion is hydrogen bonded by this highly conserved arginine residue. Site-directed mutagenesis of human PP2C α and enzymatic assays showed that this arginine residue (Arg-33 of human PP2C α) is important for binding *p*-nitrophenyl phosphate (pNPP), since the variant R33A show a 8-fold higher K_m than wild-type phosphatase (12). The crystal structures of MspP in complex with phosphate homologue molecules sulphate and cacodylate were also resolved (6). In the crystal structure of MspP with the sulphate ion, the conserved arginine residue (Arg-17 of MspP) could make hydrogen bond with this sulphate ion which is far away from the catalytic center of MspP. It implies Arg-17 might assist MspP bind or release inorganic phosphate (6). In the crystal structure of MspP with cacodylate, MspP Arg-17 makes a hydrogen bond with a water instead of one oxygen atom of cacodylate, since the only two oxygen atoms of cacodylate are coordinated by M1 and M2. A *Sa*STP (a PP2C member from *Streptococcus agalactiae*) crystal with four monomers (A, B, C, and D) in the asymmetric unit revealed monomer C in a conformation, which interacted with a flexible loop (termed FLAP subdomain) of the adjacent monomer A (7). The highly conserved arginine residue (Arg-13 of *Sa*STP) side chain shows two different conformations in the active site of *Sa*STP in monomer A and C respectively. In the monomer A structure, its conformation is similar to human PP2C α , where it binds phosphate (2). In monomers C, Arg-13 adopts a new conformation which is similar as Arg-17 of MspP in complex with a sulphate ion (6); the side chain is rotated so that the guanidine group points away from the active site and binds a serine residue (Ser155) of the monomer A. Although PP2C crystal structures revealed that the highly conserved arginine residue could interact with different ligands, all the interactions are established on the hydrogen bonds formed by the guanidium side chain of the arginine and the ligands.

In addition, the metal ions were removed from the catalytic center of human PP2C α by incubating the human PP2C α crystals with 2 mM EDTA for 12 h (2). The electron density

maps calculated using data collected from these PP2C crystals indicated dissociation of the metal ions and the phosphate ion from the catalytic center. Refinement of the metal-free human PP2C α structure revealed that it was identical to the metal-bound enzyme form with a root mean square deviation of 0.4 Å between all atoms. However, the guanidinium group of the highly conserved arginine (Arg-33 of human PP2C α) shifts by 1 Å in response to phosphate dissociation, that suggests this residue is flexible and the conformation of this residue is mutually dependent on the presence of the phosphate ion.

Although extensive atomic studies suggest this highly conserved arginine residue is an important residue for catalysis reaction, which kinds of roles it could play were not well known. Only one variant (human PP2C α R33A) of this arginine residue was generated and only *p*NPP was used as substrate to test the activity of this variant. In order to fully understand the function of this highly conserved arginine of PP2C during catalysis, the PP2C phosphatase tPphA was taken as an example and the site-directed mutagenesis of Arg-13 of tPphA was performed. The kinetic parameters of the generated variants towards different substrates were obtained to give more insights into this arginine residue.

Experimental Procedures

Cloning, Overexpression and Purification of tPphA variants

The random site-directed mutagenesis of Arg-13 was carried out following the QuikChange XL (*STRATAGENE*) protocol with two complementary primers containing three random nucleotides at Arg-13 position (Table 1). The expression plasmid pET15btPphA (pET15b hosting the gene encoding wild type tPphA) (10) was used as the template for construction of the mutation genes. The mutagenesis PCR was performed with *Pfu turbo* DNA polymerase using a program of 1 min at 95°C followed by 18 cycles of 95°C for 50 s, 60°C for 50s, 68°C for 7 min and a final extension at 68°C for 7 min. After PCR reaction, the restriction enzyme *Dpn* I was directly added to the PCR reaction tube to degrade the methylated template for 1 h at 37°C. After *Dpn* I digestion, 3 μ l PCR products containing pET15btPphA variant plasmids were transformed into *E. coli* XL-10 gold. The *E. coli* XL-10 gold cells were cultivated on the LB (Luria-Bertani) agar plate containing 100 μ g/ml ampicillin, overnight. In the next day, 48 single *E. coli* colonies were picked from the LB plate and streak cultivated on the new LB plates, overnight. 48 plasmids were extracted from these 48 kinds of *E. coli* cells by mini-prep (peqGOLD Plasmid Miniprep Kit I). The generated plasmids were transformed into *E. coli* BL21 (DE3). 48 kinds of *E. coli* BL21 (DE3) cells were grown on LB plates containing 100 μ g/ml ampicillin. In the next day, each kind of *E. coli* BL21 (DE3) cells was over grown in 2 ml liquid LB medium containing 100 μ g/ml ampicillin. When the O.D.₆₀₀ of the liquid cultures arrived at 1.0-1.5, 50 μ l aliquot cultures were collected, and at the mean time, IPTG were added into LB medium with the final concentration of 0.5 mM. After 3 hours IPTG inducing, 50 μ l aliquot cultures of

48 kinds of *E. coli* BL21 (DE3) cells were harvested. SDS-PAGEs were used to check if tPphA variants could be over expressed in these 48 kinds of *E. coli* BL21 (DE3) cells. Interestingly, all tPphA variant proteins could be induced in *E. coli* BL21 (DE3) cells and displayed strong bands on SDS-PAGE at 29 kDa. After SDS-PAGE, all 48 kinds of plasmid were checked by DNA sequencing using the T7 forward primer. The DNA sequencing revealed that 16 kinds of pET15btPphA variants were generated and 4 pET15btPphA variants (R13A, R13C, R13E and R13V) can not be generated by this random mutagenesis. R13A and R13C were obtained in new rounds site-directed mutagenesis by using the specific primers (Table 1). R13E and R13V could not be generated after two times site-directed mutagenesis attempts. The generated tPphA variant plasmids are shown in Table 2. The plasmids were transformed into *E. coli* BL21 (DE3) for protein over expression and purification as described previously (10).

Assay of phosphatase activity with pNPP as artificial substrate

The activities of the phosphatase variants towards pNPP were assayed as described previously with modifications (10). Standard assays in a volume of 250 μ l contained 0.25 μ g - 10 μ g tPphA variants in a buffer consisting of 10 mM/50mM Tris-Cl, pH 8.3, 50 mM NaCl, 1 mM DTT and 2 mM MnCl₂. Reactions were started by the addition of 2 mM pNPP at 30°C and the increase in absorbance at 400 nm was measured in an ELx808 absorbance microplate reader (BioTek, Winooski, USA) against a blank reaction without enzyme. For pNPP catalytic constants, the pNPP concentration was varied from 0.1 mM to 10 mM. From the linear slope of each reaction, the kinetic parameters K_m and V_{max} were calculated by non-linear hyperbolic fitting using the GraphPad Prism 4 program (GraphPad Software Inc.).

Reactivity of tPphA and its variants towards phosphopeptides

The activities of the phosphatase variants towards two phosphopeptides (pT-peptide, RRA(pT)VA; pS-peptide, RRA(pS)VA) were assayed as described previously (10). In a standard assay, 0.25 μ g - 10 μ g tPphA variants were reacted with 100 μ M phosphopeptides in a reaction volume of 100 μ l containing 50 mM Tris/HCl, pH 8.0, 50 mM NaCl, 2 mM MnCl₂ and 1 mM DTT. Reactions were incubated at 30°C for 2 - 10 minutes, then stopped by the addition of 50 μ l 4.7 M HCl. The released Pi was quantified colorimetrically by the malachite-green assay (13, 14). The absorbance of the solution at 630 nm was measured in ELx808 absorbance microplate reader (BioTek, Winooski, USA) against a blank reaction, which was stopped at the start point by 50 μ l 4.7 M HCl. The activity of all enzymes toward peptides was calculated with a phosphate standard.

Results and Discussion

Site-directed mutagenesis of tPphA

If one amino acid residue of the protein need to be replaced by other nineteen kinds of amino acids, then random site-directed mutagenesis is better than specific site-directed mutagenesis, since the former one only needs one pair of primer and the latter one needs at least nineteen pairs of primer. On the other hand, the procedures for one time random site-directed mutagenesis is obviously simpler than nineteen times specific site-directed mutagenesis. Therefore, random site-directed mutagenesis was used to generate different tPphA Arg-13 variants in this study. After site-directed mutagenesis PCR, *Dpn* I digestion and transformation (see the section *Cloning, Overexpression and Purification of tPphA variants*), about 500 *E.coli* XL-10 gold colonies were grown on the LB plate. 48 plasmids were extracted from 48 different *E.coli* XL-10 gold colonies. After plasmids purification, these 48 different plasmids were transformed into *E.coli* BL21 (DE3) to induce proteins. Unexpectedly, all 48 kinds of *E.coli* BL21 (DE3) cells could express a 29 kDa protein, that means all plasmids did not contain stop codon at position 13 of the variants. Probably, if there is a stop codon at position 13 of tPphA, then a short toxic peptide may be expressed in *E. coli* XL-10 gold that inhibits *E. coli* XL-10 gold continue growing on the LB plate. Therefore, it is impossible to purify a plasmid containing a stop codon at position 13 of tPphA. The DNA sequencing showed sixteen different kinds of variants were acquired from this random site-directed mutagenesis (Table 2). The gene codes at position 13 of these variants are shown in Table 2. The overall distribution probability of these gene codes follows the law of gene code. For example, the variant R13L has the highest possibility to obtain, since there are six different gene codes encoding leucine in nature. Four variants R13A, R13C, R13E, R13V were not obtained by this random site-directed mutagenesis. In order to obtain other four variants (R13A, R13C, R13E, R13V), additional site-directed mutageneses were performed with four pairs of primers (Table 1). Five times attempts to generate R13A were not successful. Interestingly, only one *E. coli* XL-10 gold colony grew on the LB plate containing plasmid pET15bR13A was obtained at the sixth time attempt. Two variants, R13E and R13V, could not be generated after two times attempts. All of the plasmids were verified by DNA sequencing.

Effect of tPphA mutations on catalytic activities: pNPP hydrolysis activity

The variant R13K has about 41% activity (K_{cat}/K_m) as compared to wild type tPphA, which is much higher than all other Arg-13 variants (Table 3, Figure 1). In many other PP2Cs, lysine was found at this position (supplementary file reference (8)). The protonated side chains of arginine and lysine under physiological conditions can participate in electrostatic interactions with different proteins. Thus, arginine or lysine in this position could give different specificity for PP2Cs. Four variants (R13L R13F, R13W and R13D) showed no activity towards pNPP. Leucine, phenylalanine and tryptophan have long and hydrophobic side chains. Aspartate has a carboxyl side chain. Since Arg-13 is close to the catalytic center, the substitutions of arginine

by either one of these four residues (leucine, phenylalanine, tryptophan and aspartate) may disturb the catalytic core of tPphA or heavily influence the binding of *p*NPP to the catalytic center of tPphA. Twelve other Arg-13 variants showed 3-7 times higher K_m than wild-type tPphA (Table 3). Especially, the K_m value of R13M is extremely high. These results proved this highly conserved arginine residue is important at binding the phosphate of *p*NPP, but whether Arg-13 is important for the initial step of catalysis or during the catalysis was still not clear. The K_{cat} values of R13A and R13G are higher than that of the other variants except R13K. Alanine and glycine have free and small side chains so that the substitution of Arg-13 by alanine and glycine may not influence the catalytic center of tPphA or tPphA binding to *p*NPP. Thus, *p*NPP still could be processed very rapidly by these two variants. The K_{cat} value of R13P is about 1.01 S⁻¹ which is also very high. Proline has a cyclic structure and a fixed ϕ angle, which could facilitate the turning of a polypeptide chain upon itself. Arg-13 is located at a β -turn connecting β_1 and β_2 sheets. Probably, proline at this position did not affect this β -turn that the catalytic center of R13P could still dephosphorylate *p*NPP. In comparison with other active variants, R13Y has the lowest K_{cat} value, whereas the variants with other aromatic side chains (R13F and R13W) have no activity at all. *p*NPP also has a aromatic ring, which might mutually attract the aromatic side chains of tyrosine, phenylalanine, and tryptophan, that change the binding properties of *p*NPP to the catalytic center of tPphA. Therefore, an aromatic side chain instead of the guanidium side chain of Arg-13 highly impair tPphA activity to *p*NPP.

Reactivity of tPphA and its variants towards phosphopeptides

Despite the fact that some variants are inactive towards *p*NPP, all variants can dephosphorylate the two phosphopeptides which have six amino acids residues (RRA(pT)VA and RRA(pS)VA) (Table 4, Figure 1). It is likely that the five residues neighbouring the phosphorylated residues (pT and pS) help anchor pT and pS to the tPphA catalytic center. After the anchoring, the phosphopeptides may affect the conformation of the catalytic centers of tPphA variants into a way that the enzyme-substrate complexes are formed and the variants can dephosphorylate these two peptides. Previously, we showed that the free phosphorylated amino acid phosphoserine and the tripeptide (G(pS)E) can not be dephosphorylated by tPphA (10). This verifies the five residues aside the phosphorylated serine of the peptide (RRA(pS)VA) could make some interactions in/around the catalytic center of tPphA. Therefore, tPphA could dephosphorylate the phosphorylated serine of RRA(pS)VA. However, the two residues aside the phosphorylated serine of the tripeptide (G(pS)E) could not help phosphorylated serine stably bind to the catalytic center of tPphA. Thus, tPphA also could not dephosphorylate this tripeptide. *p*NPP only has a phosphate group which could help *p*NPP anchor to the metal ion catalytic center of tPphA, and *p*NPP solely can not induce a conformational change of tPphA. The four variants (R13W, R13L, R13F, R13D), which show no activity towards *p*NPP, can dephosphorylate the

two phosphopeptides. This shows that the phosphopeptides recovered somewhat the catalytic centers of R13W, R13L, R13F and R13D that these four variants could dephosphorylate the two phosphopeptides. R13L still had the lowest activity towards phosphopeptides. Leucine at the position of Arg-13 may totally change the catalytic center of tPphA that even phosphopeptides could not be dephosphorylated by R13L. The fact that R13D recovered some activity towards phosphopeptides was unexpected. The carboxyl group of aspartate could exclude the phosphate of substrates. It is likely that the side chain of this aspartate was forced to adopt a conformation that the phosphate ion of the substrate could bind to the catalytic center of tPphA.

The function of Arg-13 residue of tPphA

In the crystal structure of MspP with a sulphate ion, the long guanidium side chain of the highly conserved arginine could make hydrogen bond with one oxygen atom of the sulphate molecule which is far from catalytic center. It implies that this highly conserved arginine residue could help PP2C bind or release phosphate. In this study, the kinetic parameters of tPphA Arg-13 variants towards *p*NPP are consistent with this suggestion, since all the variants showed higher K_m values than wild type tPphA. The higher K_m values of the variants not only indicate that the variants could not easily bind *p*NPP, but also indicate that the variants may not readily release the phosphate ion from the catalytic center of tPphA. In the enzymatic assays of human PP2Ca towards *p*NPP, the phosphate releasing from this enzyme was proven to be the rate-limiting step (15). If this phosphate ion could not rapidly be released from the catalytic center of tPphA, then it will influence new round of dephosphorylation reaction and the K_m value will increase and the K_{cat} value will decrease. The PP2C crystal structures revealed that the guanidium side chain of this highly conserved arginine residue could adopt different conformations indicates that this arginine residue might drag the phosphate ion from the catalytic center of tPphA by its guanidium side chain and release the phosphate ion afterwards.

In the crystal structure of SzSTP, four monomers (A, B, C, and D) in the asymmetric unit revealed monomer C interacted with the FLAP subdomain of the adjacent monomer A (7). In monomer C, the highly conserved arginine residue (Arg-13 of SzSTP) could make hydrogen bond with Ser-155 of monomer A. This interaction suggests that this highly conserved arginine may play a role in binding phosphorylated residue of the phosphopeptide. In our previously research, we showed that the phosphorylated serine as well as a tripeptide can not be dephosphorylated by tPphA (10). But tPphA can dephosphorylate two phosphopeptides containing six amino acid residues (RRA(pS)VA and RRA(pT)VA). It is likely that the five residues neighbouring the phosphorylated residues (pS and pT) in the two phosphopeptides could make some interactions with tPphA so that pS and pT could be forced into the catalytic center. Afterwards, Arg-13 may push pS or pT into the catalytic center of tPphA by forming

bifurcated hydrogen bonds with the oxygen atom of phosphorylated residue side chain and the phosphate of these phosphorylated residues.

The fact that all the variants except R13K showed significantly decreased activity towards different substrates suggests this highly conserved arginine residue may participate in tPphA dephosphorylation reaction. The guanidium side chain of Arg-13 is the closest positive charged side chain to the catalytic center. In human PP2C α and MspP crystal structures, this highly conserved arginine residue could directly make hydrogen bond with the phosphate ion. The guanidium side chain of this arginine together with the metal center could play a role in inducing the phosphate of the substrate into transition state. Without this arginine residue, although the metal ion catalytic center of PP2C could stabilize the transition state of the phosphate and catalysis the breaking of the covalent bond between phosphate and the leaving group, the catalytic efficiency of the enzyme is greatly decreased.

The molecular mechanism of PP2Cs is more and more clear, but there are still some open questions about this type phosphatase such as why there are so many isoforms in one single organism and how PP2Cs are regulated. Therefore, new biochemical studies of PP2Cs and new experimental methods will shed light on how this type phosphatases exert the functions *in vivo*.

Acknowledgements

This work was supported by grants from the DFG (Fo195/4) and the Graduiertenkolleg 685.

References

1. Shi Y (2009) Serine/threonine phosphatases: mechanism through structure. *Cell*, 139, 468-484.
2. Das AK, Helps NR, Cohen PTW, and Barford D (1996) Crystal structure of the protein serine/threonine phosphatase 2C at 2.0 angstrom resolution. *Embo Journal*, 15, 6798-6809.
3. Arino J, Casamayor A, and Gonzalez A (2011) Type 2C Protein Phosphatases in Fungi. *Eukaryotic Cell*, 10, 21-33.
4. Schlicker, C., Fokina, O., Kloft, N., Grune, T., Becker, S., Sheldrick, G. M., and Forchhammer, K. (2008) Structural analysis of the PP2C phosphatase tPphA from *Thermosynechococcus elongatus*: a flexible flap subdomain controls access to the catalytic site. *J Mol Biol* 376, 570-581.
5. Pullen, K. E., Ng, H. L., Sung, P. Y., Good, M. C., Smith, S. M., and Alber, T. (2004) An alternate conformation and a third metal in PstP/Ppp, the *M. tuberculosis* PP2C-Family Ser/Thr protein phosphatase. *Structure* 12, 1947-1954.

6. Bellinzoni, M., Wehenkel, A., Shepard, W., and Alzari, P. M. (2007) Insights into the mechanism of PPM Ser/Thr phosphatases from atomic resolution structure of a mycobacterial enzyme. *Structure* 15, 863-872.
7. Rantanen, M. K., Lehtio, L., Rajagopal, L., Rubens, C. E., and Goldman, A. (2007) Structure of *Streptococcus agalactiae* serine/threonine phosphatase: the subdomain conformation is coupled to the binding of a third metal ion. *FEBS J* 274, 3128-3137.
8. Wehenkel, A., Bellinzoni, M., Schaeffer, F., Villarino, A., and Alzari, P. M. (2007) Structural studies of the trinuclear metal center in two mycobacterial PPM Ser/Thr protein phosphatases. *J Mol Biol* 374, 890-898.
9. Melcher, K., Ng, L. M., Zhou, X. E., Soon, F. F., Xu, Y., Suino-Powell, K. M., Park, S. Y., Weiner, J. J., Fujii, H., Chinnusamy, V., Kovach, A., Li, J., Wang, Y., Li, J., Peterson, F. C., Jensen, D. R., Yong, E. L., Volkman, B. F., Cutler, S. R., Zhu, J. K., and Xu, H. E. (2009) A gate-latch-lock mechanism for hormone signalling by abscisic acid receptors. *Nature* 462, 602-608.
10. Su, J., Schlicker, C., and Forchhammer, K. (2011) A third metal is required for catalytic activity of the signal-transducing protein phosphatase M tPphA. *J. Biol. Chem.* 286, 13481-13488.
11. Shakir, S. M., Bryant, K. M., Larabee, J. L., Hamm, E. E., Lovchik, J., Lyons, C. R., and Ballard, J. D. (2010) Regulatory interactions of a virulence-associated serine/threonine phosphatase-kinase pair in *Bacillus anthracis*. *J Bacteriol.* 192, 400-409.
12. Jackson MD, Fjeld CC, and Denu JM (2003) Probing the function of conserved residues in the serine/threonine phosphatase PP2C α . *Biochemistry*, 42, 8513-8521.
13. Vanveldhoven, P. P. and Mannaerts, G. P. (1987) Inorganic and Organic Phosphate Measurements in the Nanomolar Range. *Analytical Biochemistry*, 161, 45-48.
14. Ekman, P. and Jager, O. (1993) Quantification of Subnanomolar Amounts of Phosphate Bound to Seryl and Threonyl Residues in Phosphoproteins Using Alkaline-Hydrolysis and Malachite Green. *Analytical Biochemistry*, 214, 138-141.
15. Fjeld, C. C. and Denu, J. M. (1999) Kinetic analysis of human serine/threonine protein phosphatase 2C α . *J Biol Chem.* 274, 20336-20343

Figure 1

Relative activities of tPphA and Arg-13 variants, as indicated, towards different substrates. The activities of wild-type tPphA towards five substrates were set as 100% and the activities of the tPphA variants towards these five substrates were adjusted accordingly. ρ NPP indicates the value for K_{cat}/K_m from the ρ NPP assay (Table 3). pT-peptide indicates the relative activity with RRA(pT)VA as substrate, pS-peptide indicates the activity with RRA(pS)VA peptide as substrate (from Table 4)

Figure 1

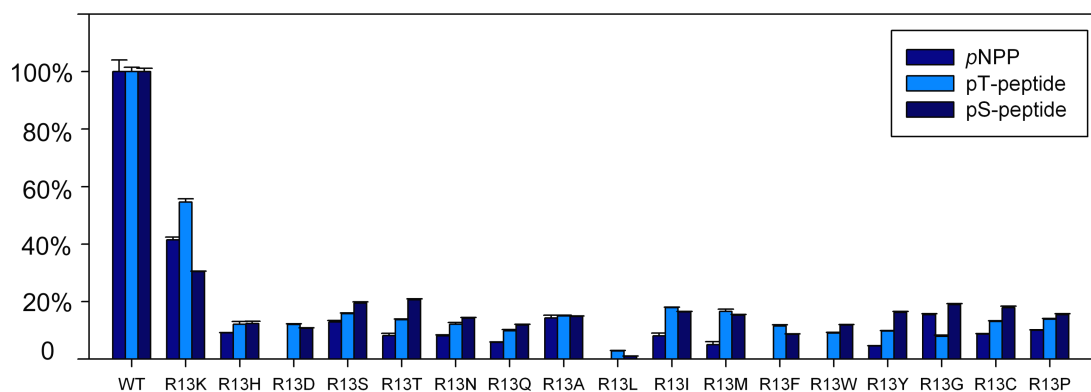


Table 1: Primers used for PCR amplification of tPphA and for site-directed mutagenesis

T7	5'; 5'-TAATACGACTCACTATAGGG-3' 3'; 5'-GCTAGTTATTGCTCAGCGG-3'
R13X	5'; 5'-CTGACTGTGGTCTGATTNNNAAAAGCAATCAGGATGC-3' 3'; 5'-GCATCCTGATTGCTTTTNNNAATCAGACCACAGTCAG-3'
R13A	5'; 5'-CTGACTGTGGTCTGATTGCTAAAAGCAATCAGGATGC-3' 3'; 5'-GCATCCTGATTGCTTTTAGCAATCAGACCACAGTCAG-3'
R13C	5'; 5'-CTGACTGTGGTCTGATTTGTAAAAGCAATCAGGATGC-3' 3'; 5'-GCATCCTGATTGCTTTTACAAATCAGACCACAGTCAG-3'
R13E	5'; 5'-CTGACTGTGGTCTGATTGAAAAAAGCAATCAGGATGC-3' 3'; 5'-GCATCCTGATTGCTTTTTTCAATCAGACCACAGTCAG-3'
R13V	5'; 5'-CTGACTGTGGTCTGATTGTTAAAAGCAATCAGGATGC-3' 3'; 5'-GCATCCTGATTGCTTTTAACAATCAGACCACAGTCAG-3'

Table 2: The generated tPphA variants from random site-directed mutagenesis and the gene codes of variants amino acids replacing wild type tPphA Arg-13. The gene code of Arg-13 of Wild type tPphA is CAC. The plasmids extracted from *E.coli* X-10 Gold colony B7, C2, D2, D5 did not yield any results in DNA sequencing.

Variants name	The gene codes of variants amino acids replacing wild type tPphA Arg-13	The name of <i>E.coli</i> X-10 Gold colony
R13L	CCT	A6
	CTC	C3
	TTA	E6
	CTT	E7
	CTC	F1
	TTA	F5
	CTT	F8
R13R	CAC	B1
	CGT	C8
	CAC	E3
	CGT	F3
R13P	CCC	A7
	CCC	B4
	CCC	D7
	CCT	F4
R13Q	CAA	B2
	CAA	B8
	CAG	C5
R13H	CAT	A2
	CAC	D4
	CAC	E5
R13G	GGA	A3
	GGG	A4
R13N	AAC	A8
	AAT	C7
R13S	TCG	B5
	TCA	D6
R13T	ACA	C1

	ACT	D8
	ACC	E8
R13D	GAT	C6
	GAC	E4
	GAC	F7
R13F	TTT	B6
	TTC	E1
R13W	TGG	A5
R13I	ATT	A1
R13K	AAA	C4
R13M	ATG	D3
R13Y	TAT	F2
Unknown variants	N*AT	B3
	NNN	D1
	CTN	E2
	CNG	F6

N* means four nucleotides AGCT could randomly appear at that position

Table 3: Kinetic parameters of tPphA and Arg-13 variants towards p NPP.

p NPP assays were carried out as described in Materials and Methods. The reaction pH is 8.3. From the apparent reaction velocities of three independent repetitions, the kinetic parameters were calculated by linear fitting using the program GraphPad Prism 4. \pm sign is a standard error. The results were obtained from single preparations of the wild-type (WT) and variant tPphA purifications and the data come from single experiments.

Classification of Arg-13 variants	Variants	K_m [mM] (p NPP)	K_{cat} [s^{-1}] p NPP	K_{cat}/K_m [$s^{-1} M^{-1}$]
Arg-13 changed to residues with electrically charged side chains	WT(R13R)	1.06 \pm 0.05	2.25 \pm 0.10	2122 \pm 94
	R13K	1.39 \pm 0.10	1.22 \pm 0.03	878 \pm 21
	R13H	3.30 \pm 0.17	0.64 \pm 0.01	194 \pm 3
	R13D	-	-	-
Arg-13 changed to residues with polar uncharged side chains	R13S	3.85 \pm 0.32	1.06 \pm 0.04	275 \pm 10
	R13T	5.37 \pm 1.00	0.94 \pm 0.08	175 \pm 15
	R13N	4.73 \pm 0.53	0.81 \pm 0.04	171 \pm 8
	R13Q	4.06 \pm 0.21	0.50 \pm 0.01	123 \pm 2
Arg-13 changed to residues with hydrophobic side chains	R13A	5.11 \pm 0.23	1.56 \pm 0.03	305 \pm 6
	R13L	-	-	-
	R13I	4.58 \pm 0.54	0.75 \pm 0.04	164 \pm 9
	R13M	7.36 \pm 2.76	0.76 \pm 0.15	103 \pm 20
Arg-13 changed to residues with aromatic side chains	R13F	-	-	-
	R13W	-	-	-
	R13Y	4.31 \pm 0.28	0.42 \pm 0.01	97 \pm 2
Arg-13 changed to residues with special side chains	R13G	3.58 \pm 0.22	1.17 \pm 0.03	327 \pm 8
	R13C	4.27 \pm 0.39	0.79 \pm 0.01	185 \pm 2
	R13P	4.77 \pm 0.17	1.01 \pm 0.02	212 \pm 4

-* means not determined.

Table 4: The activity of tPphA and Arg-13 variants towards three phosphopeptides

Reactions were performed in the buffer as described in Materials and Methods. Triplicate assays were used. \pm sign is a standard error. The results were obtained from single preparations of the wild-type (WT) and variant tPphA purifications and the data come from single experiments.

Classification of Arg-13 variants	nmol/min/ μ g	Thr peptide	Ser peptide
Arg-13 changed to residues with electrically charged side chains	WT(R13R)	9.32 \pm 0.14	5.49 \pm 0.06
	R13K	5.09 \pm 0.10	1.67 \pm 0.01
	R13H	1.13 \pm 0.08	0.68 \pm 0.04
	R13D	1.12 \pm 0.03	0.59 \pm 0.01
Arg-13 changed to residues with polar uncharged side chains	R13S	1.47 \pm 0.02	1.07 \pm 0.02
	R13T	1.28 \pm 0.02	1.13 \pm 0.02
	R13N	1.13 \pm 0.06	0.78 \pm 0.03
	R13Q	0.91 \pm 0.05	0.65 \pm 0.03
Arg-13 changed to residues with hydrophobic side chains	R13A	1.40 \pm 0.02	0.81 \pm 0.01
	R13L	0.26 \pm 0.02	0.05 \pm 0.01
	R13I	1.67 \pm 0.01	0.90 \pm 0.01
	R13M	1.55 \pm 0.07	0.84 \pm 0.01
Arg-13 changed to residues with aromatic side chains	R13F	1.07 \pm 0.04	0.47 \pm 0.01
	R13W	0.84 \pm 0.03	0.65 \pm 0.01
	R13Y	0.91 \pm 0.01	0.89 \pm 0.02
Arg-13 changed to residues with special side chains	R13G	0.74 \pm 0.04	1.04 \pm 0.02
	R13C	1.21 \pm 0.03	0.98 \pm 0.03
	R13P	1.29 \pm 0.03	0.85 \pm 0.02

Chapter 6. Additional data

6.1 The studies of P_{II} kinase

6.1.2 *In vivo* P_{II} protein phosphorylation assays

In *Synechococcus elongatus* PCC 7942 (*S. elongatus*), P_{II} protein was found to be phosphorylated at Serine-49 under low nitrogen condition (29). *In vitro* and *in vivo* experiments proved a PP2C type phosphatase PphA is the specific phosphatase of P_{II} protein in *Synechocystis* sp. PCC 6803 (48). However, the specific kinase of P_{II} protein in unicellular cyanobacteria is still not found. The crude extract of P_{II}-deficient mutant MP2 can phosphorylate unphosphorylated P_{II} purified from wild type *S. elongatus* (29). In this P_{II} phosphorylation assay, ATP was used specifically as a phosphoryl donor, and the P_{II} kinase activity was shown to be stimulated by 2-OG (29). In addition, the *S. elongatus* extract was separated by a Superdex 200 gel filtration column. The P_{II} kinase activity was mostly found in the elution fractions containing higher molecular weight proteins (47).

By checking the genome of *Synechocystis*, there is a ABC1 type kinase gene (sll1770) upstream of the PphA gene (sll1771) (48). It is possible that these two genes (sll1770, sll1771) might participate in one transduction pathway, perhaps P_{II} signal transduction pathway. Thus, if the protein encoded by sll1770 is the kinase of P_{II} was checked. The mutants of the two genes were previously generated in our lab (Δ sll1770, Δ sll1771) (48).

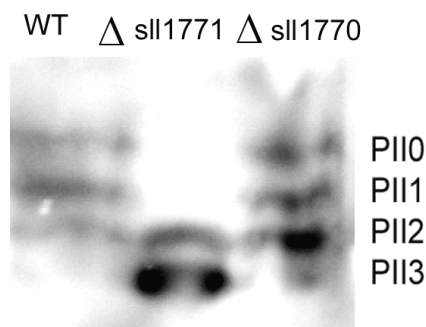


Figure 6.1. The P_{II} phosphorylation status was detected in wild type *Synechocystis*, the mutants Δ sll1770 and Δ sll1771. Wild type *Synechocystis*, Δ sll1770 and Δ sll1771 were grown in normal BG11 medium. When the OD₇₅₀ of the cultures arrived at 0.8, the cells were collected by centrifuge at 4000 rcf for 10 minutes. The cells were lysed by glass beads (Fastprep-24) for 40 seconds at 6M/s in a buffer containing 20mM K₂HPO₄, 20mM KH₂PO₄, pH 7.0, and 4mM EDTA. 20 μ g samples were loaded on Native-PAGE and analysed by western-blotting (anti-P_{II}

antibody). Figure 6.1 shows P_{II} kept in high phosphorylation status in the PphA-deficient mutant Δ sll1771. The P_{II} phosphorylation status of Δ sll1770 (ABC1 kinase-deficient mutant) was similar as wild type *Synechocystis*.

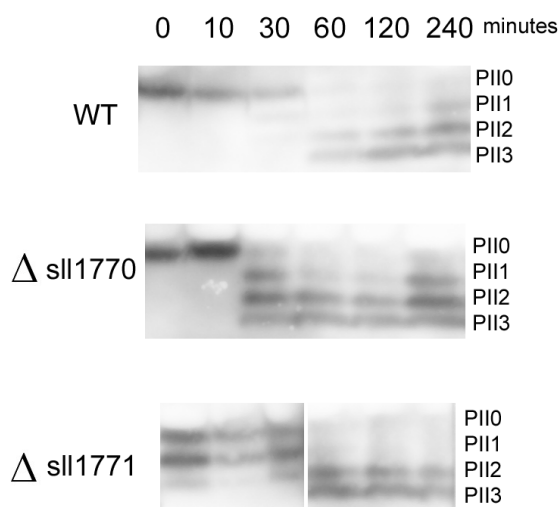


Figure 6.2. A time course assay of the P_{II} phosphorylation status of wild type *Synechocystis*, Δ sll1770 and Δ sll1771 under low nitrogen condition.

Before the cells shifted to low nitrogen condition, wild type *Synechocystis* and the mutants were growing under standard condition (BG11 medium, 50 einstein light). When the OD₇₅₀ of wild type *Synechocystis* and the mutants arrived at 1.0, the cells were centrifuged at 4000 rcf for 10 minutes. The cells were resuspended in BG11⁰ medium which contains no nitrogen. At the time points indicated at Figure 6.2, 10 ml culture was centrifuged at 4000 rcf for 10 minutes and lysed by glass beads (Fastprep-24) for 40 seconds at 6M/s in the buffer (20mM K₂HPO₄, 20mM KH₂PO₄, pH 7.0, and 4mM EDTA). 20 μ g samples were loaded on Native-PAGE and analysed by western-blotting (anti-P_{II} protein). At time 0, the mutant Δ sll1771 show more phosphorylated P_{II} (PII2, PII1, PII0) than wild type *Synechocystis* and Δ sll1770 mutant (only PII0). The P_{II} in Δ sll1771 was phosphorylated faster than the P_{II} of wild type *Synechocystis* and Δ sll1770. The P_{II} can also be phosphorylated in Δ sll1770 mutant means the protein encoded by sll1770 is not the kinase of P_{II} protein.

6.1.2 *In vitro* P_{II} protein phosphorylation assays

High purity fully phosphorylated P_{II} protein is convenient for P_{II} functional and structural analyses. The purification procedures for P_{II}-P from cyanobacteria usually need several steps (anion exchange column, gel filtration and ammonium sulphate precipitation) that most of P_{II}-P was dephosphorylated or degraded. Unfortunately, P_{II} specific kinase was not found that it is

impossible to directly phosphorylate cyano-P_{II} protein *in vitro*. Since the phosphorylate site (Serine-49) of *S. elongatus* P_{II} has a RXS motif which is a recognition site for eukaryotic PKA (29). Thus, protein kinase A (PKA) was used to phosphorylate P_{II} protein *in vitro*. Two other classical kinases (protien kinase C (PKC) and casein kinase II (CK II)) were also used to phosphorylate P_{II} protein.

The reaction condition for PKA, PKC and CK II to phosphorylate P_{II}

PKA (0.34 µg), 30°C	100 mM Tris/HCl, pH 7.5
	20 mM MgCl ₂
	0.4 mM ATP
	1.7 µg P _{II}
PKC (0.4 µg), 30°C	25 mM Tris/HCl, pH 7.5
	6.25 mM MgCl ₂
	0.125 mM CaCl ₂
	10 µM ATP
	0.05 µg/µl diolein
	0.5 µg/µl phosphatidylserine
CK II (0.4 µg), 30°C	100 mM Tris/HCl, pH 7.6
	20 mM MgCl ₂
	0.2 mM ATP
	1.7 µg P _{II}

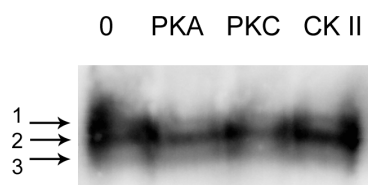


Figure 6.3. PKA, PKC, and CK II were used to phosphorylate P_{II} for 30 minutes. PKA, PKC, and CKII can not phosphorylate P_{II}.

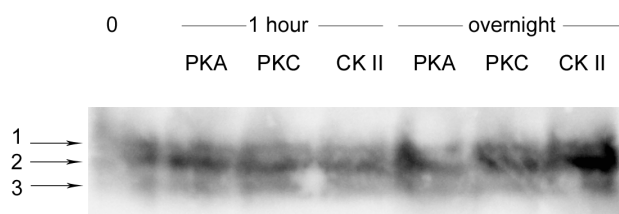


Figure 6.4. The reaction time was prolonged to overnight. PKA, PKC, and CKII still can not phosphorylate P_{II}.

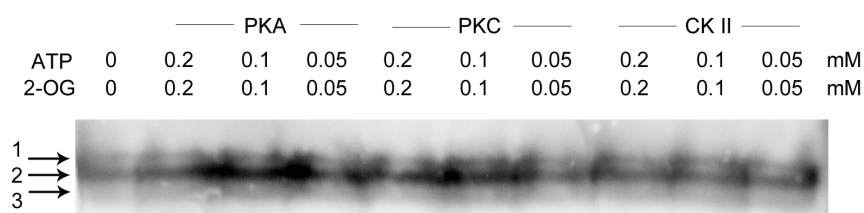


Figure 6.5. ATP, 2-OG (0.2, 0.1, and 0.05 mM as indicated) were added into the PKA, PKC, CKII reaction buffer.

Strep-tagged *S. elongatus* P_{II} was overexpressed and purified from *E. coli* RB9060 (Δ P_{II} mutant). It seems this strep-tagged P_{II} protein could interact with *E. coli* GlnK. Figure 6.3 shows three P_{II} bands (band 1, 2, 3) on the western blotting membrane after Native-PAGE separation. Band 1, 2, 3 could be cyano-P_{II}³, cyano-P_{II}²+*E. coli* GlnK¹, cyano-P_{II}¹+*E. coli* GlnK². PKA, PKC and CK II can not phosphorylate *S. elongatus* P_{II} (Figure 6.3). The reaction time was prolonged to overnight, these three kinases still can not phosphorylate P_{II} protein. 2-OG can bind in the intersubunit clefts of P_{II} that regulate the conformation of T-loop (16). ATP and 2-OG can also synergistically inhibit purified PphA dephosphorylate P_{II}-P (49). On the contrary, ATP and 2-OG may promote P_{II} phosphorylation. Therefore, ATP and 2-OG were added into the reaction solution. But PKA, PKC and CK II still can not phosphorylate P_{II} protein (Figure 7.5) in the presence of ATP and 2-OG.

6.2 tPphA could recover P_{II}-P from *S. elongatus* crude extract

In Chapter 4, a new binding assay combined with chemical cross-linking (glutaraldehyde) and pull down was used to test the binding of tPphA to P_{II}-P. tPphA was proven to specifically interact with P_{II}-P which was partially purified from *S. elongatus* crude extract (Chapter 4). In this section, His-tPphA was used to recover proteins from *S. elongatus* crude extract by the new binding assay. The recovered proteins by his-tPphA were separated by SDS-PAGE and visualized by silver staining and commassie blue staining. P_{II}-P was shown to be recovered from the *S. elongatus* crude extract by his-tPphA.

His-tPphA and *S. elongatus* crude extract were prepared as described in Chapter 4. Each step of the following binding assay was carried out on ice or 4°C. tPphA (2 μ g or 20 μ g) was incubated with *S. elongatus* crude extract (1 μ g or 10 μ g) in 10 μ l or 100 μ l of buffer I containing 1 mM Tris-Cl, pH 7.4, 2.5 mM CaCl₂, 110 mM NaCl, 0.05 mM EDTA and 0.08% (w/w) glutardialdehyde. After 60 minutes, 2.5 μ l of 1 M imidazole (pH 8.0) was added to the reaction. After further incubating on ice for 15 minutes, the reaction was diluted with 420 μ l buffer II of 2.5 mM CaCl₂, 100 mM NaCl and 0.05% v/v tween-20. To extract His-tagged tPphA, 20 μ l or 60 μ l Ni-NTA magnetic agarose beads (Qiagen, Hilden, Germany) were added. The mixture

was gently mixed by rotation for one hour. Thereafter, the Ni-NTA beads were removed with a magnet and washed four times with 1 ml washing buffer (10 mM Tris-Cl, pH 8.0, 2.5 mM CaCl₂, 100 mM NaCl, 20 mM imidazole.). Finally, the bound proteins were eluted by denaturing the sample with 50 µl SDS-sample buffer (75 mM Tris-Cl, pH 6.8, 1.5% DTT, 1% SDS, 10% glycerol, 0.04% bromphenol blue) at 95°C for 5 minutes. Subsequently, the eluted proteins were visualized by coomassie blue and silver staining.

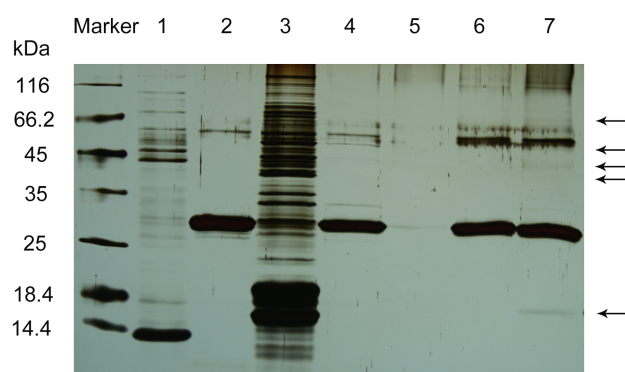


Figure 6.6. Silver staining of recovered proteins from *S. elongatus* crude extract by tPphA. Lane 1: strep-P_{II}, lane 2: 2 µg tPphA recovered by Ni-NTA magnetic agarose beads, lane 3: 1 µg *S. elongatus* crude extract, lane 4: 2 µg tPphA pull down 1 µg *S. elongatus* crude extract, lane 5: 1 µg *S. elongatus* crude extract cross-linked by glutaraldehyde and recovered by Ni-NTA magnetic agarose beads, lane 6: 2 µg tPphA cross-linked by glutaraldehyde and recovered by Ni-NTA magnetic agarose beads, lane 7: 2 µg tPphA cross-linked with 1 µg *S. elongatus* crude extract by glutaraldehyde and recovered by Ni-NTA magnetic agarose beads. In lane 7, several proteins (indicated by arrows) were recovered by tPphA from *S. elongatus* crude extract. Lane 2 shows purified his-tPphA by HIS-Select Cartridges (Sigma) from *E. coli* BL21 (DE3) could be recovered by Ni-NTA magnetic agarose beads again. Lane 4 shows tPphA could recover two proteins (one is about 50 kDa, another one is about 30 kDa) from *S. elongatus* crude extract. But these two additional proteins in lane 4 was proven to be unspecifically recovered by Ni-NTA magnetic agarose beads (See Figure 6.8 lane 1). Therefore, tPphA can not directly pull down any protein from the *S. elongatus* crude extract. But, by using the new binding assay, tPphA can recover several proteins (indicated by arrows) from *S. elongatus* crude extract (lane 7).

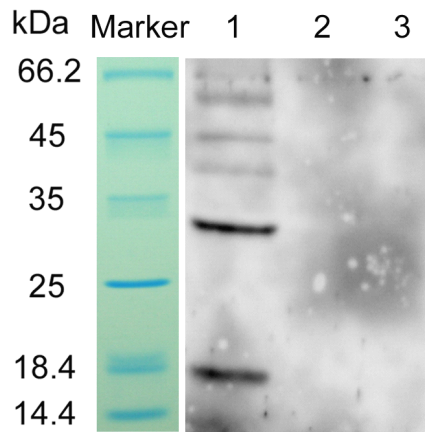


Figure 6.7. Western blot analyses (anti- P_{II} antibody) of recovered proteins by tPphA from *S. elongatus* crude extract. Lane 1 - 3 correspond to lane 5 - 7 in Figure X. Lane 1: 2 μ g tPphA cross-linked with 1 μ g *S. elongatus* crude extract by glutaraldehyde and recovered by Ni-NTA magnetic agarose beads, lane 2: 2 μ g tPphA cross-linked by glutaraldehyde and recovered by Ni-NTA magnetic agarose beads, lane 3: 1 μ g *S. elongatus* crude extract cross-linked by glutaraldehyde and recovered by Ni-NTA magnetic agarose beads. The recovered proteins were analysed by immunoblot.

Although *S. elongatus* crude extract contains a lot of other kinds of proteins (Figure 6.6 lane 3) and P_{II} -P is not a abundant protein in *S. elongatus* crude extract, tPphA could still recover P_{II} -P from this cell extract. It means tPphA could recognize P_{II} -P and the weakening interaction between tPphA and P_{II} -P can be stabilized by glutaraldehyde. Without the aid of tPphA, P_{II} -P can not be recovered by Ni-NTA magnetic agarose beads (lane 3). Besides P_{II} -P, tPphA can co-purify some other proteins (lane 7 in Figure 6.6) which may be other proteinous substrates of tPphA.

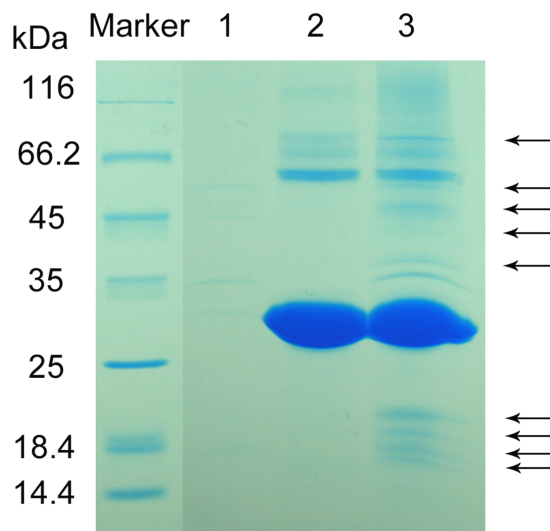


Figure 6.8. Coomassie blue staining of recovered proteins from *S. elongatus* crude extract by tPphA. Lane 1: 10 μ g *S. elongatus* crude extract cross-linked by glutaraldehyde and recovered by Ni-NTA magnetic agarose beads, some proteins from *S. elongatus* crude extract could be unspecifically recovered by Ni-NTA magnetic agarose beads, lane 2: 20 μ g tPphA cross-linked by glutaraldehyde and recovered by Ni-NTA magnetic agarose beads, lane 3: 20 μ g tPphA cross-linked with 10 μ g *S. elongatus* crude extract by glutaraldehyde and recovered by Ni-NTA magnetic agarose beads. In lane 3, several proteins (indicated by arrows) were recovered by tPphA from *S. elongatus* crude extract.

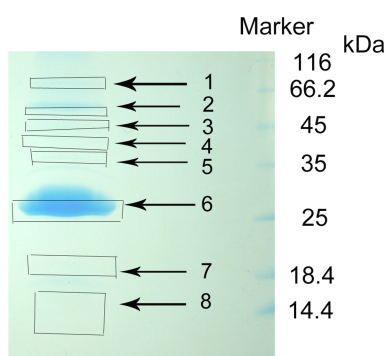


Figure 6.9 The same experiment as the lane 3 of Figure 6.8 was repeated. Eight bands containing the proteins recovered by tPphA were cut off from the gel and were sent for mass spectroscopy (MS) analyses (Proteome Center Tuebingen).

MS revealed that the 469 kinds of proteins including P_{II} were recovered by tPphA from *S. elongatus* crude extract. Most MS signals of P_{II} came from band 6 and band 8, where dimeric P_{II} and monomeric P_{II} are (see figure 6.7). P_{II} is number ten in the MS signal intensity value

ranking of all proteins recovered by tPphA. The proteins in the ranking from number one to number nine are: 1. his-tagged tPphA, 2. phycobilisome rod linker polypeptide (gene ID: Synpcc7942_1050), 3. phycocyanin beta subunit (gene ID: Synpcc7942_1047 or Synpcc7942_1052), 4. phycobilisome rod-core linker polypeptide (gene ID: Synpcc7942_2030), 5. allophycocyanin beta subunit (gene ID: Synpcc7942_0326), 6. phycobilisome rod linker polypeptide (gene ID: Synpcc7942_1049), 7. phycocyanin alpha subunit (gene ID: Synpcc7942_1048 or Synpcc7942_1053), 8. phycobilisome core-membrane linker polypeptide (gene ID: Synpcc7942_0328), 9. ribulose biphosphate carboxylase (gene ID: Synpcc7942_1426). The proteins from number two to nine are abundant protein in *S. elongatus* crude extract. It seems tPphA could inevitably recover these abundant proteins by the new binding assay, since glutaraldehyde a strong cross linker was used in this assay which may unspecifically lead to the cross-linking of tPphA to these proteins.

6.3 His-tPphA R13C variant cross-links with strep-P_{II} S49C variant

His-tPphA R13C variant (R13C) (Chapter 5) and strep-P_{II} S49C (S49C) variant (storied in our lab) were already generated. Arg-13 of tPphA is a highly conserved residue close to the catalytic center. Ser-49 of P_{II} is the phosphorylation site of P_{II}. Thus, it is possible to generate the heterodimer of R13C and S49C by oxidizing the cysteine residues of the two variants. If the cross-linking of the two variants is successful, then the heterodimer could mimic the interaction between tPphA and P_{II}-P. The crystal structure of this heterodimer could directly answer the questions about how tPphA recognizes P_{II}-P, which residues are important for tPphA binding to P_{II}-P, and what kind of role does the FLAP domain play when tPphA interact with P_{II}-P.

R13C and S49C were expressed and purified as described in Chapter 4 and Chapter 5. These two proteins were storied in a buffer containing DTT which should be removed before the cross-linking reaction, since DTT will reduce the covalent bond between two cysteine residues. 200 µg of each protein was dialysed in 1 L dialysis buffer containing 20 mM Hepes, pH 7.0, 300 mM NaCl. After dialysis, the protein concentration of the two proteins was determined by Bradford protein assay. 20 µg R13C and 10 µg S49C were incubated with 1 mM Cu²⁺(NO₃)₂ in the cross-linking buffer (20 mM Hepes, pH 7.0, 300 mM NaCl) to generate cross-linking products. Cu²⁺ was proven to be an effective oxidizer for cysteine residues in protein (82). After cross-linking at 25°C for 1 hour, the reaction solutions were mixed with SDS-PAGE loading buffer with DTT or without DTT, and incubated at 25°C for further 15 minutes. Afterwards, the samples were loaded in SDS-PAGE and visualized by coomassie blue staining.

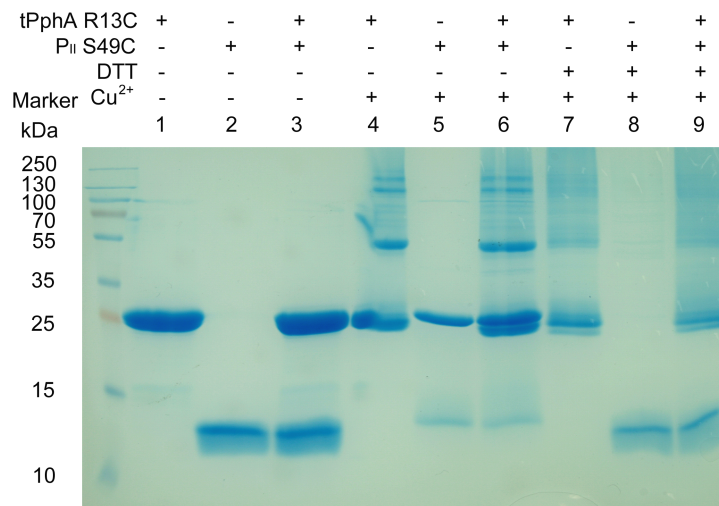


Figure 6.10 R13C cross-links with S49C by Cu²⁺(NO₃)₂.

Before the cross-linking, DTT was removed from the storage buffer of R13C and S49C. Lane 1 - 3 show the two proteins did not cross-link themselves after removing DTT. R13C and S49C could not cross-link each other without any oxidizer (lane 3). In the presence of 1 mM Cu²⁺(NO₃)₂, R13C can form homodimer, homotrimer, and homotetramer (lane 4). The main cross-linking product of R13C seems to be homodimer, which has a molecular weight about 55 kDa. In Chapter 4, tPphA was shown to form homodimer in the presence of glutaraldehyde. These results suggest tPphA might exist as dimer form under some conditions. P_{II} is a homotrimer protein. It seems a trimeric S49C molecule can only form intra cross-linking product with another trimeric S49C molecule in the presence of Cu²⁺(NO₃)₂. SDS will break the interaction of three monomer S49C but not the divalent bond form by two cysteine residues, which belong to two different trimeric S49C. Therefore, only dimeric S49C is shown in lane 5. Unfortunately, R13C and S49C could not form heterodimer (lane 6). The reason is probably, taking R13C as an example, a R13C molecule has the same properties as another R13C molecule, a R13C only like to cross-link another R13C and this cross-linking speed is different from the cross-linking speed of S49C. Thus, these two proteins only cross-link themselves. Lane 7 - 9 show DTT can reduce the covalent bond formed by two cysteines of these two protein, respectively.

7. Summary

tPphA, a PP2C type phosphatase, is the research object in this dissertation. The catalytic mechanism of tPphA was revealed and the binding of tPphA to P_{II} protein was investigated in this thesis.

PP2C crystal structures show three metal ions (M1, M2 and M3) in the catalytic center with the exception that in human PP2C α M3 is invisible in the structure. Five highly conserved aspartates form ionic bonds with these divalent cations. PP2Cs were proposed to dephosphorylate their substrates in an S_N2 mechanism. However, the proton donor for the leaving group was still not found. In the structural and functional analyses of *Mp*stP, M3 was suggested to be unimportant. However, tPphA M3 variants D119A and D193A can not dephosphorylate any substrates. The crystal structures of D119A and D193A showed only two metal ions (M1 and M2) in the catalytic center and in the D119 variant the M1-M2 core was not impaired, that proves M3 is critical important for tPphA to dephosphorylate substrates. The catalytic molecular from the crystal structure of MspP was modeled into the catalytic center of tPphA. The fitting showed one water molecule coordinated by M3 could be a proton donor for the leaving group (Figure 7.1).

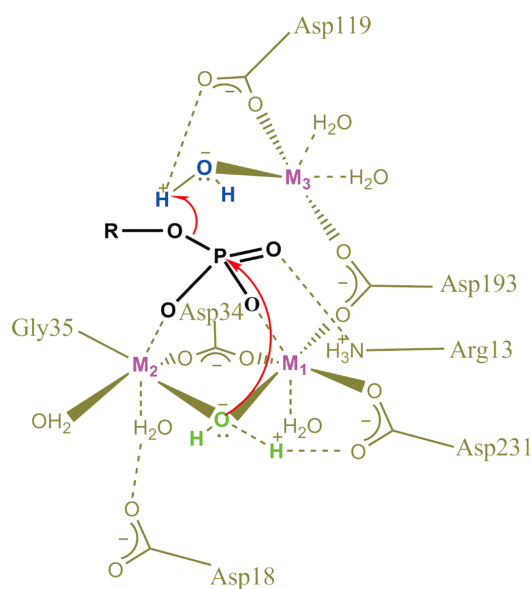


Figure 7.1 Catalytic mechanism of tPphA. The water molecule (green) in ion-dipole interaction with M1 and M2 is considered as the nucleophile, which attacks the phosphorus atom in an S_N2 mechanism. M3 activates as Lewis acid a water molecule (blue) to donate a proton for the phosphate leaving group

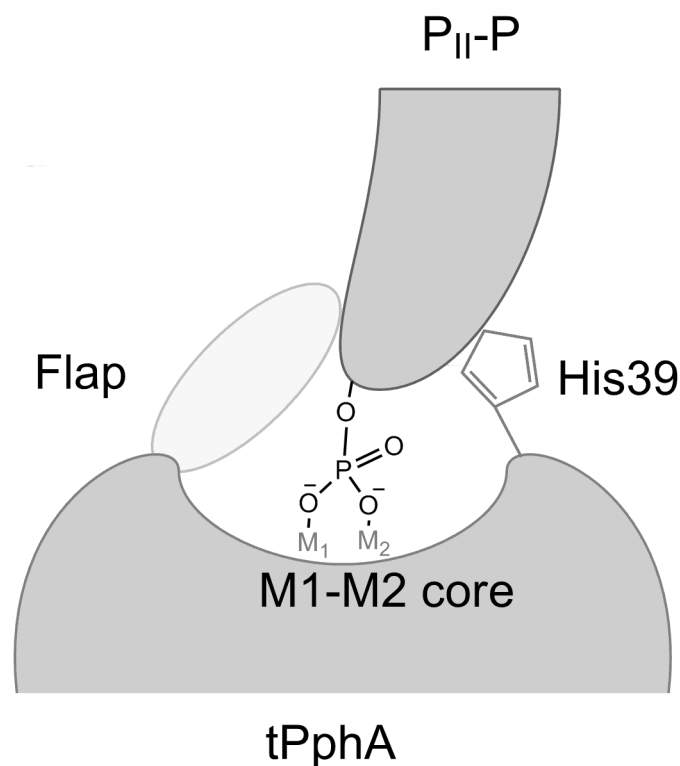


Figure 7.2 M1-M2 core, the FLAP subdomain, and His-39 residue are essential for tPphA specifically recognizing $P_{II}\text{-P}$. The phosphate group of $P_{II}\text{-P}$ is also a key factor for $P_{II}\text{-P}$ entering into the catalytic center of tPphA.

It is unlikely that PP2C without regulatory domain can directly pull down proteinous substrates since PP2C dephosphorylate substrates very rapidly. The transition binding between PP2Cs and their physiological substrates prevented the understanding of the molecular mechanism of this type phosphatase. Fortunately, chemical cross-linking, a widely used tool to determine protein-protein interactions, provided the means for capturing the transient interactions between PP2Cs and proteinous substrates. A new assay combined with chemical cross-linking and pull down was developed to test the interaction between tPphA variants and P_{II} . In the presence of Ca^{2+} and glutaraldehyde, tPphA can specifically bind to P_{II} . The M1-M2 core, the FLAP subdomain, and His-39 were proved to assist tPphA specifically recognize $P_{II}\text{-P}$ (Figure 7.2). In addition, the site-directed mutagenesis and enzymatic assays revealed tPphA that Arg-13 is important for binding phospho-substrates by making hydrogen bond with the oxygen atom of phosphate. Finally, based on the results of tPphA in this dissertation, a model of the whole dephosphorlation process of tPphA is proposed (Figure 7.3).

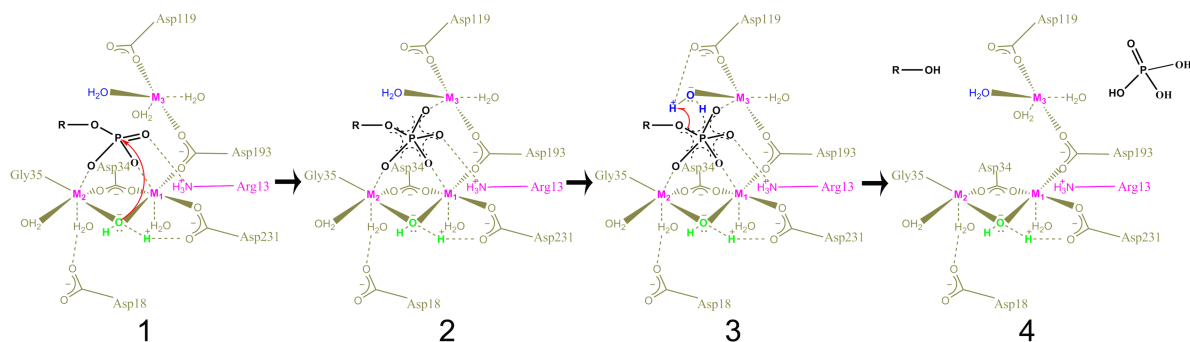


Figure 7.2 A model of how tPphA dephosphorylation substrate. 1. M1-M2 core and Arg-13 are essential for tPphA binding to the three oxygen atoms of the phosphate ion (see Chapter 4 and Chapter 5). The water molecule shared by M1 and M2 could attack the phosphate ion in an S_N2 mechanism (Chapter 3). 2. After the attacking, the phosphate ion will enter into a transition state which will temporarily have five oxygen atoms. As soon as the fifth oxygen atom appears, M3 may directly coordinate it. M1-M2 core, Arg-13 and M3 seem to stabilize the transition state of the phosphate since all of them are positive charged and close to the phosphate ion. 3. The covalent bond between the phosphate and the oxygen atom of the substrate will be broken. In the mean time, M3 could supply a water molecule as a proton donor for the leaving group (Chapter 3). 4. After dephosphorylation, the phosphate ion and the leaving group will be released from the catalytic center of tPphA.

8. Prospects

PP2Cs could regulate various signal transduction pathways in prokaryotes and eukaryotes. The highly conserved catalytic center of PP2Cs suggests they use one common mechanism to dephosphorylate substrates. But why there are many PP2C isoforms in one organism is not understood. Probably, the PP2C isoforms recognize their specific substrates by using limited regulatory domains such as FLAP subdomain. Thus, NMR study of PP2Cs in liquid condition with the substrates is essential to completely understand how the FLAP subdomain assist PP2Cs recognize different substrates.

So far it was impossible to make co-crystals of PP2Cs with the phospho-substrates since they dephosphorylate the substrates very rapidly. The analogues of substrates could be used to make co-crystal with PP2Cs. A good start is Bellinzoni's work (64) in which cacodylate and sulphate were successfully crystallized in the catalytic center of MspP. The designed analogues of substrates may also be developed as PP2C inhibitor which could be used as drug since some PP2Cs are related to cancer.

9. References

1. Zhang, X. W., Zhao, F. Q., Guan, X. G., Yang, Y., Liang, C. W., and Qin, S. (2007) *Bmc Genomics* **8**, 395.
2. Stewart, I., Seawright, A. A., and Shaw, G. R. (2008) *Adv. Exp. Med. Biol.* **619**, 613-637
3. Cavalier-Smith, T. (2000) *Trends in Plant Science* **5**, 174-182
4. Pisciotta, J. M., Zou, Y., and Baskakov, I. V. (2010) *Plos One* **5**, e10821
5. Kasting, J. F. (1993) *Science* **259**, 920–926
6. Bornet, É. and Flahault, C. (1886) *Annales des Sciences Naturelles* **180**, 224
7. Bornet, É. and Flahault, C. (1886) *Annales des Sciences Naturelles* **181**, 177-262
8. Haselkor, R. (1978) *Ann. Rev. Plant Physiol.* **29**, 319-344
9. Campbell, E. L. and Meeks, J. C. (1989) *Appl. Environ. Microbiol.* **55**, 125-131
10. <http://genome.kazusa.or.jp/cyanobase>
11. Grigorieva, G. and Shestakov, S. (1982) *Fems Microbiology Letters* **13**, 367-370
12. Yoshimura, H., Yoshihara, S., Okamoto, S., Ikeuchi, M., and Ohmori, M. (2002) *Plant and Cell Physiology* **43**, 460-463
13. Shestakov, S. V., Khyen, N. T. (1970) *Molec. Gen. Genet.* **107**, 372-375
14. Forchhammer, K. (2008) *Trends Microbiol.* **16**, 65-72
15. Forchhammer, K. (2004) *FEMS Microbiol. Rev.* **28**, 319-333
16. Fokina, O., Chellamuthu, V. R., Forchhammer, K., and Zeth, K. (2010) *Proc. Natl. Acad. Sci. U. S. A* **107**, 19760-19765
17. Shapiro, B. M. (1996). *Biochemistry* **8**, 659-670
18. Ninfa, A. J. and Jiang, P. (2005) *Curr. Opin. Microbiol.* **8**, 168-173
19. Kamberov, E. S., Atkinson, M. R., and Ninfa, A. J. (1995) *J. Biol. Chem.* **270**, 17797-17807
20. Jiang, P., Peliska, J. A., and Ninfa, A. J. (1998) *Biochemistry* **37**, 12782-12794
21. Jiang, P., Peliska, J. A., and Ninfa, A. J. (1998) *Biochemistry* **37**, 12795-12801
22. Jiang, P., Peliska, J. A., and Ninfa, A. J. (1998) *Biochemistry* **37**, 12802-12810
23. Jiang, P. and Ninfa, A. J. (2007) *Biochemistry* **46**, 12979-12996
24. Radchenko, M. V., Thornton, J., and Merrick, M. (2010) *J. Biol. Chem.* **285**, 31037-31045
25. Coutts, G., Thomas, G., Blakey, D., and Merrick, M. (2002) *Embo Journal* **21**, 536-545
26. Javelle, A. and Merrick, M. (2005) *Biochemical Society Transactions* **33**, 170-172
27. Sanders, C. E., Melis, A. and Allen, J. F. (1989) *Biochim. Biophys. Ada* **111**, 176-181
28. Tsinoremas, N. F., Castets, A. M., Harrison, M. A., Allen, J. F., and Demarsac, N. T. (1991) *Proceedings of the National Academy of Sciences of the United States of America* **88**, 4565-4569

29. Forchhammer, K. and Tandeau de, M. N. (1995) *J. Bacteriol.* **177**, 5812-5817
30. Forchhammer, K. and Hedler, A. (1997) *Eur. J. Biochem.* **244**, 869-875
31. Forchhammer, K. 1999. The PII protein in *Synechococcus* sp. PCC 7942 senses and signals 2-oxoglutarate under ATP replete conditions. in: *The Phototrophic Prokaryotes* (Hrsg: G. Peschek, W. Löffelhardt und G. Schmetterer) p. 549-553
32. Truan, D., Huergo, L. F., Chubatsu, L. S., Merrick, M., Li, X. D., and Winkler, F. K. (2010) *J. Mol. Biol.* **400**, 531-539
33. Slocum, R. D. (2005) *Plant Physiol Biochem* **43**, 729-745
34. Maheswaran, M., Ziegler, K., Lockau, W., Hagemann, M. and Forchhammer, K. (2006) *J Bacteriol* **188**, 2730-2734
35. Heinrich, A., Maheswaran, M., Ruppert, U., and Forchhammer, K. (2004) *Mol. Microbiol.* **52**, 1303-1314
36. Maheswaran, M., Urbanke, C., and Forchhammer, K. (2004) *J. Biol. Chem.* **279**, 55202-55210
37. Llacer, J. L., Contreras, A., Forchhammer, K., Marco-Marin, C., Gil-Ortiz, F., Maldonado, R., Fita, I., and Rubio, V. (2007) *Proc. Natl. Acad. Sci. U. S. A* **104**, 17644-17649
38. Mizuno, Y., Berenger, B., Moorhead, G. B., and Ng, K. K. (2007) *Biochemistry* **46**, 1477-1483
39. Espinosa, J., Forchhammer, K., Burillo, S., and Contreras, A. (2006) *Mol. Microbiol.* **61**, 457-469
40. Burillo, S., Luque, I., Fuentes, I., and Contreras, A. (2004) *J. Bacteriol.* **186**, 3346-3354
41. Herrero, A., Muro-Pastor, A. M., and Flores, E. (2001) *J. Bacteriol.* **183**, 411-425
42. Su, Z. C., Olman, V., Mao, F. L., and Xu, Y. (2005) *Nucleic Acids Research* **33**, 5156-5171
43. Llacer, J. L., Espinosa, J., Castells, M. A., Contreras, A., Forchhammer, K., and Rubio, V. (2010) *Proc. Natl. Acad. Sci. U. S. A* **107**, 15397-15402
44. Osanai, T., Sato, S., Tabata, S., and Tanaka, K. (2005) *Journal of Biological Chemistry* **280**, 34684-34690
45. Ferrario-Mery, S., Bouvet, M., Leleu, O., Savino, G., Hodges, M., and Meyer, C. (2005) *Planta* **223**, 28-39
46. Feria Bourrellier, A. B., Valot, B., Guillot, A., Ambard-Bretteville, F., Vidal, J., and Hodges, M. (2010) *Proc. Natl. Acad. Sci. U. S. A* **107**, 502-507
47. Irmeler, A., Sanner, S., Dierks, H., and Forchhammer, K. (1997) *Mol. Microbiol.* **26**, 81-90
48. Irmeler, A. and Forchhammer, K. (2001) *Proc. Natl. Acad. Sci. U. S. A* **98**, 12978-12983
49. Ruppert, U., Irmeler, A., Kloft, N., and Forchhammer, K. (2002) *Mol. Microbiol.* **44**, 855-864

50. Barford, D., Das, A. K., and Egloff, M. -P. (1998) *Annu. Rev. Biomol. Struct.* **27**, 133-164
51. Rigden, D. J. (2008) *Biochem. J.* **409**, 333-348
52. Shi, Y. G. (2009) *Cell* **139**, 468-484
53. Das, A. K., Helps, N. R., Cohen, P. T. W., and Barford, D. (1996) *Embo Journal* **15**, 6798-6809
54. Egloff, M. -P., Cohen, P. T. W., Reinemer, P., and Barford, D. (1995) *J. Mol. Biol.* **254**, 942-956
55. Goldberg, J., Huang, H., Kwon, Y., Greengard, P., Nairn, A. C., and Kuriyan, J. (1995) *Nature* **376**, 745-753
56. Ghosh, A., Shuman, S., and Lima, C. D. (2008) *Mol. Cell* **32**, 478-490
57. Kamenski, T., Heilmerier, S., Meinhardt, A., and Cramer, P. (2004) *Mol. Cell* **15**, 399-407
58. Lammers, T. (2007) *Crit Rev Biochem Mol Biol.* **42**, 437-461
59. Arino, J., Casamayor, A., and Gonzalez, A. (2011) *Eukaryot Cell.* **10**, 21-33
60. Schweighofer, A., Hirt, H., and Meskiena, I. (2004) *Trends Plant Sci.* **9**, 236-243
61. Melcher, K., Ng, L. M., Zhou, X. E., Soon, F. F., Xu, Y., Suino-Powell, K. M., Park, S. Y., Weiner, J. J., Fujii, H., Chinnusamy, V., Kovach, A., Li, J., Wang, Y., Li, J., Peterson, F. C., Jensen, D. R., Yong, E. L., Volkman, B. F., Cutler, S. R., Zhu, J. K., and Xu, H. E. (2009) *Nature* **462**, 602-608
62. Miyazono, K., Miyakawa, T., Sawano, Y., Kubota, K., Kang, HJ, Asano, A., Miyauchi, Y., Takahashi, M., Zhi, Y., Fujita, Y., Yoshida, T., Kodaira, KS., Yamaguchi-Shinozaki, K., and Tanokura, M. (2009) *Nature* **462**, 609-614
63. Dupeux, F., Antoni, R., Betz, K., Santiago, J., Gonzalez-Guzman, M., Rodriguez, L., Rubio, S., Park, S. Y., Cutler, S. R., Rodriguez, P. L., and Marquez, J. A. (2011) *Plant Physiol* **156**, 106-116
64. Bellinzoni, M., Welhenkel, A., Shepard, W., and Alzari, P. M. (2007) *Structure* **15**, 863-872
65. Wehenkel, A., Bellinzoni, M., Schaeffer, F., Villarino, A., and Alzari, P. M. (2007) *J. Mol. Biol.* **374**, 890-898
66. Shi, L. and Zhang, W. (2004) *Microbiology* **150**, 2247-2256
67. Kennelly, P. J. (2002) *FEMS Microbiol. Lett.* **206**, 1-8
68. Duncan, L., Alper, S., Arigoni, F., Losick, R., and Stragier, P. (1995) *Science* **270**, 641-644
69. Vijay, K., Brody, M. S., Fredlund, E., and Price, C. W. (2000) *Mol. Microbiol.* **35**, 180-188
70. Obuchowski, M., Madec, E., Delattre, D., Boel, G., Iwanicki, A., Foulger, D., and Seror, S. J. (2000) *J. Bacteriol.* **182**, 5634-5638
71. Shakir, S. M., Bryant, K. M., Larabee, J. L., Hamm, E. E., Lovchik, J., Lyons, C. R., and Ballard, J. D. (2010) *J. Bacteriol.* **192**, 400-409

72. Treuner-Lange, A., Ward, M. J., and Zusman, D. R. (2001) *Mol. Microbiol.* **40**, 126-140
73. Rajagopal, L., Clancy, A., and Rubens, C. E. (2003) *J. Biol. Chem.* **278**, 14429-14441
74. Boitel, B., Ortiz-lombardia, M., Duran, R., Pompeo, F., Cole, S. T., Cervenansky, C., and Alzari, P. M. (2003) *Mol. Microbiol.* **49**, 1493-1508
75. Chopra, P., Singh, B., Singh, R., Vohra, R., Koul, A., Meena, L. S., Koduri, H., Ghildiyal, M., Deol, P., Das, T. K., Tyagi, A. K., and Singh, Y. (2003) *Biochem. Biophys. Res. Commun.* **311**, 112-120
76. Jang, J., Wang, L., Jeanjean, R., and Zhang, C. C. *Mol. Microbiol.* **64**, 347-358
77. Jackson, M. D. And Denu, J. M. (2001) *Chem. Rev.* **101**, 2313-2340
78. Jackson, M. D., Fjeld, C. C., and Denu, J. M. (2003) *Biochemistry* **42**, 8513-8521
79. Pullen, K .E., Ng, H. L., Sung, P. Y., Good, M. C., Smith, S. M., and Alber, T. (2004) *Structure* **12**, 1947-1954
80. Rantanen, M. K., Lehtio, L., Rajagopal, L., Rubens, C. E., and Goldman, A. (2007) *Febs Journal* **274**, 3128-3137
81. Schlicker, C., Fokina, O., Kloft, N., Grune, T., Becker, S., Sheldrick, G. M., and Forchhammer, K. (2008) *J. Mol. Biol.* **376**, 570-581
82. Pappa, H. S. and Poulos, T. L. (1995) *Biochemistry* **34**, 6573-6580

Contribution to publications/manuscripts

Chapter 3: A third metal is required for catalytic activity of the signal-transducing PPM phosphatase tPphA

I performed all experiments, with the exception of the crystal structures. I purified the proteins (D119A and D193A) and Dr. Christine Schlicker made the crystallization and X-ray analysis.

Chapter 4-6.

I performed all experiments

Curriculum vitae

Name:	Jiyong Su 苏纪勇	Age:	31
Place of born	Hebei, China 河北, 中国	Email:	susion888@yahoo.com.cn

School experience:

2008—2011	Ph.D candidate, Microbiology II, Uni-Tübingen, Germany
2007—2008	Diploma, Microbiology II, Uni-Tübingen, Germany
2004—2007	Master, Biophysics, Nankai University, Tianjin, China
1999—2003	Bachelor, Biotechnology, Hebei University, Hebei, China
1996—1999	27th high school of Shijiazhuang City, Hebei, China

Abbreviations

°C Grad Celsius	PP2C PP2C type phosphatase
μ Micro-	PphA Protein-Phosphatase A
2 OG 2-oxoglutarate	tPphA <i>Thermosynechococcus</i> -Protein-Phosphatase A
ADP Adenosine Diphosphate	Tris Tris(dibenzylideneacetone)dipalladium
APS Ammonium persulfate	UV Ultraviolet
ATP Adenosine Triphosphate	NMR Nuclear magnetic resonance
BSA Bovine Serum Albumin	
DTT dithiothreitol	
EDTA ethylenediaminetetraacetic acid	
<i>E.coli Escherichia coli</i>	
Fig figure	
GDP Guanosine diphosphate	
GTP Guanosine triphosphate	
Hepes 4-(2-hydroxyethyl)piperazine-1-erhanesulfonic acid	
IPTG Isopropyl β- D -1-thiogalactopyranoside	
kDa Kilodalton	
M mol/l	
min Minute	
Np-40 Nonidet P-40	
O. D optical density	
PAGE polyacrylamide gel electrophoresis	
Pi inorganic phosphate	
PCR polymerase chain reaction	
PP2C Protein phosphatase 2C	
PphA Protein-Phosphatase A	
PMSF Phenylmethanesulphonylfluoride	
<i>p</i> -NPP <i>p</i> -Nitrophenyl Phosphate	
rpm Revolutions per minute	
SDS sodium dodecyl sulfate	
TEMED N, N, N', N'-	
Tetramethylethylenediamine	
PPM Mg ²⁺ -Mn ²⁺ dependent phosphatase	